The Role of Muscular TDP-43 in Neuromuscular Junction Development and Progress of ALS

Thesis

The Role of Muscular TDP-43 in Neuromuscular Junction Development and Progress of ALS

Nina Strah

A thesis submitted in fulfilment of the requirements of The Open University, United Kingdom, for the degree of Doctor of Philosophy

Neurobiology Group, International Centre for Genetic Engineering and Biotechnology (ICGEB), Trieste, Italy

Director of Studies: Fabian Feiguin, MD, PhD

External Supervisor: Serena Zacchigna, MD, PhD

September 2019

The thesis is dedicated to my grandfather Alojz.

ABSTRACT

Amyotrophic lateral sclerosis (ALS) is a fatal disease with fast progression. Patients usually die three to five years after diagnosis. The main characteristics are progressive neurodegeneration, following muscular weakness, and atrophy. The most common cause of death is respiratory muscle failure. Studies have shown that the highlight of the disease is TDP-43 inclusions in neuronal cytoplasm. The symptoms of ALS can be recapitulated in *Drosophila melanogaster*. The *Drosophila*‘s ortholog is called TBPH. TBPH knockout flies show locomotion problems, shorter lifespan, and anatomical changes in the neuromuscular junction (NMJ).

Our studies aimed to reveal the function of TBPH in muscles. We took advantage of RNA interference and silenced the protein exclusively in muscles. Moreover, we expressed TBPH in *tbph*$^{\Delta 23}$/- fly and tried to understand whether it can rescue reduced mobility, lifespan, and anatomical properties of NMJ. We observed changes in lifespan, motility, and NMJ structure when TBPH was silenced in muscles. Expression of the protein in *tbph*$^{\Delta 23}$/- *Drosophila* completely recovered the motility of larvae and the level of proteins located in the postsynaptic compartment of NMJ. One of the proteins was Disc large (Dlg), known as scaffold protein involved in NMJ development and maintenance of NMJ structure. Expression of Dlg recovered the phenotype in terms of mobility, lifespan, and NMJ formation. We also demonstrated that the drop of Dlg levels

could be seen in neuroblastoma cells and differentiated iPS cells of ALS patients. With that been discovered, not only have we confirmed the relevance of our studies, but we have also opened a new possibility for drug development and treatment. Moreover, with the research, we contributed to a recent hypothesis that muscles can be involved in the onset of ALS.

Acknowledgments

First, I would like to thank Director of Studies, Dr Fabian Feiguin, who accepted me and allowed me to work in the laboratory three years ago, work on my thesis and learn a lot about science, research, and *Drosophila.* The studies would not have been possible without the financial support. Thus, special thanks go to the ICGEB for awarding a fellowship to me and enabled my studies.

I am deeply grateful to Dr Serena Zacchigna for being my support and guide. I appreciated all your pieces of advice and time that you dedicated to me. I want to express my gratitude to Dr Giulia Romano and Raffaella Klima, who taught me all the techniques and gave me a hand whenever I needed it. Thank you, Raffa, for all the nights you have dedicated to my thesis. I owe my deepest gratitude to all members of the laboratory. For a long time, Marina and Alessio, we were the “Three Musketeers”, battling our everyday struggles. You were always there, patting my back, and made me keep going on. I wish you both to live a life of your dreams – this is the least you deserve. Nik, thank you for all the pieces of advice and pleasant moments that we had shared. Monsurat, I owe you a lot. Being my support, friend, and guide, you have shown me that things were not just black and white and that every hard situation can also have a positive side. Nora and Matea, you were not just students, but also a great help

and inspiration. Thank you for all your questions and all discussions about everything we could have imagined. I would like to thank Dr Aram Megighian for accepting me in his laboratory in Padova and help me with the experiments regarding the electrophysiology of our model.

I would like to express the most profound appreciation to my mother Branka, father Jože, brothers Rok and Matic, grandfather Alojz, and late grandparents Terezija and Franc. Without you, I would not have succeeded at all. You had always pushed me, supported me financially and morally, and enabled me to become the person I am today. I cannot thank Muli enough, being right beside me at my lowest and highest, always finding the right words to make me feel better. You are my rock and inspiration. My sincere appreciation goes to Monika, Brigita, Tina, and Maruša. You are my sisters I had always wished for. No matter how many kilometres separate us, our paths always join at one point. I love you all to the moon and back.

Table of content

ABSTRACT 1

List of Abbreviations 24

1. INTRODUCTION 29

1.1. Amyotrophic Lateral Sclerosis 30

1.1.1. The symptoms and stages of the disease 30

1.1.2. The pathogenesis of ALS 32

1.1.3. The diagnosis of ALS 39

1.1.4. The treatment and management of ALS 40

1.1.5. Role of the muscles in ALS 44

1.2. TDP-43 47

1.2.1. TDP-43 structure 48

1.2.2. TDP-43 function 49

1.2.3. TDP-43 and muscles 53

1.3. TDP-43 and neurodegeneration 55

1.3.1. TDP-43 pathology in ALS 56

1.4. TBPH: the ortholog of TDP-43 in Drosophila melanogaster 58

1.5. Drosophila melanogaster 62

1.5.1. Drosophila life cycle 62

1.5.2. Drosophila in biology 65

1.5.3. Genetic in *Drosophila melanogaster* 66

1.5.4. Drosophila neuromuscular junction 73

1.6. *tbph*$^{\Delta 23}$/- *Drosophila* model 80

2. AIMS AND OBJECTIVES 84
3. RESULTS 86
3.1. Silencing TBPH in muscles 87
3.1.1. Flies show locomotive problems and shorter lifespan 87
3.1.2. Boutons are misshaped, and Futsch level drops with TBPH silencing in muscles 100
3.1.3. Dlg and glutamate receptors are downregulated 104
3.2. TBPH rescue in *tbph*$^{\Delta 23}$/- flies 107
3.2.1. The motility in larvae but not in adult flies is recovered 108
3.2.2. NMJ growth and shape are recovered 116
3.2.3. Dlg and glutamate receptors are recovered, as well as NMJ function 120
3.3. Dlg rescues *tbph*$^{\Delta 23}$/- flies 124
3.3.1. Expression of Dlg in muscles rescues the phenotype in larvae, as well as in adult flies 125
3.3.2. Expression of Dlg in muscles contributes to NMJ growth and function 129
3.3.3. Expression of Dlg in neurons improve the mobility of larvae 134
3.4. TBPH directly binds *dlg* mRNA 142
3.5. TDP-43 in human cells regulates Dlg levels 145
4. DISCUSSION 148
4.1. Silencing of TBPH in muscles affects locomotion, life span, NMJ shape and function 149
4.2. Expression of TBPH in muscles rescues TBPH$^{-/-}$ phenotype, NMJ function, and structure 152

4.3. Dlg protein regulates NMJ shape and function 155
4.4. Dlg1 (SAP79) is downregulated in SH-SY5Y cells and ALS patients . 157
4.5. Conclusions and future perspective 159
Translational potential for patients 162
5. MATERIAL AND METHODS 163
5.1. Fly strains 164
5.2. Drosophila techniques 167
5.2.1. Fly stocks and crosses 167
5.2.2. Phenotypic analysis in *Drosophila* 168
5.2.3. Immunohistochemistry studies 171
5.2.4. Electrophysiology on NMJ of the third instar larva preparation 175
5.3. Biochemical techniques 176
5.3.1. Immunoprecipitation 176
5.3.2. Protein extraction 179
5.3.3. SDS-PAGE 179
5.3.4. Western blot 180
5.4. Cell culture techniques 181
5.4.1. Cell culture and RNA interference 181
5.5. Statistical analysis 182
REFERENCES 183

List of Figures

Figure 1: Two onsets of the disease. Patients can experience different early symptoms of ALS, depending on the onset. 31
Figure 2: Proteins carrying the mutations in patients diagnosed with FALS and SALS, and their frequencies (Zou et al., 2017). 33
Figure 3: Regions of FUS where mutations were found (marked with arrows) in ALS patients. NES = nuclear export signal, RRM = RNA recognition motif, RGG = Arg-Gly-Gly repeat region, ZNF = zinc-finger motif, NLS = nuclear localisation signal 37
Figure 4: Potential factors that could lead to motor neuron death – the main characteristic of ALS. Gene mutations and environment could contribute to cellular dysfunctions, which cause cell death (The image modified by (Vijayakumar et al., 2019)). 38
Figure 5: The structure and the mechanism of riluzole. A) The chemical structure of riluzole. B) Riluzole acts neuroprotective. It blocks the influx of sodium ions and prevents the release of glutamate. It also increases the reuptake of glutamate in glial cells. It is adapted from http://www.mdpi.com/1420-3049/20/5/7775/htm. 41
Figure 6: The main parts of the TDP-43 protein. NLS = nuclear localisation sequence, RRM1 and RRM2 = RNA recognition motive 1 and 2, NES = nuclear export sequence and GRR = glycine-rich region. (customised by (Cohen et al., 2011)) 48
Figure 7: TDP-43 functions in the cell. 1) TDP-43 binds directly to the promoter regions and regulates the transcription. 2) TDP-43 is involved in the alternative splicing by binding to introns or exons and recruiting specific proteins. 3) TDP-43 stabilises mRNA and is involved in the transport. 4) TDP-43 controls the assembly of stress granules. 5) TDP-43

binds to Drosha and Dicer, and controls microRNA processing (customised by (Budini et al., 2017)). 50
Figure 8: The main characteristic of ALS is TDP-43 cytoplasmatic aggregates. There are two hypotheses of how these aggregates affect cell function. Either TDP-43 aggregates prevent the protein from functioning, or the aggregates are toxic for the cell. 57
Figure 9: Comparison between human TDP-43 and TBPH. The difference between the two is mainly in C-terminal part. TBPH C-terminal is longer than the one of TDP-43. (The image is customized by (Romano et al. 2012).) 58
Figure 10: Chromosomal location of tbph gene (second chromosome), and representation of its transcripts and the relative CDS. It is adapted from www.flybase.org. 59
Figure 11: The parallel between human TDP-43 (upper line) and TBPH Drosophila amino acid sequence (bottom line). Amino acids, identical (*) or similar (:), between the two proteins are indicated. Red squares indicate the RNA recognition domains, RRM1 and RRM2. (Uniprot accession no. Q13148 and O97468 resp.) 60
Figure 12: The Drosophila life cycle. Three different stages of larva follow the egg stage, and then larva eventually develops in a pupa and forms an adult fly. Customised by http://www.zoology.ubc.ca/~bio463/lecture_13.htm. 63
Figure 13: Female versus male Drosophila melanogaster. The two most identifiable features in males are claspers at the tip of the abdomen and sex comb at the front leg. Females are usually bigger and have a light tip of the abdomen. 64
Figure 14: Schematic presentation of autonomous and nonautonomous P-elements. Nonautonomous P-element has the majority of the transposase gene deleted (customised by Anthony J.F. Griffiths, 2015). 68

Figure 15: The bacterial vector with nonautonomous P-element containing a DNA segment of interest. After injection with the autonomous vector, transposase integrates DNA with the P-element into Drosophila chromosome (customised by Anthony J.F. Griffiths, 2015). 69
Figure 16: GAL4/UAS system. In the GAL4/UAS system, two transgenic fly lines are created. In the responder strain, the transgene is placed downstream of a UAS activation domain that consists of binding sides where GAL4 binds when present. Driver strain has GAL4 protein, yeast transcriptional activator. The progeny of the cross has GAL4 and UAS combined, so the gene or RNAi is expressed (modified by https://smallscienceworks.com/tag/uas-gal4/.) 71
Figure 17: $GAL80^{ts}$ and GAL 4 are expressed independently. At lower temperature, $GAL80^{ts}$ binds to GAL4 and blocks its promotion of gene transcription. When the temperature is higher, $Gal80^{ts}$ no longer binds to GAL4, and tissue-specific transcription is possible (Image customized by McGuire et al., 2003)..... 73
Figure 18: Larval body wall. The wall is divided into seven segments. Each segment presents a group of 30 different muscles that are precisely arranged. 74
Figure 19: A scheme of muscles and three primary nerve roots (ISN, SN, and TN). The scheme represents a group of 30 muscles and their distribution (muscle 7 and 6 are specially marked) in one half of one segment. The position of the muscles in larvae is shown in the bottom left corner. Three primary roots innervate different groups of the muscles in the segment. The image was customised by (Hoang and Chiba, 2001). 75
Figure 20: The structure of Dlg-A protein. It contains 3 PDZ domains, SH3 domain, and GUK domain, which however is not active. (The image customised by (Woods and Bryant, 1991))..... 79

Figure 21: Mutant flies had the same body characteristics as wildtype control, but they lived a significantly shorter time. When expressing TBPH or human TDP-43 in neurons, the life span was partially recovered (Feiguin et al., 2009). 81
Figure 22: Mutant adult flies did not climb, and their walking was significantly impaired. When TBPH was expressed in neurons, the phenotype was recovered (Feiguin et al., 2009)..... 82
Figure 23: The characterisation of the larval phenotype. (A) Confocal images of motoneurons presynaptic terminals at muscles 6 and 7 (abdominal segment III) in wild type third instar larvae stained with anti-HRP antibodies reveal the branching pattern and the presence of big (arrowhead) and small (arrow) synaptic boutons. (B) and (C) Similar staining and anatomical position for TBPHΔ23 and TBPHΔ142 homozygous larvae respectively show reduced axonal branching pattern and the number of synaptic boutons. (D) TBPHΔ23 third instar larvae rescued by expressing UAShTDP-43 in motoneurons with D42-GAL4 shows recovery of presynaptic complexity with increased formation of synaptic boutons and axonal terminal branching. (E) The number of peristaltic waves observed for two minutes. (F) Quantification of big synaptic boutons present in consecutive abdominal segments. (G) Analysis of small synaptic boutons. (H) Quantification of presynaptic terminals branches in wild type, TBPHΔ23 and hTDP-43/TBPH rescued third instar larva. Scale: 10μm. (Feiguin et al., 2009). 83
Figure 24: Larval movement was significantly impaired when TBPH in muscles was silenced. Counting peristaltic waves significantly dropped in larvae expressing UAS-TBPH-IR comparing to larvae expressing UAS-GFP-IR. *p<0.05 calculated by T-test, error bars SEM. N=20 larvae per genotype. 88

Figure 25: Larval motility was impaired in animals with silenced TBPH. Counting peristaltic waves significantly dropped in larvae expressing UAS-TBPH-IR comparing to larvae expressing UAS-GFP-IR. ***p<0.001 calculated by T-test, error bars SEM. N=20 larvae per genotype. 89
Figure 26: Larvae with silenced TBPH in wild type background performed worse than the control group. Counting peristaltic waves significantly dropped in larvae expressing UAS-TBPH-IR comparing to larvae expressing UAS-GFP-IR. ***p<0.001 calculated by T-test, error bars SEM. N=20 larvae per genotype. 91
Figure 27: Larvae with TBPH silenced have impaired mobility. Counting peristaltic waves significantly dropped in larvae expressing UAS-TBPH-IR comparing to larvae expressing UAS-GFP-IR. ***p<0.001 calculated by T-test, error bars SEM. N=20 larvae per genotype. 92
Figure 28: Flies' ability in climbing was impaired. The percentage of flies that reached the top of the cylinder significantly dropped in flies expressing UAS-TBPH-IR comparing to flies expressing UAS-GFP-IR on day 4, 7 and 14. On day 21, the difference was not significant. ***p<0.001 calculated by two-way ANOVA, error bars SEM. N=200 flies per genotype. 93
Figure 29: Flies had a significantly shorter lifespan when TBPH in muscles was silenced in early time points. The percentage of death events in silencing flies compared to their control was higher at the beginning of the measurement. The statistical difference was calculated by the Gehan-Breslow-Wilcoxon test, *p<0.05. N=200 flies per genotype. 94
Figure 30: Flies climbed significantly less when TBPH in muscles was silenced. The percentage of flies that reached the top of the cylinder significantly dropped in flies expressing UAS-TBPH-IR comparing to flies expressing UAS-GFP-IR on day 1, 4, 7 and 14. **p<0.01 and ***p<0.001 calculated by two-way ANOVA, error bars SEM. N=200 flies per genotype. 96

Figure 31: Flies lived a significantly shorter time when TBPH in muscles was silenced. Silencing of TBPH affects the overall life span (log-rank test), including with early events evaluation (Gehan-Breslow-Wilcoxon test). ***p<0.001. N=200 flies per genotype. 98
Figure 32: With one-way ANOVA test statistically the strongest difference show TBPH silencing with MHC-GAL4 in heterozygous background. ns = not significant **p<0.01 and ***p<0.001 calculated by one-way ANOVA. Error bars SEM. N=20 larvae per genotype..... 100
Figure 33: In larvae with silenced TBPH in muscles number of branches did not significantly change. Confocal images of the third instar NMJ terminals in muscle 6 / 7, second segment stained with anti-HRP (in green) are represented. The representative terminals are shown, together with the quantification. ns= not significant, calculated by T-test, error bars SEM. N = 20 larvae per genotype. 101
Figure 34: Silencing TBPH in muscles affected the bouton shape. Confocal images of the third instar NMJ terminals in muscle 6 / 7, second segment stained with anti-HRP (in green). The representative bouton shapes are shown, together with the quantification. **p<0.01, calculated by T-test, error bars SEM. N = 20 larvae per genotype. 102
Figure 35: Futsch was significantly reduced in flies with silenced TBPH in muscles. Confocal images of third instar NMJ terminals in muscle 6 / 7 second segment stained with anti-HRP (in green) and anti-Futsch (in red) in MHC-Ctrl ($tbph^{\Delta 23}$/ +; MHC-GAL4/UAS-GFP-IR) and MHC-TBi ($tbph^{\Delta 23}$/+; MHC-GAL4/UAS-TBPH-IR). Arrows show boutons with reduced levels or absence of Futsch in boutons. Quantification of Futsch intensity was normalised on control. ***p<0.001, calculated by T-test, Error bars SEM. N=20 larvae per genotype. 103
Figure 36: Dlg protein level was reduced by TBPH silencing in muscles. Confocal images of the third instar NMJ terminals in muscle 6 / 7 second

segment stained with anti-HRP (in green) and anti-Dlg (in red) in MHC-Ctrl ($tbph^{\Delta 23}$/ +; MHC-GAL4/UAS-GFP-IR) and MHC-TBi ($tbph^{\Delta 23}$/+; MHC-GAL4/UAS-TBPH-IR) together with the quantification of Dlg intensity normalised on ctrl. Arrows point to the absence of the protein in the postsynaptic part of NMJ. ***p<0.001, calculated by T-test, Error bars SEM. N=20 larvae per genotype. 104
Figure 37: Glutamate receptors (subunit GluRIIA) are downregulated by TBPH silencing in muscles. Confocal images of the third instar NMJ terminals in muscle 6 / 7 second segment stained with anti-HRP (in green) and anti-GluRIIA (in red) in MHC-Ctrl ($tbph^{\Delta 23}$/ +; MHC-GAL4/UAS-GFP-IR) and MHC-TBi ($tbph^{\Delta 23}$/+; MHC-GAL4/UAS-TBPH-IR) together with the quantification of GluRIIA intensity normalised on ctrl. ***p<0.001, calculated by T-test, Error bars SEM. N=20 larvae per genotype. 106
Figure 38: TBPH and hTDP expression with co-expression of $GAL80^{ts}$ did not affect larval phenotype at 25°C. Calculated by one-way ANOVA with Bonferroni correction, error bars SEM. N=20 larvae per genotype. 108
Figure 39: Larval motility was recovered by expressing TBPH or hTDP2 in muscles. The number of peristaltic waves significantly raised in larvae expressing UAS-TBPH and UAS-TDP-43. **p<0.01, ***p<0.001 calculated by one-way ANOVA with Bonferroni correction, error bars SEM. N=20 larvae per genotype. 109
Figure 40: TBPH and TDP-43 expressing in muscles do not improve the climbing ability. The percentage of flies that reached the top of the cylinder was not significantly higher in flies expressing UAS-TBPH or UAS-TDP-43 comparing to the negative control group (UAS-GFP) on day 4 and 7. *p<0.05 and ***p<0.001 calculated by one-way ANOVA with a Bonferroni correction, error bars SEM. N=200 flies per genotype. 111
Figure 41: Flies expressing TBPH in muscles walked a greater distance. Walking assay analysis of flies expressing UAS-GFP and UAS-TBPH

using Mef2-GAL4 at day 2. ***p<0.001 calculated by t-test, error bars SEM. N = 50 flies per genotype. 112
Figure 42: TBPH and TDP-43 expression in muscles did not rescue the phenotype. The lifespan of flies expressing TBPH, TDP-43, and GFP. Statistical analysis was calculated with the log-rank test. ***p<0.001. N=200 flies per genotype. 113
Figure 43: Flies expressing TBPH or TDP-43 climbed worse than the wild type. The percentage of flies that reached the top of the cylinder is significantly lower in flies expressing UAS-TBPH or UAS-TDP-43 comparing to a positive control group (UAS-GFP) on day 4. *p<0.05 and **p<0.01 calculated by one-way ANOVA with a Bonferroni correction, error bars SEM. N=200 flies per genotype. 114
Figure 44: Lifespan was significantly shorter in flies expressing TBPH and TDP-43 in muscles. The lifespan of flies expressing TBPH, TDP-43, and GFP in a wild-type background. Statistical analysis was calculated with the log-rank test. **p<0.01 and ***p<0.001. N=200 flies per genotype. 116
Figure 45: The number of branches was recovered in larvae expressing TBPH in muscles. Confocal images of the third instar NMJ terminals in muscle 6 / 7, second segment stained with anti-HRP (in green). The representative terminals are shown, together with the quantification. ***p<0.001, calculated by one-way ANOVA with Bonferroni correction, error bars SEM. N = 20 larvae per genotype. 118
Figure 46: The percentage of regular boutons increases when TBPH was expressed in larval muscles. Confocal images of the third instar NMJ terminals in muscle 6 / 7, second segment stained with anti-HRP (in green). The representative bouton shapes are shown, together with the quantification. ***p<0.001, calculated by one-way ANOVA, error bars SEM. N = 20 larvae per genotype. 119

Figure 47: Dlg protein level was recovered after overexpression of TBPH in muscles. Confocal images of the third instar NMJ terminals in muscle 6 / 7 second segment stained with anti-HRP (in green) and anti-Dlg (in red) in Ctrl ($tbph^{\Delta 23}GAL80^{ts}$/+; Mef2-GAL4/+), Δtb-GFP ($tbph^{\Delta 23}$ $GAL80^{ts}/tbph^{\Delta 23}$; Mef2-GAL4/UAS-GFP) and Δtb-TBPH ($tbph^{\Delta 23}$ $GAL80^{ts}/tbph^{\Delta 23}$UAS-TBPH; Mef2-GAL4/+), together with the quantification of Dlg intensity normalised on ctrl. ***p<0.001, calculated by one-way ANOVA with Bonferroni correction, Error bars SEM. N=20 larvae per genotype. 121
Figure 48: Level of glutamate receptors was recovered in mutant larvae expressing TBPH in muscles. Confocal images of the third instar NMJ terminals in muscle 6 / 7 second segment stained with anti-HRP (in green) and anti-GluRIIA (in red) in Ctrl ($tbph^{\Delta 23}GAL80^{ts}$/+; Mef2-GAL4/+), Δtb-GFP ($tbph^{\Delta 23}$ $GAL80^{ts}/tbph^{\Delta 23}$; Mef2-GAL4/UAS-GFP) and Δtb-TBPH ($tbph^{\Delta 23}$ $GAL80^{ts}/tbph^{\Delta 23}$UAS-TBPH; Mef2-GAL4/+) together with the quantification of GluRIIA intensity normalised on ctrl. ***p<0.001, calculated by one-way ANOVA with Bonferroni correction, Error bars SEM. N=20 larvae per genotype. 122
Figure 49: Evoked junctional potential in mutant larvae expressing TBPH was recovered. Representative EJPs evoked by segmental nerve stimulation of Ctrl ($tbph^{\Delta 23}GAL80^{ts}$/+; Mef2-GAL4/+), Δtb-GFP ($tbph^{\Delta 23}$ $GAL80^{ts}/tbph^{\Delta 23}$; Mef2-GAL4/UAS-GFP) and Δtb-TBPH ($tbph^{\Delta 23}$ $GAL80^{ts}/tbph^{\Delta 23}$UAS-TBPH; Mef2-GAL4/+) in muscle fibre 6 / 7 of A3 in third instar larvae. For each fibre 5, EPPs following 0.5Hz stimulation were considered. **p<0.01, ***p<0.001 calculated by one-way ANOVA with Bonferroni correction, error bars SEM. N = 10 larvae per each genotype. 123

Figure 50: UAS-DLG expression with Mef2-GAL4 did not affect larval phenotype at 25°C. Calculated by t-test, error bars SEM. N=20 larvae per genotype. 125
Figure 51: Dlg expression in muscles rescued the larval phenotype. The number of peristaltic waves significantly raised in larvae expressing UAS-DLG comparing to larvae expressing UAS-GFP. **p<0.01, ***p<0.001 calculated by one-way ANOVA with Bonferroni correction, error bars SEM. N=20 larvae per genotype. 126
Figure 52: Climbing performance was significantly improved when Dlg was expressed in muscles. The percentage of flies that reached the top of the cylinder was significantly higher in flies expressing UAS-DLG comparing to the negative control (UAS-GFP) on day 4. ***p<0.001 calculated by one-way ANOVA with a Bonferroni correction, error bars SEM. N=200 flies per genotype. 128
Figure 53: Flies expressing Dlg had a longer lifespan than mutant flies. The lifespan of flies expressing only driver Mef2-GAL4, UAS-GFP and UAS-DLG. Statistical analysis was calculated with the log-rank test. ***p<0.001. N=200 flies per genotype. 129
Figure 54: NMJ shape was recovered by Dlg expression. Confocal images of the third instar NMJ terminals in muscle 6 / 7, second segment stained with anti-HRP (in green). The representative terminals are shown, together with the quantification. ***p<0.001, calculated by one-way ANOVA with Bonferroni correction, error bars SEM. N = 20 larvae per genotype. ... 130
Figure 55: Larvae expressing Dlg had a higher percentage of regular boutons and a lower percentage of irregular ones. Confocal images of the third instar NMJ terminals in muscle 6 / 7, second segment stained with anti-HRP (in green). The representative bouton shapes are shown, together with the quantification. ***p<0.001, calculated by one-way ANOVA, error bars SEM. N=20 larvae per genotype..... 132

Figure 56: Dlg expression in muscles recovered the glutamate receptors level. Confocal images of the third instar NMJ terminals in muscle 6 / 7 second segment stained with anti-HRP (in green) and anti-GluRIIA (in red) in Ctrl ($tbph^{\Delta 23}$/+; Mef2-GAL4/+), Δtb-GFP ($tbph^{\Delta 23}$/$tbph^{\Delta 23}$; Mef2-GAL4/UAS-GFP) and Δtb-Dlg ($tbph^{\Delta 23}$ /$tbph^{\Delta 23}$UAS-DLG; Mef2-GAL4/+), together with the quantification of GluRIIA intensity normalised on ctrl. ***p<0.001, calculated by one-way ANOVA with Bonferroni correction, Error bars SEM. N=20 larvae per genotype..... 133
Figure 57: The evoked junctional potential was rescued when Dlg was expressed in muscles. Representative EJPs evoked by segmental nerve stimulation of $tbph^{\Delta 23}$/+; Mef2-GAL4/+, $tbph^{\Delta 23}$/$tbph^{\Delta 23}$; Mef2-GAL4/UAS-GFP and $tbph^{\Delta 23}$ /$tbph^{\Delta 23}$UAS-DLG; Mef2-GAL4/+ in muscle fibre 6 / 7 of A3 in third instar larvae. For each fibre 5, EPPs following 0.5Hz stimulation were considered. **p<0.01, ***p<0.001 calculated by one-way ANOVA with Bonferroni correction, error bars SEM. N = 10 larvae per each genotype. 134
Figure 58: In TBPH mutants, Dlg levels were downregulated. Expression of TBPH recovered the intensity. Western blot analysis of lane 1 (w^{1118}), lane 2 ($tbph^{\Delta 23}$/$tbph^{\Delta 23}$), lane 3 ($tbph^{\Delta 142}$/$tbph^{\Delta 142}$) and lane 4 ($tbph^{\Delta 23}$UAS-TBPH /$tbph^{\Delta 23}$ Elav-GAL4). Adult brains, one day old, were probed with anti-Dlg and alpha-tubulin antibodies. The same membrane was probed with the two antibodies, and the bands of interest were cropped. Quantification of normalised amounts was reported below each lane. n=3 (biological replicates). 135
Figure 59: UAS-DLG gene expression with nSyb-GAL4 did not affect larval phenotype at 25°C. Calculated by t-test, error bars SEM. N=20 larvae per genotype. 137
Figure 60: Dlg expression in neurons rescued the larval phenotype. The number of peristaltic waves significantly raised in larvae expressing UAS-

DLG comparing to larvae expressing UAS-GFP. ***p<0.001 calculated by one-way ANOVA with Bonferroni correction, error bars SEM. N=20 larvae per genotype. 138
Figure 61: Dlg expressed in neurons recovered the number of branches. Confocal images of the third instar NMJ terminals in muscle 6 / 7, second segment stained with anti-HRP (in green). The representative terminals are shown, together with the quantification. **p<0.01 and ***p<0.001, calculated by one-way ANOVA with Bonferroni correction, error bars SEM. N = 20 larvae per genotype. 140
Figure 62: Glutamate receptor level was higher when expressing Dlg. Confocal images of the third instar NMJ terminals in muscle 6 / 7 second segment stained with anti-HRP (in green) and anti-GluRIIA (in red) in Ctrl ($tbph^{\Delta 23}$/+;nSyb-GAL4/+), Δtb-GFP ($tbph^{\Delta 23}$/$tbph^{\Delta 23}$;nSyb-GAL4/UAS-GFP) and Δtb-Dlg ($tbph^{\Delta 23}$ /$tbph^{\Delta 23}$UAS-DLG;nSyb-GAL4/+), together with the quantification of GluRIIA intensity normalised on ctrl. **p<0.01 and ***p<0.001, calculated by one-way ANOVA with Bonferroni correction, Error bars SEM. N=20 larvae per genotype..... 142
Figure 63: Dlg mRNA levels were enriched in flies' muscles overexpressing TBPH. qRT-PCR analysis of mRNAs immunoprecipitated by Flag-tagged TBPH (UAS-TBPH/+; Mef2-GAL4/+, IP-TBPH) and its mutant variants $TBPH^{F/L}$ (+/+; UAS-TBPH $^{F/L}$/Mef2-GAL4, IP-$TBPH^{F/L}$) in adult thoraces. The dlg enrichment-folds was referred to as rpl-11 (negative control), hdac6 has been used as a positive control. n=3 (biological replicates). 143
Figure 64: Dlg mRNA levels were enriched when TBPH was overexpressed in flies' neurons. qRT-PCR analysis of mRNAs immunoprecipitated by Flag-tagged TBPH (Elav-GAL4/UAS-TBPH/+;+/+, IP-TBPH) and its mutant variants $TBPH^{F/L}$ (Elav-GAL4/+; UAS-TBPH $^{F/L}$/+, IP-$TBPH^{F/L}$) in adult heads. The dlg enrichment-folds was referred to rpl-

11 (negative control), syntaxin has been used as a positive control. n=3 (biological replicates). 144
Figure 65: Dlg levels were downregulated when TDP-43 was silenced. A) Western blot analysis on human neuroblastoma (SH-S5Y5) cell line probed for anti-Dlg, anti-GAPDH, and anti-TDP-43 in siGFP (GFP ctrl) and siTDP-43 (TDP-43 silenced). The same membrane was probed with the three antibodies, and the bands of interest were cropped. B) Quantification of normalised protein amount (Dlg). C) Quantification of normalised protein amount (TDP-43). ****p=0.0001, using t-test. n=3 (biological replicates). 146
Figure 66: ALS patients have decreased levels of Dlg in differentiated neuronal cells. Western blot analysis probed for anti-Dlg and anti-GAPDH on human differentiated motoneurons derived from iPSCs of an ALS patient (ALS patient #1 and ALS patient #2) and a non-ALS affected control (Ctrl #1 and Ctrl #2). The same membrane was probed with the two antibodies, and the bands of interest were cropped. Quantification of normalised protein amount was reported below each lane. **p<0.01, ***p<0.001, ****p< 0.0001 calculated by one-way ANOVA, error bars SEM. 147
Figure 67: The alignment of D. melanogaster Dlg and human Dlg1. Equal amino acids (*) and similar amino acids (:) are marked (Source: https://www.uniprot.org/) 158
Figure 68: The model of TBPH function in NMJ. TBPH in muscles and neurons binds dlg mRNA and regulates mRNA metabolism. Dlg is expressed and located in NMJ, whereby to-Dlg-bound proteins anchor the Dlg protein on the other side of NMJ, and so their functions can be executed. 161
Figure 69: Divided glass cylinder prepared for the climbing assay. 170
Figure 70: Walking assay plate with the 1cm x 1cm grid beneath it. 171

Figure 71: When an equal diameter on both axes of the bouton is observed, the bouton is considered regular. Irregular boutons come in different sizes and shapes, with a different diameter on both axes.....173
Figure 72: Scheme of branches in NMJ and their hierarchy. 174
Figure 73: The scheme of measuring the EJPs.....176

Publications

The paper is under revision at BMC Biology.

Preprint:

Strah, N., Romano, G., Introna, C., Klima, R., Megighian, A., Nizzardo, M., and Feiguin, F. (2019). TDP-43 regulates the expression levels of Disc-large in skeletal muscles to promote the assemble of the neuromuscular synapses in Drosophila. BioRxiv 716423.

List of Abbreviations

AD	Alzheimer's disease
ALS	amyotrophic lateral sclerosis
AMPA	α-amino-3-hydroxy-5-methyl-4-isoxazole propionic acid
bp	base pair
CDS	coding sequence
CNS	central nervous system
COX IV	cytochrome C oxidase subunit IV
CSF	cerebrospinal fluid
Ctrl	control
CyO	curly O
Dlg	disc large
DNA	deoxyribonucleic acid
DPR	dipeptide repeat protein
DSHB	Developmental Studies Hybridoma Bank
EDTA	ethylenediaminetetraacetic acid
eGFP	enhanced green fluorescent protein
EGTA	ethylene glycol-bis(β-aminoethyl ether)-N,N,N′,N′-tetra acetic acid
EJP	excitatory junction potential
EMS	ethyl methane sulfonate

EPSP	excitatory postsynaptic potential
ER	endoplasmic reticulum
ERRα	estrogen-related receptor alpha
FALS	familial amyotrophic lateral sclerosis
FDA	food and drug administration
FTLD	frontotemporal lobar degeneration
FUS/TLS	fused in sarcoma/translocated in sarcoma
GAPDH	Glyceraldehyde 3-phosphate dehydrogenase
GFP	green fluorescent protein
GluR	glutamate receptor
GRR	glycine rich region
GUK	guanylate kinase
HD	Huntington’s disease
HDAC4/6	histone deacetylase 4/6
HEPES	4-(2-hydroxyethyl)-1-piperazineethanesulfonic acid
HL-3	hemolymph-like solution
hnRNP	heterogeneous nuclear ribonucleoprotein
HRP	horseradish peroxidase
hTDP-43	human TAR DNA-binding protein 43
IBM	inclusion body myositis
iPSC	induced pluripotent cell

ISN	intersegmental nerve root
LMN	lower motor neuron
MADD	MAP kinase-activating death domain
MAGUK	membrane-associated guanylate kinase
Mef2	myocyte enhancer factor 2
miRNA	microRNA
NES	nuclear export signal
NGS	normal goat serum
NLS	nuclear localisation signal
NMDA	N-methyl-D-aspartate
NMJ	neuromuscular junction
NRF1	nuclear respiratory factor
PBS	phosphate buffer saline
PCR	polymerase chain reaction
PD	Parkinson disease
PDZ	postsynaptic density protein/Drosophila disc large tumour suppressor/zonula occludens-1
PFA	paraformaldehyde
PGC-1α	peroxisome proliferator-activated receptor-gamma coactivator 1 alpha
PNS	peripheral nervous system

POLDIP3/SK	polymerase delta-interacting protein 3
AR	
PSD	postsynaptic density
RAN	repeat-associated non-ATG
RBP	RNA binding protein
RGG	Arg-Gly-Gly repeat region
RISC	RNA-induced silencing complex
RNA	ribonucleic acid
RNAi	RNA interference
ROS	reactive oxygen species
rpl11	ribosomal protein L11 gene
RRM	RNA recognition motive
RT	room temperature
SALS	sporadic amyotrophic lateral sclerosis
SC	satellite cell
SDS	sodium dodecyl sulphate
SEM	standard error of the mean
SH3	Src homology 3
siRNA	silencing RNA
SN	segmental nerve root
SNP	single-nucleotide polymorphism

SOD	superoxide dismutase
SORT1	sortilin 1
SR protein	serine-arginine protein
SSR	subsynaptic reticulum
STAG2	cohesin subunit SA-2 gene
TAR	trans-activation response element
TARGET	temporal and regional gene expression targeting
TBPH	TAR DNA-binding protein-43 homolog
TDP-43	TAR DNA-binding protein 43
TEMED	tetramethyl ethylenediamine
TN	transverse nerve
Tris	tris(hydroxymethyl)aminomethane
UAS	upstream activation sequence
UMN	upper motor neuron
UTR	untranslated region
VDRC	Vienna Drosophila Resource Center
ZNF	zinc finger motif

1. INTRODUCTION

1.1. Amyotrophic Lateral Sclerosis

Amyotrophic lateral sclerosis (ALS), also known as Lou Gherig or Charcot disease, is a fatal neurodegenerative disease with rapid progression. The incidence is 1 in 100,000 people and the prevalence of 6 – 8 in 100,000 people per year (Pasinelli and Brown, 2006; Shaw et al., 2001).

With rare exceptions, the onset of ALS occurs at the age of 45 – 60 years, with higher prevalence in men. However, some reports indicate similar prevalence between the genders (Worms, 2001; Zoccolella et al., 2008).

1.1.1. The symptoms and stages of the disease

The disease mainly affects upper and lower motoneurons. Its progress is divided into three stages. In the early stage, symptoms are usually limited to one body region. The initial symptoms depend on the onset of the disease. There are two types of onset: limb onset, where lower motoneurons (LMN) are affected, and bulbar onset, where upper motoneurons (UMN) are degenerated first (Figure 1). Patients with the limb onset first notice changes in lower or upper limbs. Their muscles are weak and soft or stiff, tight and spastic, often presenting cramping and twitching. Patients feel fatigued, poor balance, weak grip, and tripping. Patients with the bulbar onset experience dysarthria of speech. In rare cases, dysphagia occurs before speech problems (Wijesekera and Leigh, 2009).

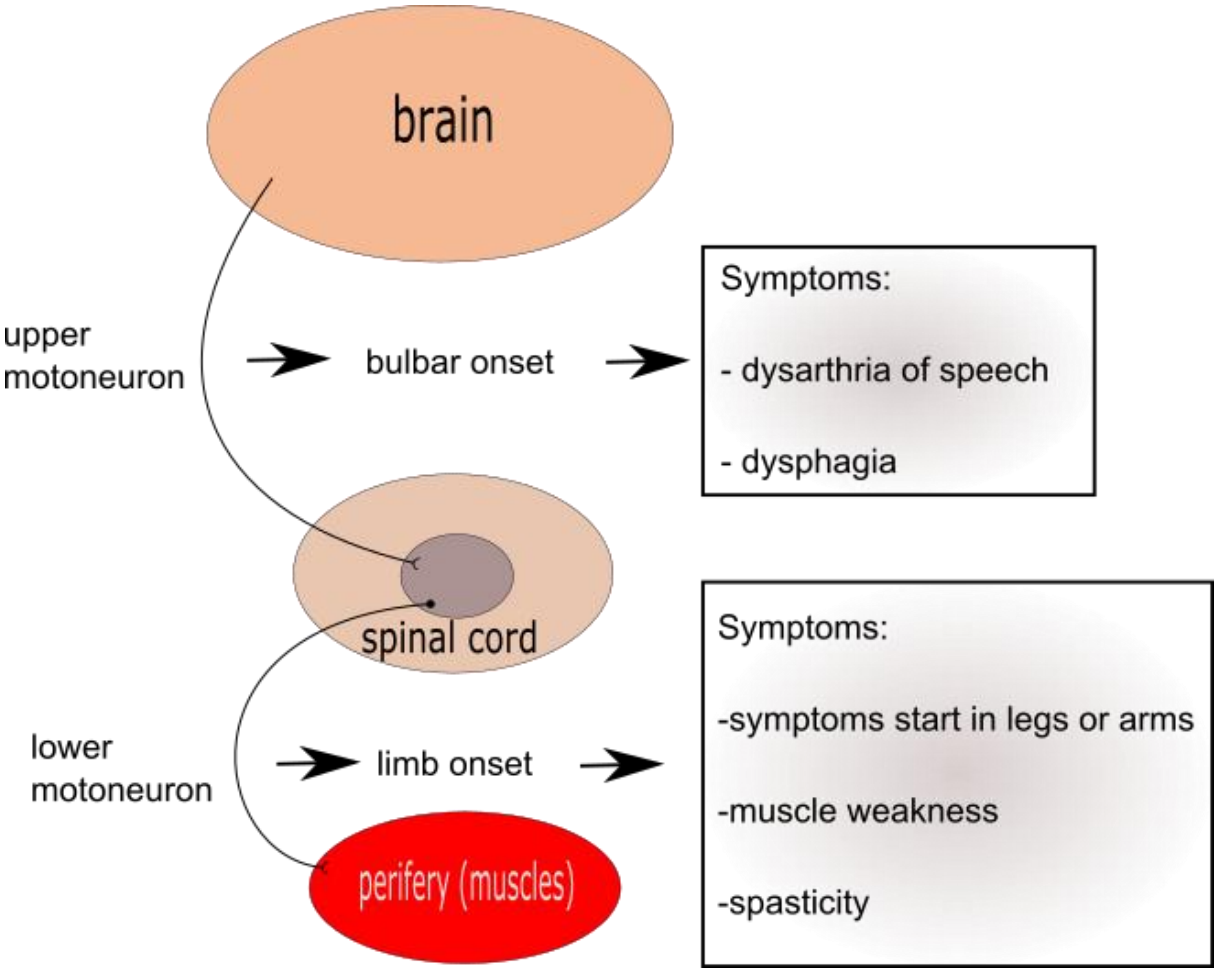

Figure 1: Two onsets of the disease. Patients can experience different early symptoms of ALS, depending on the onset.

During the middle stage, the symptoms spread to other parts of the body. Muscles can be either paralysed, weakened, or unaffected. Patients experience stiff, painful, and sometimes deformed joints, difficulties in eating, respiratory insufficiency, and some of them may be uncontrollably and inappropriately laughing or crying (pseudobulbar symptoms).

Finally, in the late stage, most voluntary muscles are paralysed. Breathing muscles are more and more affected. Patients are incapable of moving. Breathing is hard. Speech, eating, and drinking are barely possible.

Eventually, most ALS patients die of respiratory failure (Vijayakumar et al., 2019).

The involuntary nervous system, sensory nerves, and cognitive function are, in most cases, preserved and unaffected. Even though, some people with sporadic cases can suffer from dementia or cognitive dysfunction (Phukan et al., 2007; Strong and Yang, 2011). The involvement of cognitive dysfunction has been poorly investigated and probably underestimated. The biggest problem is a difficult diagnosis (Strong and Yang, 2011).

1.1.2. The pathogenesis of ALS

ALS is classified into two major groups: familial ALS (FALS) and sporadic ALS (SALS). 90% of all patients diagnosed with ALS have SALS. The remaining 10% suffer from FALS, which is caused by the inheritance of an autosomal dominant mutation.

Since 1990, pieces of the research described up to 30 mutated genes that cause ALS. However, mutations are present just in 66% of patients with FALS and approximately 15% of patients with SALS. The most frequent are mutations of *c9orf72* (23% of FALS mutations and 3% of SALS mutations), *sod1* (19% of FALS mutations and 1% of SALS mutations), *fus* (3% of FALS mutations and 0,4% of SALS mutations), and *tdp-43* (3% of

FALS mutations and 0,5% of SALS mutations) genes (van Es et al., 2017; Vijayakumar et al., 2019; Zou et al., 2017) (Figure 2).

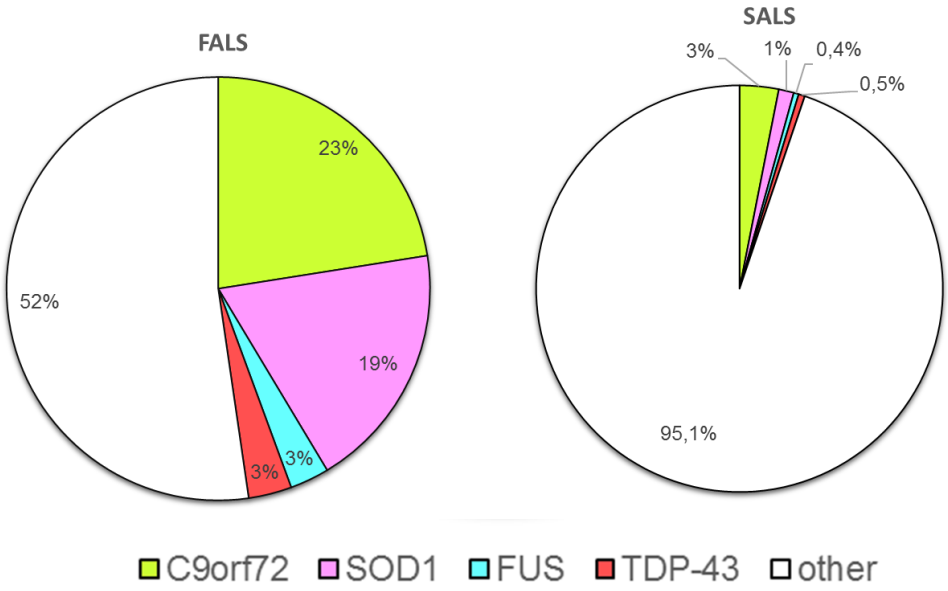

Figure 2: Proteins carrying the mutations in patients diagnosed with FALS and SALS, and their frequencies (Zou et al., 2017).

- ***C9orf72* mutations**

C9orf72 is a gene coding for C9 protein. The role of the protein in the cells is not entirely known. There are some evidence that show one of the two isoforms of the C9 protein being involved in autophagy, endosomal trafficking, modulation of actin dynamics, immune pathway regulation, and glutamate signalling (Fomin et al., 2018; O'Rourke et al., 2016; Sellier et al., 2016; Sivadasan et al., 2016; Webster et al., 2016).

In 2011, two research groups (DeJesus-Hernandez et al., 2011; Renton et al., 2011) discovered that the most common genetic cause of ALS was a hexanucleotide GGGGCC repeat expansion. The ALS-nonaffected

people have around 11 or less repeats, while ALS patients have from 700 to up to 1,600 repeats. The abnormality is linked to three different hypotheses of how the pathology is triggered.

The first one is a loss-of-function hypothesis. The expansion of the repeats can cause lower levels of transcription and consequently lower levels of the protein.

The second hypothesis describes a toxic gain of function of sense and antisense *c9orf72* repeat RNA. These RNAs form secondary structures (hairpins, G-quadruplexes, DNA-RNA heteroduplexes, RNA duplexes, and i-motifs), which sequestrate RNA-binding proteins, which are not available for other functions in the cell (Balendra and Isaacs, 2018).

Thirdly, repetitive RNAs can be transcribed in every reading frame and form five different dipeptide repeat proteins (DPRs) via a mechanism called repeat-associated non-ATG (RAN) translation (Zu et al., 2013). DPRs form neuronal cytoplasmic inclusions, which are hypothetically toxic for the neurons (Balendra and Isaacs, 2018).

- **Superoxide dismutase (SOD1, CuZnSOD) mutations**

Copper-zinc superoxide dismutase is an antioxidant enzyme located in the cytosol, nucleus, peroxisomes, and mitochondrial intermembrane space. It is a 32-kDa homodimer with one zinc- and one copper-binding site. Its

essential role is to catalyse disproportionation of superoxide into dioxygen (O_2) and hydrogen peroxide (H_2O_2) (Valentine et al., 2005).

The first mutation of the gene for SOD1 protein in FALS patients was observed in 1993 (Rosen et al., 1993). Up until now, more than 180 mutations have been recorded (Mathis et al., 2019). Different mutations cause difference in the severity of the disease: A4V mutated cases have a disease course of fewer than 12 months, while in cases with G93C or D90A mutations, the disease usually lasts more than five or even ten years. However, patients with *sod-1* gene mutation ALS show some common characteristics such as the earlier onset of the disease and legs are predominantly affected (Andersen et al., 1997; Corcia et al., 2012). However, it is debatable whether all mutations express as ALS (Mathis et al., 2019).

Several mechanisms have been proposed to describe how SOD1 mutations can affect neuronal cells and trigger ALS. In SOD1 mutant mice (transgenic model of ALS), the excessive glutamate release was found, which caused excitotoxicity (Milanese et al., 2011). Moreover, loss of glutamate receptors GluR2 increase the influx of Ca^{2+}, which is also toxic for the cell (Van Damme et al., 2007).

The next mechanism proposed is increased oxidative stress. SOD1 functions typically as an antioxidative enzyme. However, oxidative stress

is not the consequence of a lack of enzymatic activity. Mutated SOD1 increases the production of reactive oxygen species (ROS) and consequently promotes oxidative stress (Harraz et al., 2008).

Furthermore, it has been found that endoplasmic reticulum (ER) stress can contribute to the loss of neurons in mice with mutated SOD1 protein (Saxena et al., 2009). SOD1 mutant mice also show mitochondria dysfunction. By releasing cytochrome C, the neuronal cell undergoes the apoptosis (Hayashi et al., 2016).

Three more mechanisms have been recently mentioned. These are axonal transport disruption, prion-like propagation, and non-cell autonomous toxicity of neuroglia. Recent pieces of evidence also suggest that misfolded wildtype SOD1 protein promotes ALS in sporadic cases (Hayashi et al., 2016).

- **Fused in sarcoma / translated in liposarcoma (FUS/TLS or FUS) mutations**

FUS / TLS is a DNA / RNA ribonucleic binding protein that plays a role in the maintenance of dendritic integrity and neuronal plasticity (Fujii and Takumi, 2005; Fujii et al., 2005). It is involved in processes such as RNA biogenesis, regulation of transcription by binding to the chromatin, immediate response to DNA damage, embryogenesis, and transcription of basal levels manganese *sod* gene (Mathis et al., 2019).

FUS-positive and TDP-43-positive inclusions have been found in both, sporadic and familial ALS patients, and represent a hallmark of the disease. The accumulation of the aggregates in the cytoplasm reduces the levels of FUS in the nucleus, and consequently, one can obtain loss of function of FUS (Ishigaki and Sobue, 2018). Studies have shown several mutations of FUS protein in the patients (

Figure 3). Some of them are used to replicate ALS symptoms in animal models (Shang and Huang, 2016).

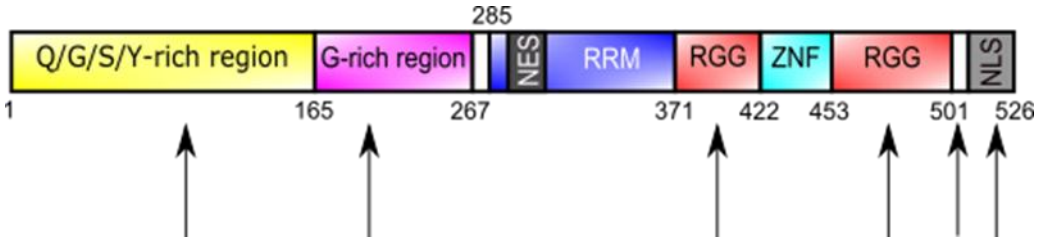

Figure 3: Regions of FUS where mutations were found (marked with arrows) in ALS patients. NES = nuclear export signal, RRM = RNA recognition motif, RGG = Arg-Gly-Gly repeat region, ZNF = zinc-finger motif, NLS = nuclear localisation signal

- **Other causes**

Most of ALS cases do not possess any mutations. It is predicted that environmental exposure (epigenetic modification, viral infections) can have a contribution to the development of the disease.

One cannot exclude the combination of different parameters. However, all changes lead to cellular dysfunctions of motor neurons and surrounding cells. The most common defects are abnormal protein aggregations, which became a synonym for ALS. Furthermore, dysregulation of RNA processing, secretion of neurotoxic vesicles from astrocyte and muscles, glutamate excitotoxicity and mitochondrial disorganisation and dysfunction can be observed in an affected organism. Consequently, all the pathological changes lead to motor neuron death (Vijayakumar et al., 2019) (Figure 4).

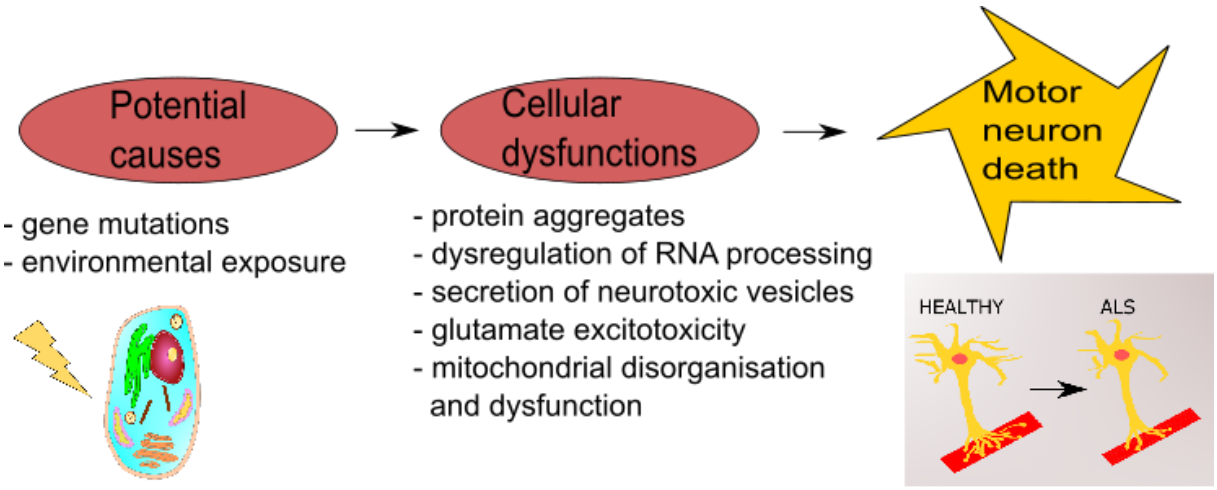

Figure 4: Potential factors that could lead to motor neuron death – the main characteristic of ALS. Gene mutations and environment could contribute to cellular dysfunctions, which cause cell death (The image modified by *(Vijayakumar et al., 2019)*).

1.1.3. The diagnosis of ALS

El Escorial World Federation of Neurology set the criteria for the diagnosis of ALS (Brooks et al., 2000). The diagnosis of ALS requires the presence of LMN degeneration, confirmed by clinical, electrophysiological or neuropathological examination, or clinical examination evidence of UMN degeneration, or progressive spread of symptoms within a region or to other regions, proved by history or examination. Furthermore, the diagnosis also requires the absence of other disease confirmed by electrophysiological, pathological indications, and neuroimaging (Brooks et al., 2000).

First, patients are clinically examined. Depending on the presence of LMN or UMN signs, they are classified into 5 different groups: clinically definite ALS, clinically probable ALS, clinically probable ALS – laboratory-supported ALS, clinically possible ALS, and clinically suspected ALS (Brooks et al., 2000).

After clinical examination, several studies should be done in order to define the diagnosis more precisely (Wijesekera and Leigh, 2009). To begin with, patients with the diagnosis of ALS should undergo electrophysiological studies to confirm LMN dysfunction in clinically affected regions, to detect electrophysiological evidence of LMN dysfunction in clinically uninvolved regions, and to exclude other

pathophysiological processes (Brooks et al., 2000). The studies performed are nerve conduction studies, conventional electromyography, transcranial magnetic stimulation and central motor conduction studies, as well as quantitative electromyography (Wijesekera and Leigh, 2009).

Another type of studies is neuroimaging studies. The primary purpose of these studies is to exclude the presence of structural lesions, which resemble ALS and can be treated. However, patients diagnosed with clinically definite ALS with bulbar or pseudobulbar involvement do not undergo these studies (Brooks et al., 2000).

Moreover, other examinations can be done, but are not essential. They include muscle biopsy, levels of muscle enzymes (serum creatine kinase), levels of serum creatinine, bicarbonate levels, and elevation of cerebrospinal fluid (CSF) protein (Brooks et al., 2000; Wijesekera and Leigh, 2009).

1.1.4. The treatment and management of ALS

There is no cure for ALS. The only drugs available are riluzole (2-amino-trifluoromethoxybenzotiazole) (Figure 5) and edaravone. Riluzole prevents the release of glutamate by blocking sodium channels. Though it slows down the progression of the disease, it does not cure it completely (Rowland and Shneider, 2001).

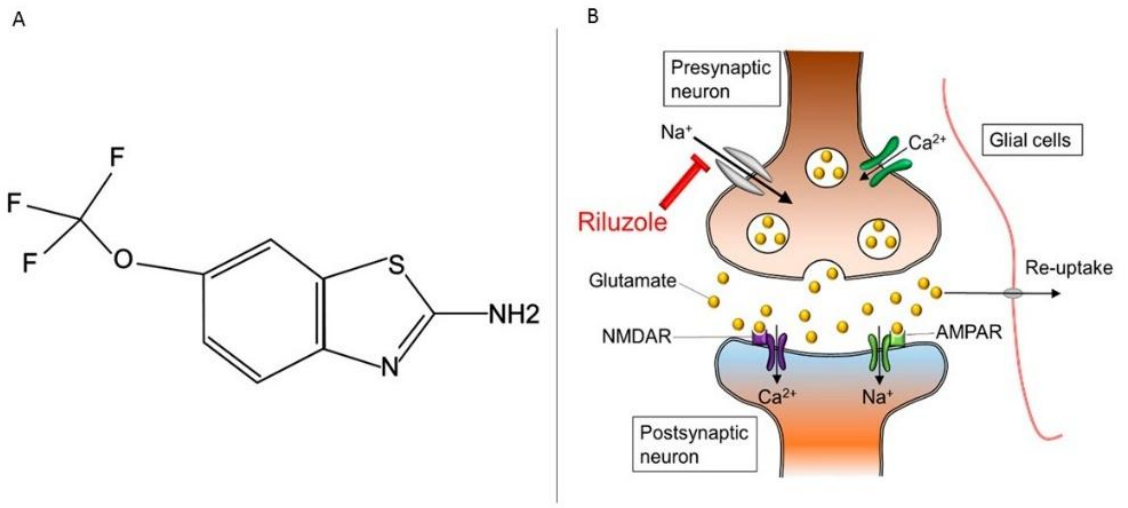

Figure 5: The structure and the mechanism of riluzole. A) The chemical structure of riluzole. B) Riluzole acts neuroprotective. It blocks the influx of sodium ions and prevents the release of glutamate. It also increases the reuptake of glutamate in glial cells. It is adapted from http://www.mdpi.com/1420-3049/20/5/7775/htm.

Edaravone was approved in May 2017 after six months of clinical studies by the FDA. It is a potent antioxidant and reduces the oxidative stress in neurons. It slows down the progression of the ALS in patients (Bhandari et al., 2018; Traynor, 2017). However, it is licensed just in Japan and under considerations in the USA (Ng et al., 2017).

Many of the symptoms arising during the development of the disease can be cured, and so the quality of patients' life can be improved (Table 1).

Table 1: The list of symptoms and symptomatic treatments (Andersen et al., 2005; Ng et al., 2017).

symptom	drugs	other treatments
pain	• non-steroidal anti-inflammatory drugs • opioids (later stages)	-
cramps	• quinine sulphate • alternatives: Mg^{2+}, carbamazepine, phenytoin, verapamil, gabapentin	• physiotherapy • physical exercise • hydrotherapy
spasticity	• baclofen • tizanidine • dantrolene • gabapentin • memantine • botulinum toxin type a	• physiotherapy • hydrotherapy in heated pools
depression	• amitriptyline • selective serotonin reuptake inhibitor	• psychological support
insomnia	• amitriptyline • zolpidem • diphenhydramine	• comfort
anxiety	• bupropion • diazepam or lorazepam	• psychological support
sialorrhea	• amitriptyline • atropine • hyoscine • glycopyrrolate	• the mechanical home suction device • irradiation of the salivary glands

bronchial secretions	• n-acetylcysteine • propranolol • metoprolol	• assisted cough insufflator – exsufflator • home suction device
pseudobulbar emotional lability	• Only if necessary! • amitriptyline • fluvoxamine • citalopram	-

Apart from symptomatic drug treatments, ALS patients also require ventilatory and nutritional management (Wijesekera and Leigh, 2009). Patients with ALS usually suffer from dysphagia. Difficulty in swallowing is common. They choke and cough. The problems arise with time, and the most common result is weight loss, which additionally promotes muscle loss (Reich-Slotky et al., 2013). It has been recommended that when the patient loses 10% of their weight, they should undergo gastrostomy, to enable feeding and drug intake (Stavroulakis et al., 2016).

Gradually with time, patients develop difficulties in breathing. Therefore, non-invasive ventilation is recommended (van Es et al., 2017). With a randomised controlled trial with patients who have ALS without severe bulbar dysfunction, non-invasive ventilation improved survival with an improvement in the quality of life. The survival benefit with this type of management was much higher than with currently available neuroprotective therapy (Bourke et al., 2006).

1.1.5. Role of the muscles in ALS

For a long time, ALS was considered a motor neuron degradation disease. With time, it has been shown that the surrounding tissue may also contribute to the progression of the disease (Tsitkanou et al., 2016). It has been proposed that the degeneration starts in the neuromuscular junction. One of the hypothesis was that muscles could contribute to retrograde signalling and consequently, to the degeneration of motor neurons (Moloney et al., 2014). Mechanisms responsible for maintaining healthy skeletal muscle mass and functions are disturbed in ALS. Three main processes are satellite cell (SC) activity, mitochondrial biogenesis, and miRNA regulation (Tsitkanou et al., 2016).

Satellite cells are responsible for muscle regeneration and reside under the basal lamina of muscle fibres (Ehrhardt and Morgan, 2005; Pradat et al., 2011). Manzano et al. checked the SCs activity during the progress of ALS in SOD1 mutant mice (Manzano et al., 2013). The difference in the number of SC and their activation depends on the stage of disease and muscle fibre type. In the early presymptomatic stage, 40 days of age (post-natal 40 (p40)), the number of SCs is reduced in both fibre types (slow and fast). In the late presymptomatic stage (p60), the number of SCs in slow muscle fibres is increased, and the number is unchanged in fast muscle fibres comparing to the wildtype control. In the symptomatic stage (p90),

the number of SCs in slow fibres is decreased, and on the contrary, in fast fibres, the number of SCs increased. Finally, at the end stage (p120), the SC count resembled the observations in the p60 stage. Every measurement was controlled with wildtype mouse muscle fibres. In terms of activation, in p90, SCs were more active in both fibre types than in the wild type control, but at the p120 stage, the activation was unchanged in comparison with the wildtype control (Manzano et al., 2012, 2013; Tsitkanou et al., 2016). The hypothesis of increased activity and the number of SCs describes the attempt of muscles to repair the damage caused by mitochondrial dysfunction, oxidative stress, protein aggregation and denervation (Manzano et al., 2013; Tsitkanou et al., 2016). However, there was no difference in the number of SCs in ALS patients, yet their activity was reduced compared to healthy age-matched control (Pradat et al., 2011).

The second feature observed in ALS mouse models and patients is mitochondrial dysfunction and along with that also oxidative stress. Defects in morphology and biochemical properties of mitochondria were found in both familial and sporadic ALS cases (Zhou et al., 2019). Muscle samples and $SOD1^{G93A}$ ALS mouse model show significantly reduced levels of mRNA and protein peroxisome proliferator-activated receptor-γ coactivator-1α (PGC-1α), which is responsible for mitochondrial

biogenesis and enhances mitochondrial function (Russell et al., 2013; Tsitkanou et al., 2016). What is more, several effectors of mitochondrial function (nuclear respiratory factor (NRF-1), estrogen-related receptor α (ERRα) and cyclooxygenase subunit IV (COX IV)) downstream of PGC-1α, are downregulated in ALS patients (Russell et al., 2013). The downregulation of the proteins causes defective mitochondrial respiratory chain complex and elevates oxidative stress (Zhou et al., 2019).

The third observed change in ALS patients and ALS mouse models is connected to microRNA (miRNA) expression and their regulation of other processes in skeletal muscles such as regulation of myogenesis, mitochondrial biogenesis and NMJ innervation (Tsitkanou et al., 2016). miRNAs are essential for the regulation of protein expression. Either they participate in post-transcriptional modification or bind directly to target mRNA and enhance its stability or degradation (Di Pietro et al., 2018). The primary miRNAs found in muscles are miR-1, miR-133a, miR-133b, miR-206, miR-208a, miR-208b, miR-499, and miR-486 (Nie et al., 2015). However, only miR-206 was consistently upregulated in the $SOD1^{G93A}$ mouse model (Williams et al., 2009) and ALS patients (Toivonen et al., 2014). miR-206 suppresses muscular histone deacetylase 4 (HDAC4) protein levels (Williams et al., 2009). It has been proposed as a prominent marker for ALS (Di Pietro et al., 2018; Toivonen et al., 2014).

1.2. TDP-43

TAR DNA binding protein 43 (TDP-43) belongs to the family of heterogeneous ribonucleoprotein (hnRNP). It is very well conserved among different species such as *Rattus norvegicus*, *Mus musculus*, *Drosophila melanogaster*, *Xenopus laevis* or *Caenorhabditis elegans* (Ayala et al., 2005; Wang et al., 2004). High level of sequence conservation suggests that TDP-43 may play an essential role in the regulation of fundamental cellular mechanisms. Apart from the brain, TDP-43 is also present in other tissues such as muscles, heart, pancreas, spleen, testis, ovary, lung, placenta, and kidney (Buratti & Baralle, 2001). In physiological conditions, the protein predominantly localises in the cell nucleus. However, it can also be found in the cytoplasm, because it can shuttle between the nucleus and cytoplasm (Ayala et al., 2008b).

Even though the *tdp-43* gene may be transcribed in eleven different isoforms, results of western blots and immunoprecipitation from a variety of human tissues and cell lines show only one major protein of 43 kDa (Wang et al., 2004). Complex post-translational modifications such as hyperphosphorylation, abnormal ubiquitination or protein cleavages were described in pathological conditions indicating that these alterations may

affect TDP-43 metabolism or function (Arai et al., 2006; Buratti et al., 2001; Neumann et al., 2006).

1.2.1. TDP-43 structure

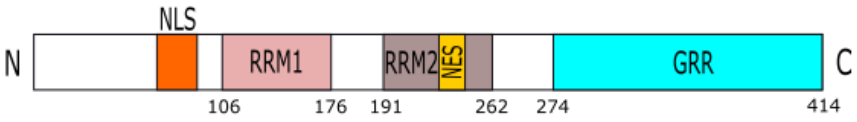

Figure 6: The main parts of the TDP-43 protein. NLS = nuclear localisation sequence, RRM1 and RRM2 = RNA recognition motive 1 and 2, NES = nuclear export sequence and GRR = glycine-rich region. (customised by (Cohen et al., 2011))

The N-terminal part of the protein contains two highly conserved RNA Recognition Motifs RRM1 and RRM2. It also has a nuclear localisation signal (from residue 82 to 98) and a nuclear export signal, which is located at the end of the RRM2 domain (Cohen et al., 2011). The C-terminal domain consists of a glycine-rich area and a low complexity region that is more variable among species (Figure 6) (Buratti & Baralle, 2008).

RRMs domains of TDP-43 are essential for RNA-protein interactions and are highly conserved domains. The amino acid identity of RRM domains is 79% between human and Drosophila's ortholog (Ayala et al. 2005). It was demonstrated that they could bind single-stranded TG nucleotide stretches with high-affinity (Buratti & Baralle, 2001). The RRM1 domain is the only one necessary and sufficient for the binding of the protein to its target. Moreover, it was demonstrated that two point mutations, leading to

corresponding changes in the amino acid sequence (from Phenylalanine to Leucine in position 147 and from Phenylalanine to Leucine in position 149, F147L and F149L) in the RRM1 region, prevented the interaction of the protein with its target RNA (the same construct is also available in *Drosophila melanogaster*, called $TBPH^{F/L}$). On the contrary, similar mutations or complete deletion of the RRM2 domain did not affect the functionality of the protein (Buratti et al., 2001).

The C-terminal part of the protein is, as mentioned above, less conserved. It contains a glycine-rich region, which is responsible for protein-protein interactions. The most common interactions are with other proteins of the hnRNP family, especially hnRNP A2/B1 and hnRNP A1 (Buratti et al., 2005; D'Ambrogio et al., 2009). It was found that 2 – 3% of ALS patients carry specific missense mutations in this region (Banks et al., 2008; Sreedharan et al., 2008; Van Deerlin et al., 2008).

1.2.2. TDP-43 function

TDP-43 has many roles. It interacts with RNAs, DNA, and some proteins. It is mainly involved in RNA metabolism, which includes RNA transcription, RNA splicing, mRNA transport and stability, stress granules formation and microRNA processing (Figure 7) (Budini et al., 2017).

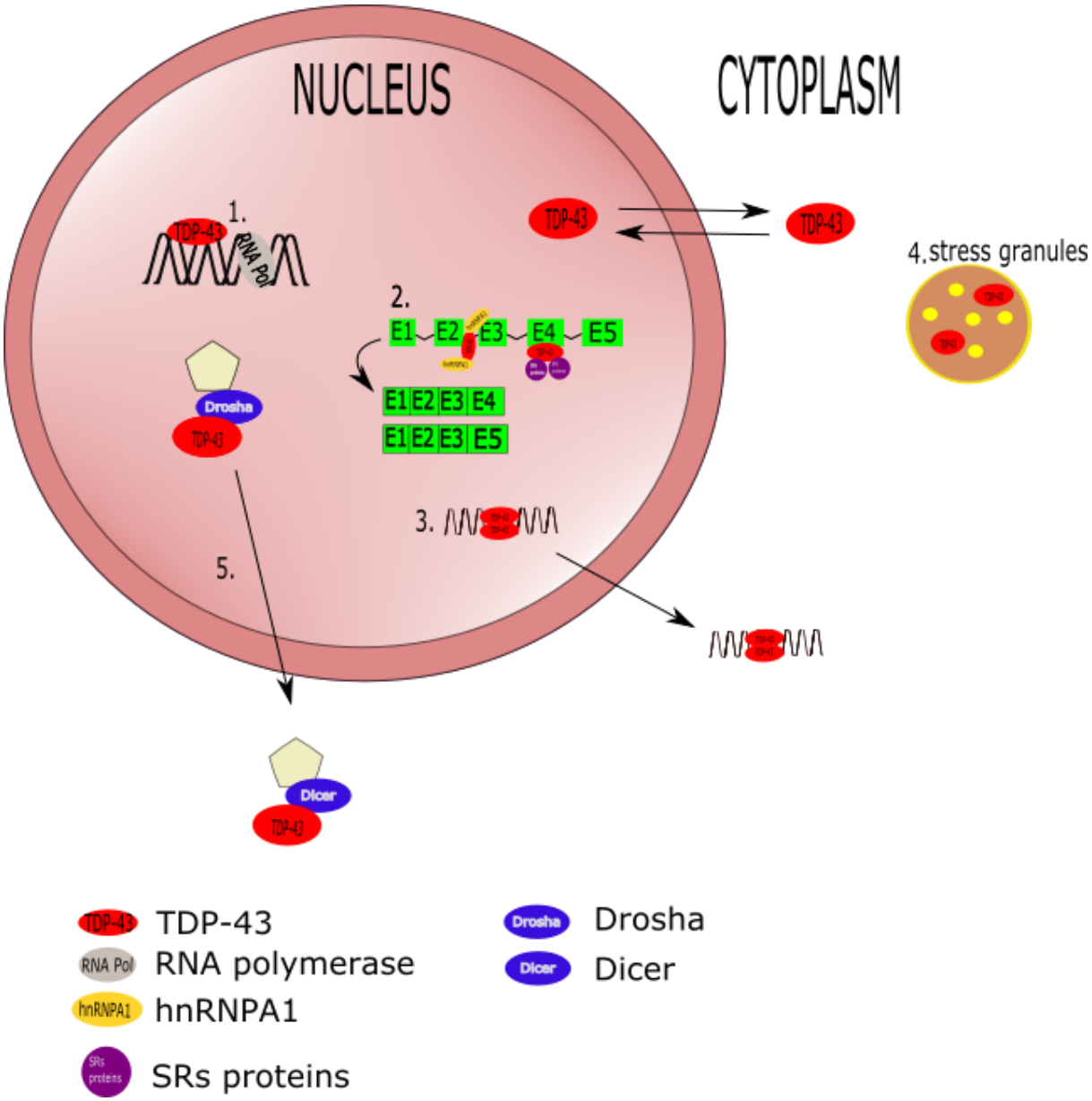

Figure 7: TDP-43 functions in the cell. 1) TDP-43 binds directly to the promoter regions and regulates the transcription. 2) TDP-43 is involved in the alternative splicing by binding to introns or exons and recruiting specific proteins. 3) TDP-43 stabilises mRNA and is involved in the transport. 4) TDP-43 controls the assembly of stress granules. 5) TDP-43 binds to Drosha and Dicer, and controls microRNA processing (customised by *(Budini et al., 2017)*).

- **Transcription and Pre-mRNA splicing**

TDP-43 directly binds to multiple promotor regions and regulates the transcription of the corresponding genes. However, the most known role of TDP-43 is alternative splicing. TDP-43 binds to introns or exons and recruits other hnRNP proteins, preferably hnRNPA1 (heterogeneous nuclear ribonucleoproteins) and serine-arginine proteins (SRs proteins) (Budini et al., 2017). The first record of TDP-43 regulation of pre-mRNA splicing was in connection to exon 9 in the CFTR gene. This gene plays a crucial role in the development of cystic fibrosis. However, it is highly unlikely that the regulation of this particular gene is involved in neuronal metabolism (Buratti et al., 2001; Ratti and Buratti, 2016). Over time, there were more direct targets identified, such as POLDIP3/SKAR (Fiesel et al., 2012; Shiga et al., 2012), SORT1 (Prudencio et al., 2012), STAG2 and MADD (De Conti et al., 2015).

Moreover, TDP-43 autoregulates its splicing by binding to its 3'UTR region. This autoregulation is fundamental to keep protein levels within a physiological range (Ayala et al., 2011; Ratti and Buratti).

- **mRNA stability and transport**

TDP-43 is mainly present in the nucleus, but it also shuttles to the cytoplasm where it exerts an essential role in mRNA regulation, particularly in controlling mRNA stability. TDP-43 interacts with the 3'UTR

region of mRNAs, and so influences their half-life either positively or negatively (Colombrita et al., 2012; Gerstberger et al., 2014; Sephton et al., 2011). Loss of function of TDP-43 may affect levels of mRNA or their products and consequently, have adverse effects on neuronal viability (Ratti and Buratti, 2016).

TDP-43 interacts with mRNAs, and together they form ribonucleoprotein granules, which transport the mRNA to the most peripheral parts of the cells, such as axons and dendrites (Prasad et al., 2019). The mRNA transport in neurons is crucial to maintain neuronal activity and synaptic plasticity (Swanger and Bassell, 2011). It has been shown that TDP-43 is actively transported along the axons and colocalises with other transport RBPs in RNA granules (Fallini et al., 2012).

Moreover, mRNAs encoding for proteins involved in synaptic function bind directly to TDP-43 (Narayanan et al., 2013). The impairment of mRNA transport in neurons and TDP-43 loss of function can be one of the reasons for neuronal loss. TDP-43 seems to be essential for synapses' formation, which is impaired in ALS patients (Alami et al., 2014).

- **TDP-43 and stress granules**

Stress granules form upon exposed stress and act like sorting stations for mRNAs. They determine whether mRNA will be either translated, sequestrated, or degraded. The involvement of TDP-43 in the regulation

of stress granules depends on cell and stressor type. Stress granule assembly is affected when TDP-43 is either overexpressed or knocked down. In the first case, stress granules are more prominent and form faster, while in the second case, stress granules assembly is delayed (Dewey et al., 2012).

- **miRNA processing**

TDP-43 was found in Drosha complex together with FUS/TLS (Gregory et al., 2004). This is in agreement with the hypothesis that TDP-43 could be involved in miRNA processing. Several reports describe the dysregulation of multiple miRNAs when TDP-43 is depleted (Ratti and Buratti, 2016). Furthermore, some reports claim that TDP-43 stabilises the Drosha protein during neuronal differentiation (Di Carlo et al., 2013). However, overall, the contribution of TDP-43 to the regulation of miRNAs and how that contributes to the diseases remain unknown.

1.2.3. TDP-43 and muscles

TDP-43 is ubiquitously expressed in the organism. It can be found in muscles. In cells C2C12 (Vogler et al., 2018) and Drosophila muscles (Diaper et al., 2013), TDP-43 is predominantly localised in the nucleus. In the study in 2018, Vogler (Vogler et al., 2018) discovered that TDP-43 forms amyloid-like myo-granules (amyloids are long fibres made up of building blocks of the misfolded disease proteins arranged in a highly

organised manner (Becker and Gitler, 2018)) that are located in the cytoplasm during the muscle recovery after an injury. Granules are also involved in the regulation of healthy skeletal muscle formation. Moreover, his group proved that TDP-43 binds to the exons of mature sarcomere mRNAs and localises them to newly forming sarcomeres.

Another role of TDP-43 in muscles that has recently been observed is involved in the metabolism of glucose. Over-expression of TDP-43 can lead to significant weight gain, increased fat deposition, adipocyte hypertrophy, and abnormal insulin-mediated Glut4 translocation in skeletal muscle in A315T TDP-43 mutant mice (Stallings et al., 2013). The supporting hypothesis proposes the regulation of Tbc1b1, which has already been linked to human familial obesity (Chiang et al., 2010; Stallings et al., 2013).

In 2014, additional TDP-43 function in muscles was discovered (King et al., 2014). As described above, consistent downregulation of miR-206 was reported in the muscles of ALS mouse models and ALS patients (Williams et al., 2009). Targeted deletion of miR-206 prevents efficient reinnervation of the neuromuscular junction after an injury. The cause of inefficient regeneration is upregulation of histone deacetylase 4 (HDAC4) (Bruneteau et al., 2013; Williams et al., 2009). King et al. (King et al., 2014)

proposed a mechanism in which TDP-43 negatively regulates miR-206 by preventing the bound miRNAs to the RISC complex (King et al., 2014).

In 2018, Cykowski et al. (Cykowski et al., 2018) showed that phosphorylated TDP-43 aggregates can be found in muscles of SALS and FALS patients. They tracked more aggregates in axial muscle group than in appendicular. Additionally, they reported colocalisation of pTDP-43 aggregates with the protein p62 and suggested the autophagic processes in muscles of ALS patients, which is also a characteristic of inclusion-body myositis (IBM).

1.3. TDP-43 and neurodegeneration

Neurodegenerative diseases include a large group of disorders. They are all characterised by a progressive loss of neurons and their dysfunction in both the central nervous system (CNS) and the peripheral nervous system (PNS). They tend to progress with aging. Among them, the most common are the Parkinson's disease (PD), Alzheimer's disease (AD), amyotrophic lateral sclerosis (ALS), frontotemporal lobar degeneration (FTLD), and Huntington's disease (HD) (Gao et al., 2018).

TDP-43 was linked to neurodegenerative diseases when found as a component of ubiquitin-positive protein inclusions in patients with ALS and frontotemporal lobar degeneration (FTLD) (Arai et al., 2006; Gao et al.,

2018; Neumann et al., 2006). Later on, there were reports about genetic mutations of TDP-43 in patients affected by these two disorders (Gao et al., 2018; Kabashi et al., 2008; Kwiatkowski et al., 2009; Vance et al., 2009).

1.3.1. TDP-43 pathology in ALS

The main characteristic observed in neurons from patients diagnosed with ALS is TDP-43 cytoplasmic inclusions. Analysis of these formations showed abnormal C-terminal fragments of TDP-43 that were ubiquitylated and phosphorylated (Mackenzie and Rademakers, 2008).

In most cases, TDP-43 was not mutated. Mutations were found just in 3 – 6% of all cases. Mutations were recorded mainly in the glycine-rich region and the C-terminal domain (Mackenzie and Rademakers, 2008).

Two hypotheses potentially explain the onset of the symptoms. The first one is centred on the loss of function of the protein. If TDP-43 is aggregated and trapped in the cytoplasm, it is not present in the nucleus where its primary function cannot be exerted (Budini et al., 2015; Feiguin et al., 2009) (Figure 8).

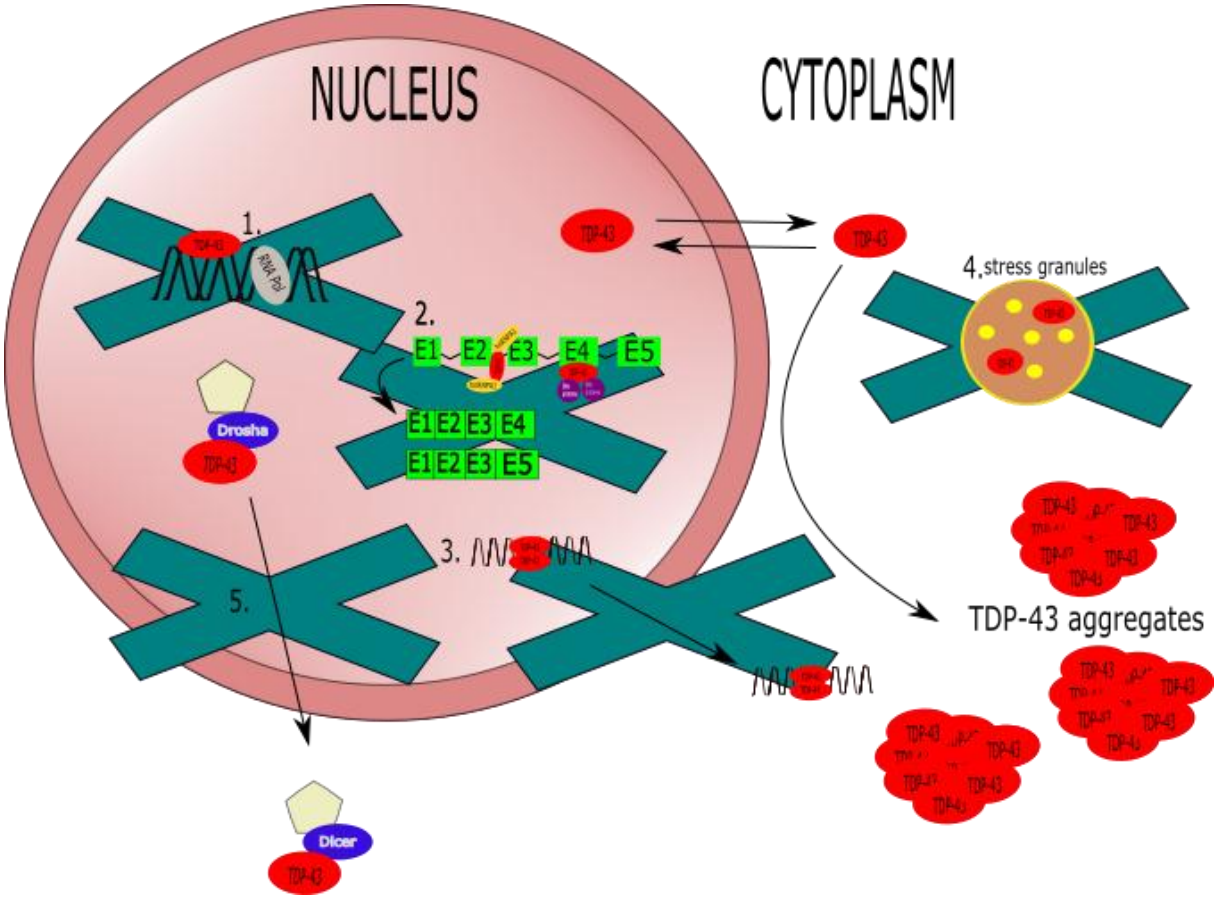

Figure 8: The main characteristic of ALS is TDP-43 cytoplasmatic aggregates. There are two hypotheses of how these aggregates affect cell function. Either TDP-43 aggregates prevent the protein from functioning, or the aggregates are toxic for the cell.

On the other hand, some studies support a gain-of-function hypothesis. These works show that TDP-43 inclusions are toxic and therefore cause cell death (Johnson et al., 2008, 2009; Zhang et al., 2009) (Figure 8).

1.4. TBPH: the ortholog of TDP-43 in Drosophila melanogaster

Human TDP-43 is highly conserved in *Drosophila melanogaster,* even though these two species are phylogenetically distant (Figure 9). The ortholog of TDP-43 in flies is called TBPH, and its gene is located on the second chromosome (2R: 19746589-19750104). There are six transcripts reported that code for six different protein isoforms by alternative splicing (Figure 10). However, western blot reports show only one protein of approximately 58 kDa (*www.flybase.org*).

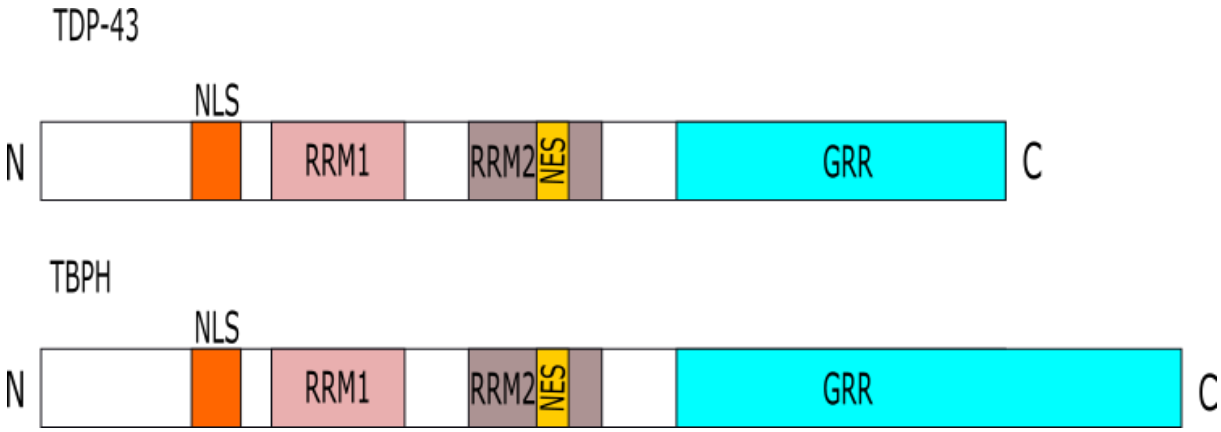

Figure 9: Comparison between human TDP-43 and TBPH. The difference between the two is mainly in C-terminal part. TBPH C-terminal is longer than the one of TDP-43. (The image is customized by (Romano et al. 2012).)

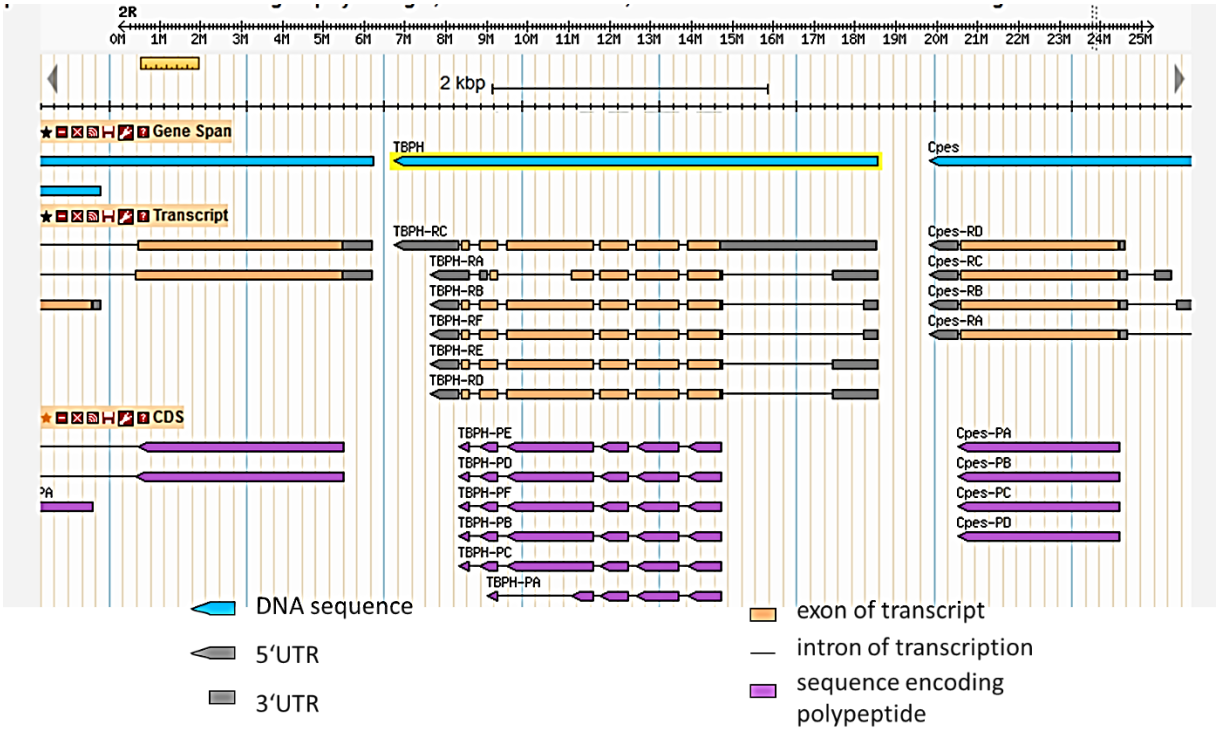

Figure 10: Chromosomal location of tbph gene (second chromosome), and representation of its transcripts and the relative coding sequence (CDS). It is adapted from www.flybase.org.

The overall homology between the fruit fly and the human proteins is 11.8%, while the identity is 34.4%. hTDP-43 and TBPH show higher conservation of the region that includes RRM1 and RRM2 than of the C-terminal region. RRM regions have 59% identity and 77% similarity, while C-terminus has 18% identity and 22% similarity (Figure 11) (Romano et al., 2012).

Figure 11: The parallel between human TDP-43 (upper line) and TBPH Drosophila amino acid sequence (bottom line). Amino acids, identical (*) or similar (:), between the two proteins are indicated. Red squares indicate the RNA recognition domains, RRM1 and RRM2. (Uniprot accession no. Q13148 and O97468 resp.)

The degree of conservation between human and Drosophila orthologs is not only at the level of the sequence but also includes functional properties (Ayala et al., 2011; Buratti et al., 2001). Both proteins have the same tendency to bind $(UG)_n$ rich region of RNA sequences (Ayala et al., 2005). Additionally, *in vivo* studies have confirmed that C-terminals of both proteins (TBPH and hTDP-43) can interact with the same nuclear partners

(hnRNPA2, hnRNPA1, hnRNPC, and hnRNPB1) (D'Ambrogio et al., 2009; Romano et al., 2012).

1.5. Drosophila melanogaster

Drosophila melanogaster is a Diptera and belongs to the family of *Drosophilidae*. The common name is a fruit fly or vinegar fly, and it is widely used as a model in biology. These insects were introduced to the laboratory by Thomas Hunt Morgan. He and his students were the first ones who identified the first genetic mutations in the early 1900s (Morgan, 1910). This studies and others set the basis of modern genetics.

1.5.1. Drosophila life cycle

The development of *Drosophila* depends on the temperature. At 25°C, the whole transformation from an egg to an adult fly takes 9 – 10 days (Figure 12).

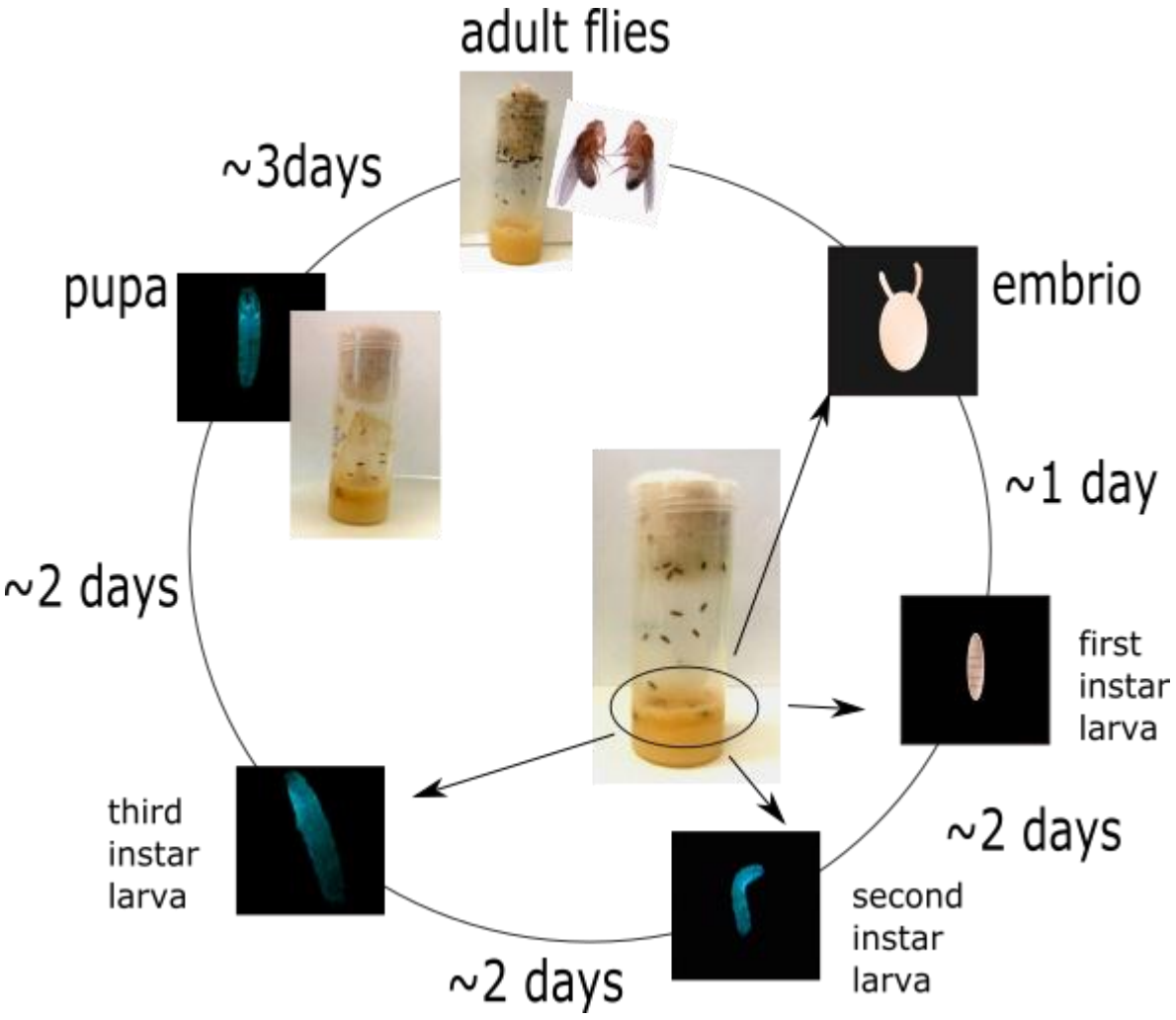

Figure 12: The Drosophila life cycle. Three different stages of larva follow the egg stage, and then larva eventually develops in a pupa and forms an adult fly. Customised by http://www.zoology.ubc.ca/~bio463/lecture_13.htm.

The embryogenesis in Drosophila starts with the deposition of eggs. 18 to 22 hours after egg laying embryos develop into first instar larvae, followed by the second and third stage, respectively occurring at 48 and 72 hours after laying eggs. The larvae then transform into pupae during the subsequent three to four days. After completion of the metamorphosis, the adult fly breaks the pupal shall case. Newly born flies have wings still

closed, and the body pigmentation is evident. A few hours later, the wings open and the body gets normal pigmentation. The females sexually mature approximately 12 hours after hatching. Wild-type *Drosophila* has red eyes, and the body is segmented with transversal black rings across the abdomen. Because of sexual dimorphism, male and female flies can be easily distinguishable. Male flies have a sex comb, a row of dark bristles on forelegs. Female flies have a long abdomen composed of seven segments pointed towards the anus. Males have a dark tip of the abdomen, and their body size is smaller than the one of females. They only have five segments (

Figure 13).

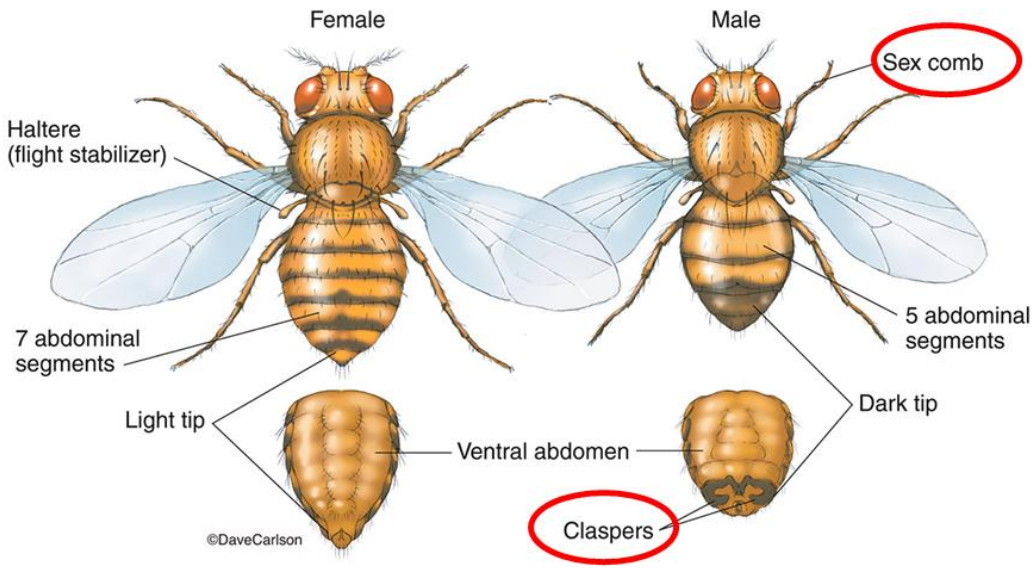

Figure 13: Female versus male Drosophila melanogaster. The two most identifiable features in males are claspers at the tip of the abdomen and sex comb at the front leg. Females are usually bigger and have a light tip of the abdomen.

1.5.2. Drosophila in biology

The use of cell lines in experimental biology is the easiest and cheapest approach, which can provide relevant information in multiple instances. However, cell lines are not always enough to explain complex processes in the context of an intact organism. Mammalian models offer several *in vivo* opportunities and extensive similarity to the human organism. The main disadvantage of this type of model is the time required to perform experiments. *Drosophila melanogaster*, on the contrary, is a model with relatively short generation time and many descendants in one single cycle. Drosophila also possesses a small annotated genome, with the absence of genetic redundancy. Moreover, their genetic is simpler. There are only four pairs of chromosomes and 12,000 genes (humans have 23 pairs of chromosomes and 25,000 genes) (Johnston, 2002).

Even though the number of chromosomes and genes is significantly lower than in humans, the conservation with vertebrates is very high. Approximately 75% of the human genes involved in diseases have *Drosophila* ortholog (Fortini et al., 2000). This fact allows the research of complex mechanisms behind human pathologies like neurological

disorders, cancer, metabolic diseases, cardiovascular diseases, and immune system deficits (Bier, 2005).

In neurobiology, the nervous system of *Drosophila* (~200,000 neurons) is simpler than the human brain (1 billion neurons). Flies can perform complex motor behaviours such as flying, climbing, and walking (Ambegaokar et al., 2010). The fly's brain is organised into different areas that perform specialised functions and includes zones for learning, memory, vision, and olfaction. Moreover, the synaptic connections are well and extensively characterised, thus allowing the identification of pathological modifications occurring in diseased animals (Menon et al., 2013). Several genetic and molecular tools allow manipulating part of the Drosophila genome to determine the role of different molecules in development and diseases.

1.5.3. Genetic in *Drosophila melanogaster*

Several genetic approaches in *Drosophila melanogaster* offer the opportunity to study the molecular function of genes involved in human disease.

MUTAGENESIS IN DROSOPHILA

The genetic screens became possible when methods for creating mutations were developed. The first and the most efficient one is feeding the flies with ethyl methanesulfonate (EMS). EMS induces point mutations

and disrupts gene function. In the past, it was difficult to map point mutations, but with time single nucleotide polymorphism (SNP) maps were created and facilitated the recognition of the SNPs (Berger et al., 2001). The second disadvantage is that the progeny of mutagenised males is often mosaic, and the mutation is not passed to a second generation (F_1). Therefore, the screenings of F_1 often include x-ray irradiation that causes double-stranded DNA brakes and so do not cause the mosaicism (Johnston, 2002).

Another well-known strategy for mutant screening uses P-element insertions. P-elements are transposable elements found in *Drosophila melanogaster* and can cause the germline transformation (Castro and Carareto, 2004). The method allows the specific insertion of DNA segments into a germline and results in their stable inheritance in subsequent generations (Rubin and Spradling, 1982). With the P-element, chosen genes can be disrupted or tagged. Moreover, it can be used for inducible gene expression or repression. In the case of P-element mutation, mutated gene can be easily and also quickly identified (Johnston, 2002).

P-elements are divided into two groups, autonomous and nonautonomous. Autonomous P-elements are 2912 bp long and encode for a protein transposase that is in charge of P-element translocation.

Nonautonomous P-element can also move to a new genomic location but needs a transposase from autonomous P-element. It consists of the first 200 bp and final 200 bp of the autonomous element and includes the sequence that the transposase needs to recognise for transposition. Moreover, any DNA sequence inserted in between the ends will be transposed, as well (Anthony J.F. Griffiths, 2015) (Figure 14).

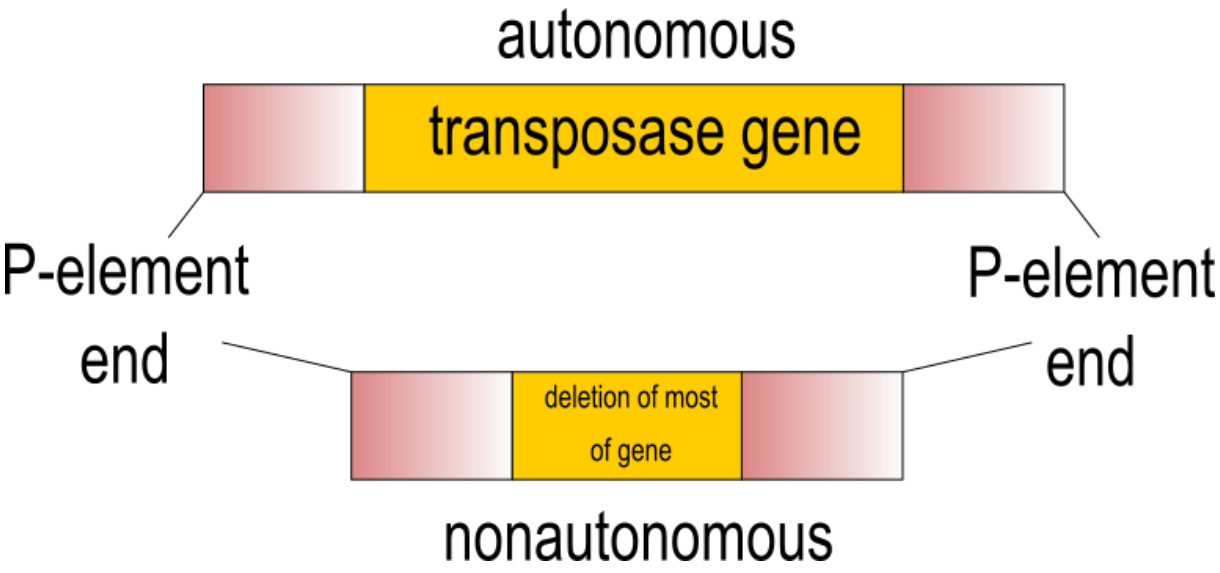

Figure 14: Schematic presentation of autonomous and nonautonomous P-elements. Nonautonomous P-element has the majority of the transposase gene deleted (customised by Anthony J.F. Griffiths, 2015).

For a transgenic fly creation, two types of bacterial plasmids need to be injected into the early Drosophila embryo. One carries an autonomous P-element (P helper plasmid) that can express the transposase. The second is an engineered nonautonomous P-element with incorporated cloned

DNA of the transgene (between the two P-element ends) (Figure 15). The P transposase expressing from autonomous P-element catalyses the insertion of the chosen gene. Only one copy of the gene of interest is inserted at a specific location (Anthony J.F. Griffiths, 2015).

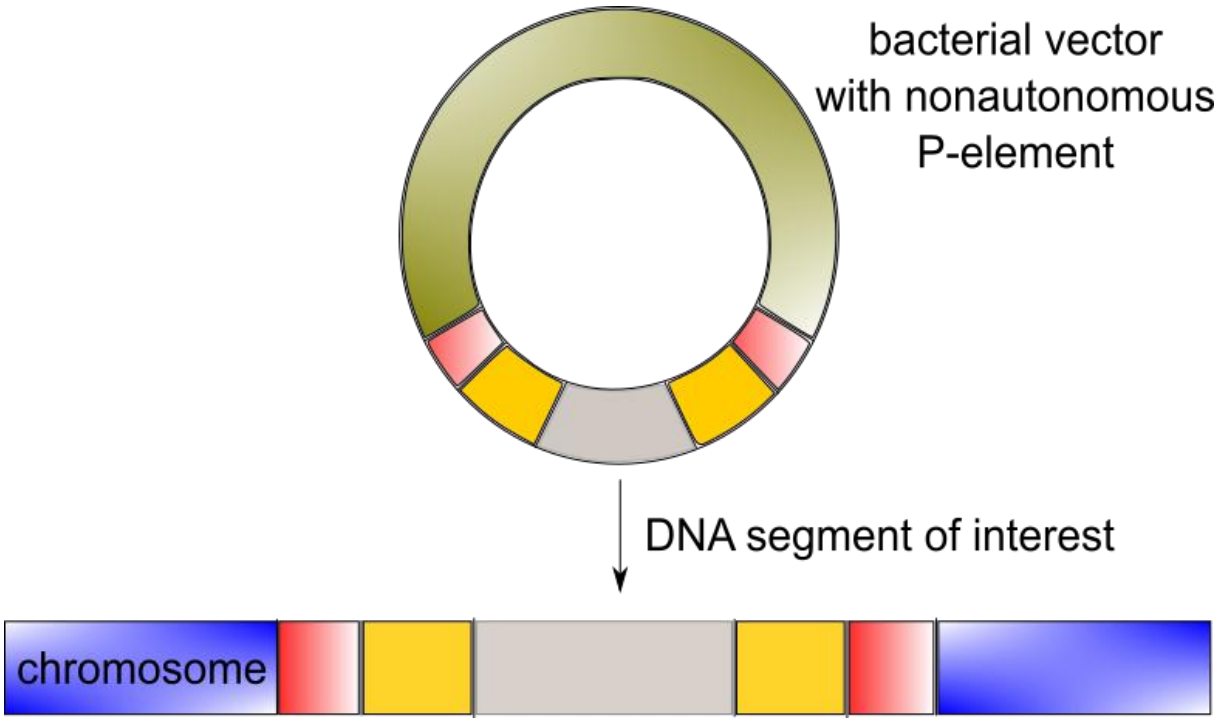

Figure 15: The bacterial vector with nonautonomous P-element containing a DNA segment of interest. After injection with the autonomous vector, transposase integrates DNA with the P-element into Drosophila chromosome (customised by Anthony J.F. Griffiths, 2015).

REGULATION OF GENE EXPRESSION

Gene expression can be reduced, eliminated, or increased, with obvious consequences on the levels of the corresponding protein product. As a

result, new phenotypes can be obtained. The most commonly used fly models are using the GAL4/UAS (upstream activating sequence) system. The system enables the expression of a particular protein in a tissue-specific manner (Brand and Perrimon, 1993). The yeast transcriptional factor GAL4 controls the expression of the gene of interest. In front of the gene, upstream activating sequence (UAS) is inserted. In the absence of GAL4, the transgene is not active, and it is not expressed. When crossing two flies, one with GAL4 expressed in a specific tissue and one with the transgene under the control of a UAS sequence, the transgenic protein can be expressed, and the phenotype generated easily analysed (Figure 16).

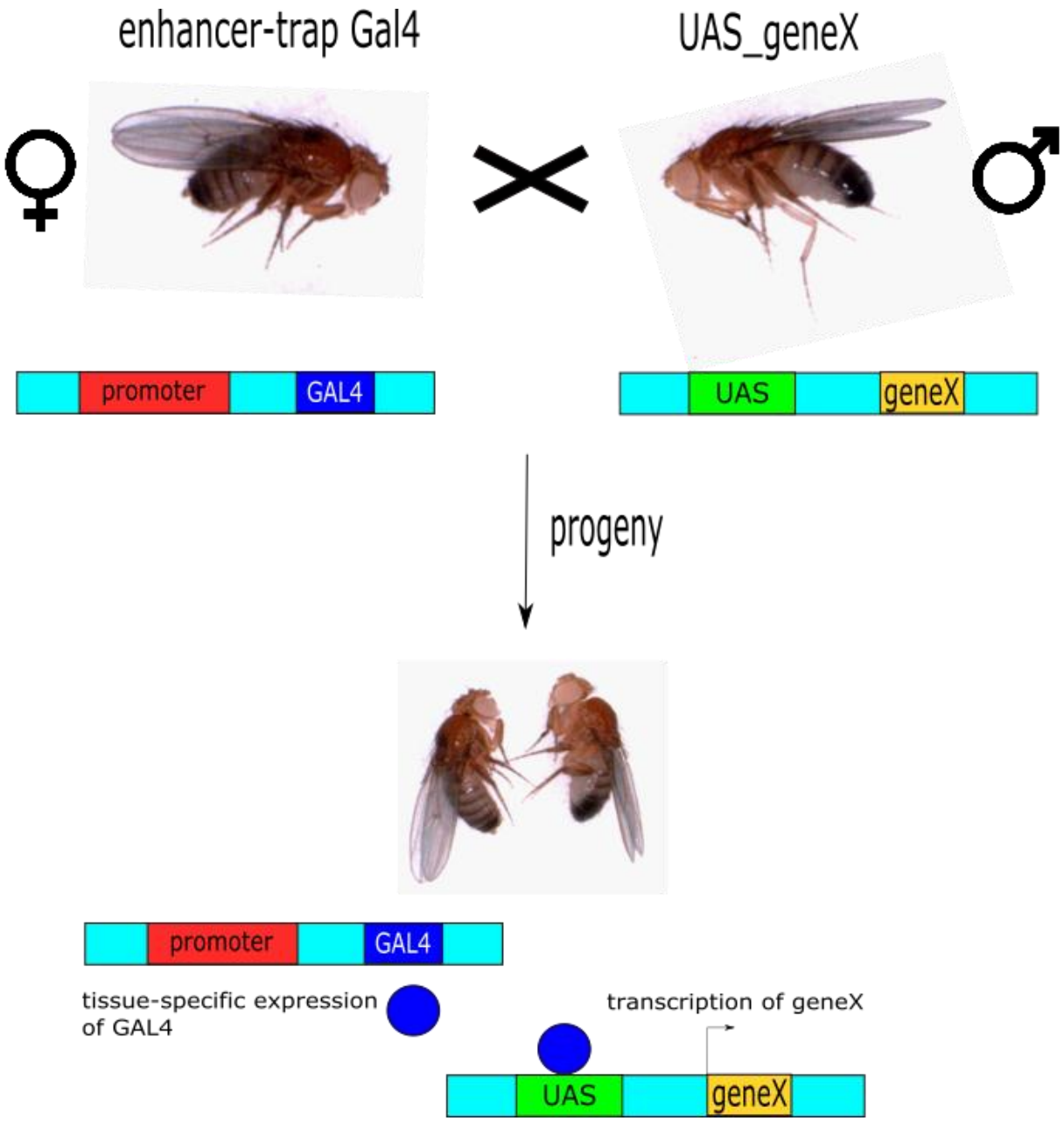

Figure 16: GAL4/UAS system. In the GAL4/UAS system, two transgenic fly lines are created. In the responder strain, the transgene is placed downstream of a UAS activation domain that consists of binding sides where GAL4 binds when present. Driver strain has GAL4 protein, yeast transcriptional activator. The progeny of the cross has GAL4 and UAS combined, so the gene or RNAi is expressed (modified by https://smallscienceworks.com/tag/uas-gal4/.)

TEMPORAL CONTROL OF THE GAL4 SYSTEM

One approach regulating the expression of UAS-gene with GAL4 system is the use of the GAL80 yeast protein. This protein is regulating the expression in yeast when there is no galactose. It binds to a specific amino acid sequence on GAL4 protein and prevents the transcription of the genes responsible for galactose catabolism (Ma and Ptashne, 1987).

Lee and Luo (Lee and Luo, 1999) first introduced the GAL80 regulation of the GAL4/UAS system in Drosophila. They ubiquitously expressed GAL80 under control of *tubulin 1α,* repressing the activity of GAL4 in all tissues. The main problem was that GAL80 repressed the expression of the genes regarding the conditions flies were exposed to.

The promising step towards efficient gene expression control was the development of the temporal and regional gene expression targeting (TARGET) technique (McGuire et al., 2003). The group developed a thermosensitive GAL80 protein ($GAL80^{ts}$) under *tubulin 1α* promotor. The expression of the gene was blocked when flies were kept at 19°C and the gene was expressing when flies were exposed to high temperature (30°C) (McGuire et al., 2003) (Figure 17).

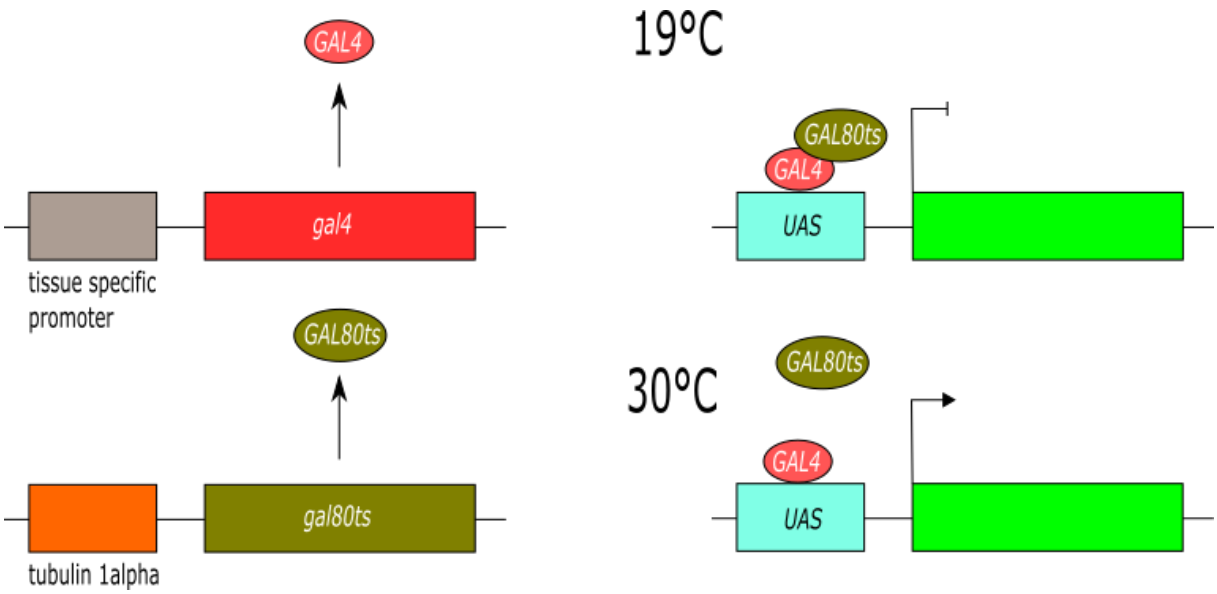

Figure 17: GAL80^{ts} and GAL 4 are expressed independently. At lower temperature, GAL80^{ts} binds to GAL4 and blocks its promotion of gene transcription. When the temperature is higher, Gal80^{ts} no longer binds to GAL4, and tissue-specific transcription is possible (Image customized by McGuire et al., 2003).

1.5.4. Drosophila neuromuscular junction

NMJs in *Drosophila* larvae are similar to the synapses in the central nervous system in vertebrates. NMJs are glutamatergic and use ionotropic glutamate receptors. They are orthologs of AMPA-type glutamate receptors found in the mammalian brain. They also have postsynaptic densities (PSDs) – large protein complexes, located in the postsynaptic part – containing orthologs of mammalian scaffold proteins, including PSD-95 (Menon et al., 2013).

Drosophila larval body is divided into seven segments labelled from A1 to A7 (Figure 18). They present a group of 30 different muscles that are precisely arranged, reproducing the same arrangement in every segment.

Muscles are innervated by specific motoneurons that target individual muscle fibres (Gramates and Budnik, 1999; Keshishian and Chiba, 1993). The relatively small number of muscles and neurons allows us to study the interactions present at the NMJs in detail and with high reproducibility. On average, there are six nerve branches with 32 motoneurons in total that innervate a specific muscle (Hoang and Chiba, 2001).

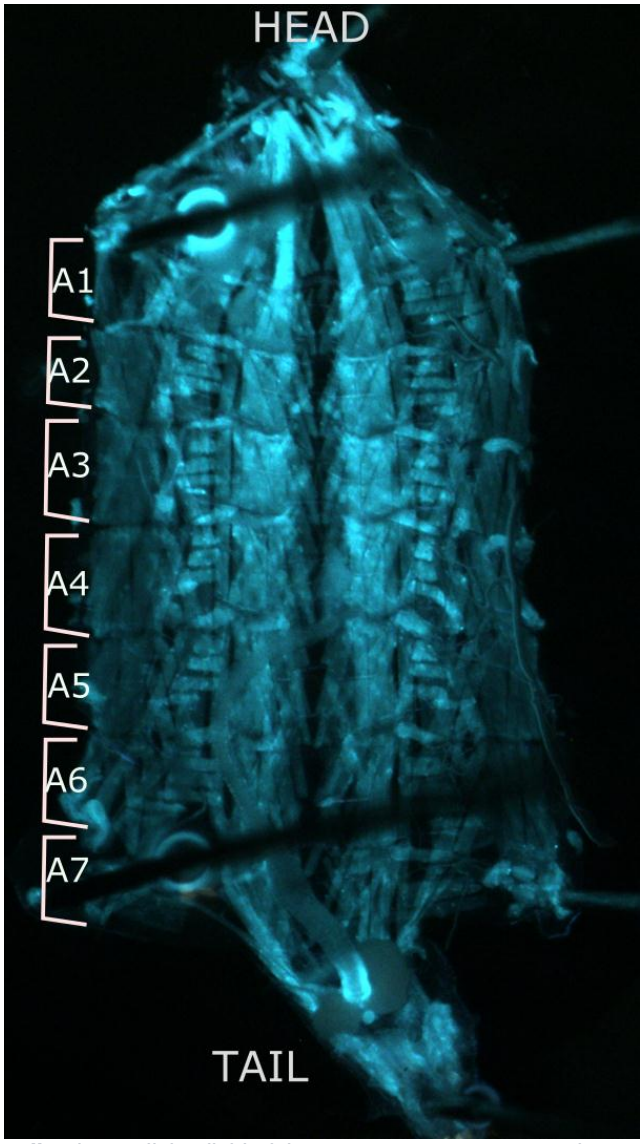

Figure 18: ***Larval body wall.*** *The wall is divided into seven segments. Each segment presents a group of 30 different muscles that are precisely arranged.*

During the embryonic development, motor neurons extend their axons into the musculature. They create three different pathways leading from CNS to the muscles: segmental nerve root (SN), which splits into SNa, SNb, SNc and SNd, intersegmental nerve root (ISN), and transverse nerve (TN) (Menon et al., 2013) (Figure 19). Every pathway and root innervates their specific group of muscles (Hoang and Chiba, 2001).

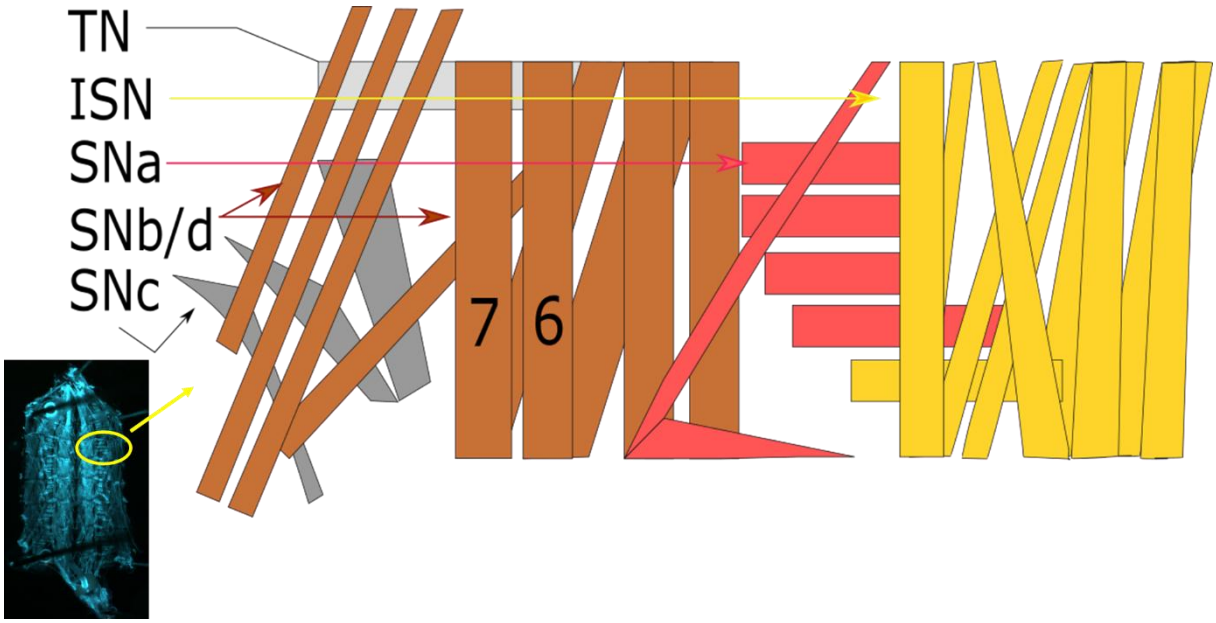

Figure 19: A scheme of muscles and three primary nerve roots (ISN, SN, and TN). The scheme represents a group of 30 muscles and their distribution (muscle 7 and 6 are specially marked) in one half of one segment. The position of the muscles in larvae is shown in the bottom left corner. Three primary roots innervate different groups of the muscles in the segment. The image was customised by (Hoang and Chiba, 2001).

All roots form structures of functional connections between an axon of a motoneuron and the surface of a muscle called neuromuscular synapse.

The axon reaches the muscle through synaptic boutons. These structures are well characterised based on their size; they can be classified into four major categories:

- Type Ib boutons are the largest found in all muscles (3 – 6μm). The neurotransmitter is glutamate (Johansen et al., 1989).
- Type Is are smaller (2 – 4μm) and are present in all muscles, similar to Ib, and are glutamatergic (Johansen et al., 1989).
- Type II are the smallest among all bouton types (1 – 2μm), they have developed branches and cannot be found in all muscles. They use either glutamate or octopamine as neurotransmitters (Monastirioti et al., 1995).
- Type III are medium in size (2 – 3μm). They are present only in muscle 12 and contain glutamate and insulin, as putative hormone neurotransmitter (Gorczyca et al., 1993).

In the thesis, we examined NMJ innervating muscles 6 and 7 (Figure 19). The NMJ originates from the SNb root. The single motoneuron axon innervates the cleft of muscles 6 and 7 with Ib boutons. SNb/d root has one single Is motoneuron axon that innervates all SNb/d muscles groups, consequently also 6 and 7. Our results are the outcomes of Ib analysis, so the largest boutons innervating larval body wall are using glutamate as a neurotransmitter (Hoang and Chiba, 2001; Menon et al., 2013).

- **Glutamate receptors**

There are two families of glutamate receptors. Ones are ionotropic receptors, ligand-gated channels. The second type is a metabotropic glutamate receptor, and it is coupled with G-protein. Ionotropic receptors are further divided into N-methyl-D-aspartate (NMDA), a-amino-3-hydroxy-5-methyl-4-isoxazolepropionic acid (AMPA), and kainate receptor subfamilies. Their names refer to the chemical agonist that selectively binds to the subfamily (Willard and Koochekpour, 2013). In *D. melanogaster,* both types can be found. Metabotropic glutamate receptors have mainly neuromodulatory role, and ionotropic receptors mediate fast synaptic transmission, resulting in muscle depolarisation. The last-mentioned is the most studied in this particular model (DiAntonio, 2006). Based on sequences of the genome, all types of ionotropic receptors can be found in Drosophila (Littleton and Ganetzky, 2000). However, the majority of the literature describing Drosophila NMJ receptors deals with AMPA/kainate receptors (DiAntonio, 2006).

Muscles express five different subunits: GluRIIA (IIA), GluRIIB (IIB), GluRIIC (IIC, also called GluRIII), GluRIID (IID), and GluRIIE (IIE). The progeny with the absence of IIA or IIB separately is viable. Double

mutation induces embryonic paralysis, and the progeny die at that stage (DiAntonio et al., 1999).

GluRIIC, D, and E form the receptor and are essential for its function. In particular, IIC is essential for the transmission of the signal, IID, and IIE are essential for viability (DiAntonio, 2006). The studies show that iGluR in *Drosophila* consists of four different subunits: IIC, IID, IIE, and either IIA or IIB. Depending on the last two subunits, GluRIIA (IIA, IIC, IID and IIE subunits) and GluRIIB (IIB, IIC, IID and IIE subunits) compete with each other for synaptic localisation, differ in synaptic currents (IIB channels desensitise ten times faster than IIA), second messenger regulation and localisation patterns (DiAntonio, 2006; DiAntonio et al., 1999). In our study, we analysed the levels of GluRIIA receptors that are in high levels present opposite to Ib boutons (Marrus et al., 2004).

- **Dlg protein**

The disc-large protein belongs to a family of membrane-associated guanylate kinases (MAGUKs). It shares high homology with the major protein component of the brain postsynaptic density, PSD-95. Dlg protein is expressed at septate epithelial junctions in insects, which are similar to tight junctions in vertebrates, but can also be found in the fly central nervous system (CNS) and muscles. The absence of Dlg results in a neoplastic growth of larval imaginal disc, poor adhesion between epithelial

cells, and abnormal cell polarity. Mutations of *dlg* locus in the brain result in brain tumour (Lahey et al., 1994).

The most characterised product of *dlg* gene, Dlg-A, contains 3 PDZ (postsynaptic density 95 (PSD-95)/Disc large (Dlg)/zona occludens-1 (ZO-1)) domains, Src homology 3 (SH3) domain and a guanylate kinase-like domain (Woods and Bryant, 1991) (Figure 20).

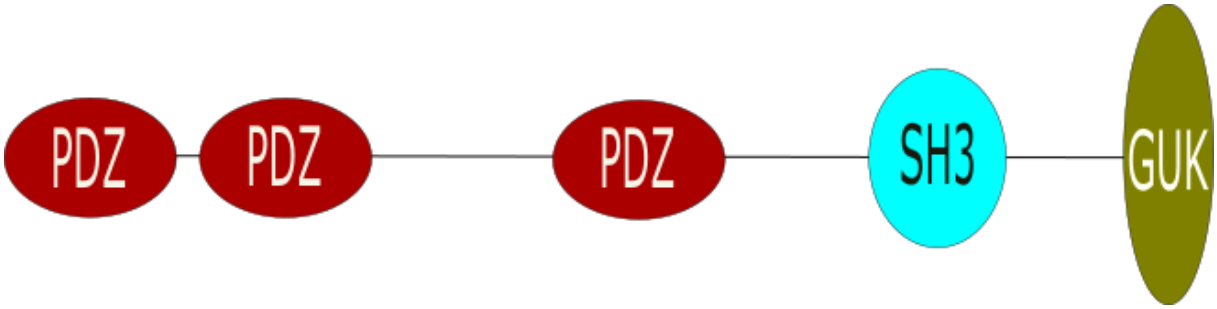

Figure 20: The structure of Dlg-A protein. It contains 3 PDZ domains, SH3 domain, and GUK domain, which however is not active. (The image customised by (Woods and Bryant, 1991)).

Most of the Dlg protein is located postsynaptically in boutons type I. The findings that mutation of *dlg* locus causes poorly developed and much simpler subsynaptic reticulum (SSR) support the model that Dlg is involved in the development of synaptic structure (Guan et al., 1996). It has been characterised as a scaffold protein. PDZ domains are responsible for binding proteins and deliver them to the NMJ. The first characterised protein that Dlg binds is a shaker-type K^+ channel following with Fasiciclin II and glutamate receptors (reviewed by (Koh et al., 2000)).

Dlg appears a few hours before the first larval stage when the SSR is generated. It is in larval development, particularly at the beginning of the third instar larval stage, when the SSR undergoes a dramatic expansion. However, Dlg mutants do not have any misshaped boutons (Guan et al., 1996). In general, hypomorphic *dlg* alleles display underdeveloped subsynaptic reticulum, larger glutamate receptor fields, and increased size of synaptic boutons, active zones, and vesicles (Astorga et al., 2016).

1.6. *tbph*$^{\Delta 23}$/- *Drosophila* model

The starting point of our laboratory research was a mutant fly with deletion of *tbph* gene. Two different stocks were created, with different parts of the protein deleted. The *tbph*$^{\Delta 23}$/- flies possess deletion of 1616 bp with break points from base pair 19748477 to 19750093. *tbph*$^{\Delta 142}$/- deletion is located from base pair 19749289 to 19750093 in total with deletion of 1138 bp. Both deletions resulted in the complete absence of TBPH protein (Feiguin et al., 2009). The lines were named after the corresponding number of the tube, from where the stock was created.

The *tbph*$^{\Delta 23}$/- and *tbph*$^{\Delta 142}$/- flies had the same body characteristics as W^{1118} flies (wild type). However, the phenotype was quite different. Both mutant flies lived significantly shorter time. They died already on day three after hatching. When TBPH or human TDP-43 were expressed in neurons, the phenotype was recovered (Figure 21) (Feiguin et al., 2009).

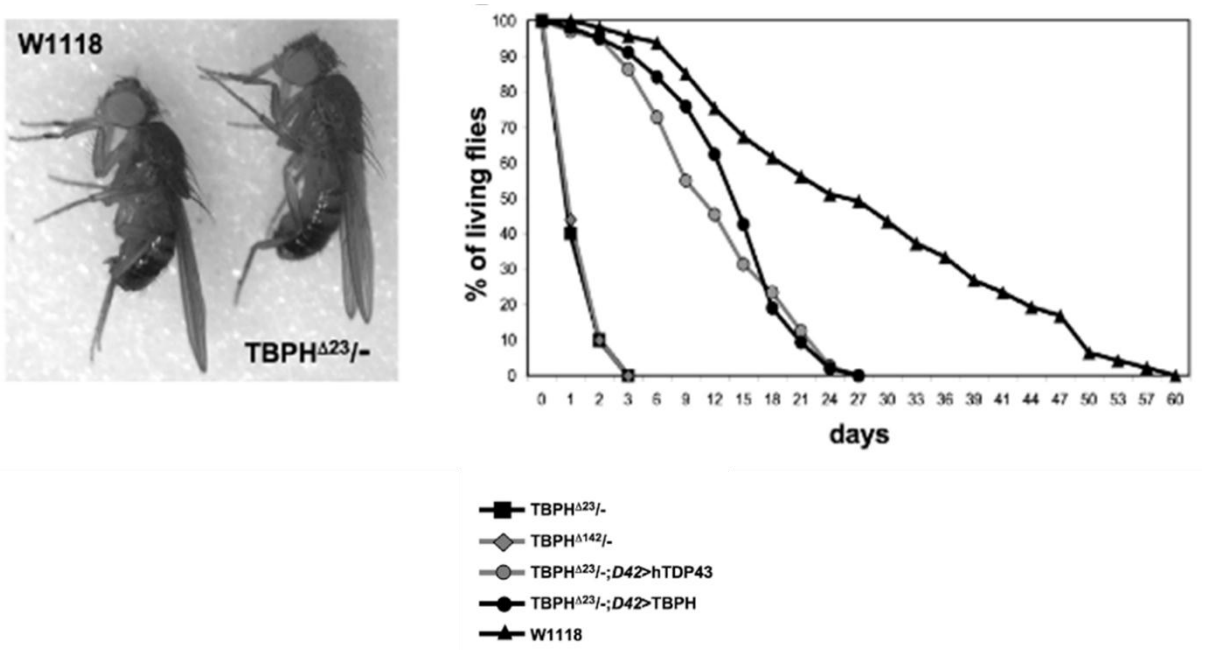

Figure 21: Mutant flies had the same body characteristics as wildtype control, but they lived a significantly shorter time. When expressing TBPH or human TDP-43 in neurons, the life span was partially recovered (Feiguin et al., 2009).

Not only life span, but also locomotion was affected. Mutant adult flies were tested for climbing and walking. Climbing the glass cylinder demands strength and motoric skills that mutant flies did not possess. The performance was also evaluated with walking. $TBPH^{-/-}$ walked a significantly shorter distance than wildtype control. Flies expressing TBPH or human TDP-43 in neurons recovered the abilities of climbing and walking (Figure 22) (Feiguin et al., 2009).

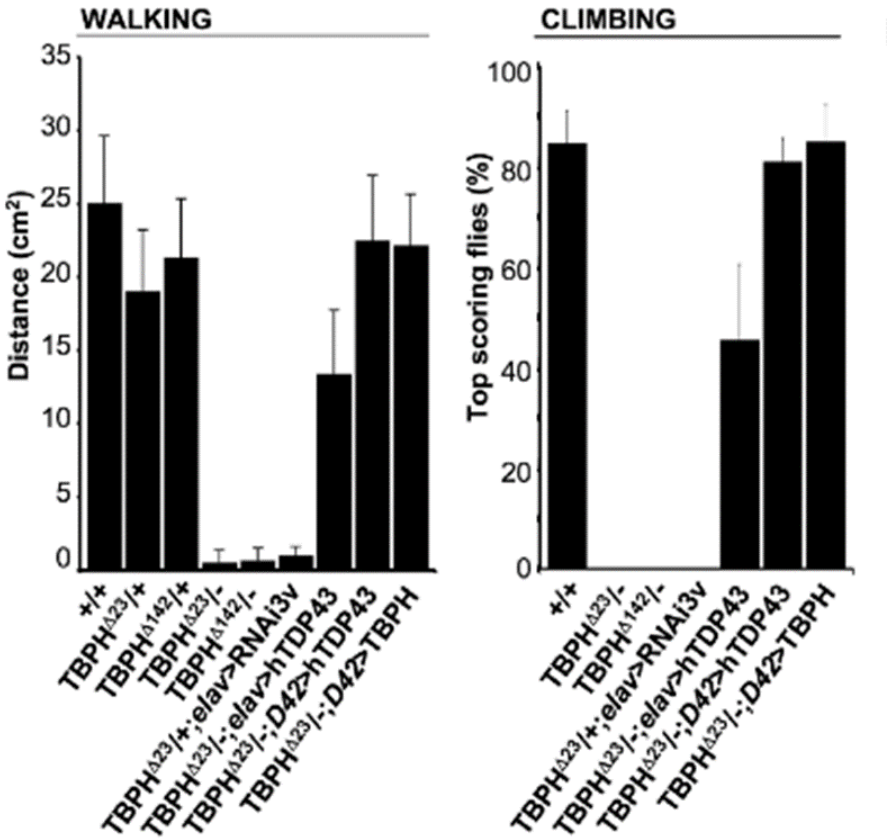

Figure 22: Mutant adult flies did not climb, and their walking was significantly impaired. When TBPH was expressed in neurons, the phenotype was recovered (Feiguin et al., 2009).

The phenotype was evident also in larvae (Figure 23). They moved significantly slower with 30 peristaltic waves in two minutes. Their NMJ had on average two to three branches and 10 to 15 boutons less than wild type control. However, the phenotype was reversible, since expressing TBPH or human TDP-43 in neurons recovered all tested aspects of a larval phenotype (Feiguin et al., 2009).

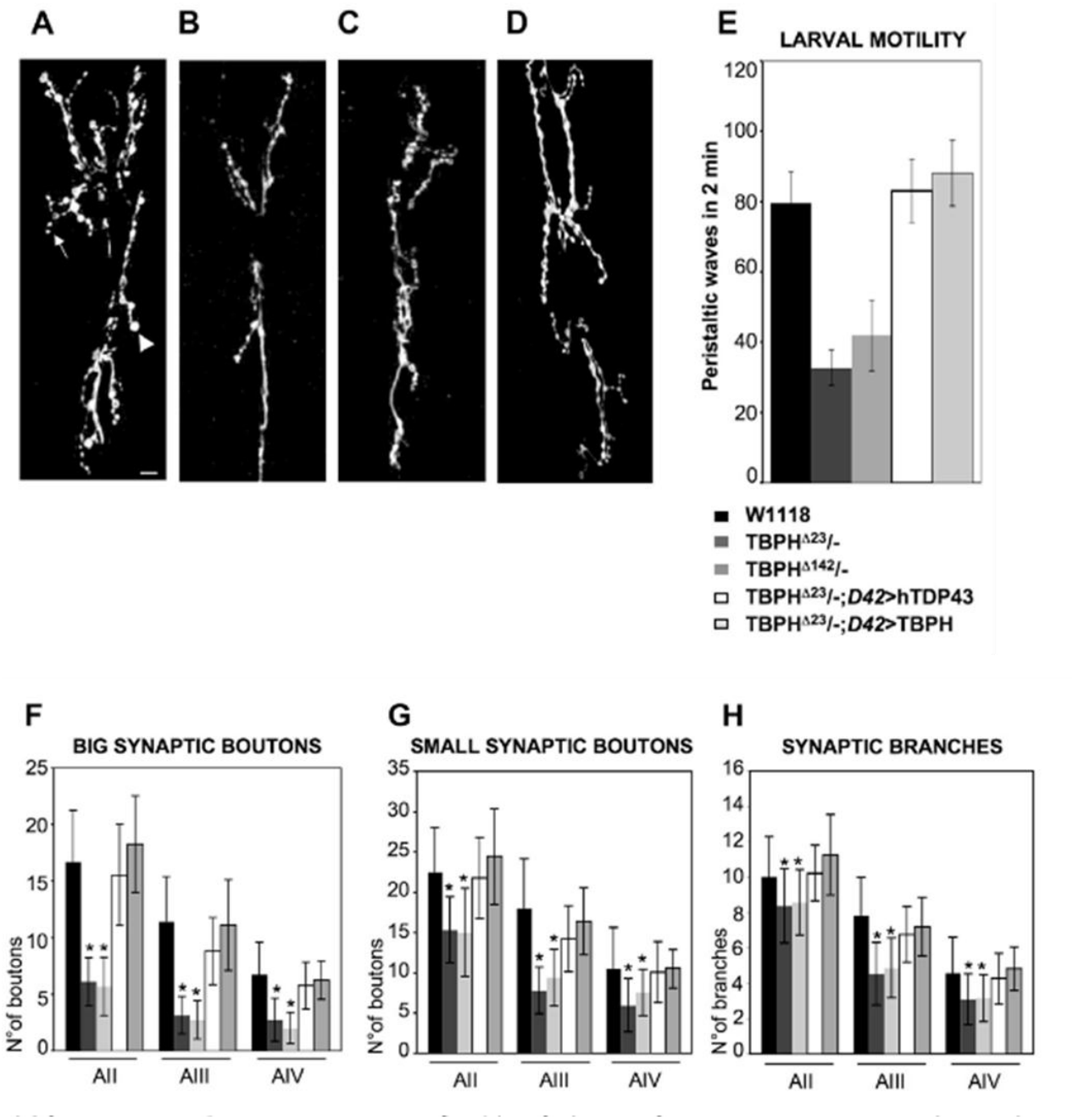

Figure 23: The characterisation of the larval phenotype. (A) Confocal images of motoneurons presynaptic terminals at muscles 6 and 7 (abdominal segment III) in wild type third instar larvae stained with anti-HRP antibodies reveal the branching pattern and the presence of big (arrowhead) and small (arrow) synaptic boutons. (B) and (C) Similar staining and anatomical position for TBPHΔ23 and TBPHΔ142 homozygous larvae respectively show reduced axonal branching pattern and the number of synaptic boutons. (D) TBPHΔ23 third instar larvae rescued by expressing UAShTDP-43 in motoneurons with D42-GAL4 shows recovery of presynaptic complexity with increased formation of synaptic boutons and axonal terminal branching. (E) The number of peristaltic waves observed for two minutes. (F) Quantification of big synaptic boutons present in consecutive abdominal segments. (G) Analysis of small synaptic boutons. (H) Quantification of presynaptic terminals branches in wild type, TBPHΔ23 and hTDP-43/TBPH rescued third instar larva. Scale: 10μm. (Feiguin et al., 2009).

2. AIMS AND OBJECTIVES

The aim of the project was to investigate the role of TBPH in muscles and its contribution to neuromuscular junction development and onset in ALS. To address this aim, we used several objectives:

- To determine the phenotype and NMJ shape and function, when TBPH in muscles is silenced;
- To investigate whether expression of TBPH in muscles can recover the ALS-like phenotype;
- To track the proteins that are regulated by TBPH and determine their role in NMJ development, shape and function.

3. RESULTS

3.1. Silencing TBPH in muscles

3.1.1. Flies show locomotive problems and shorter lifespan

In order to explore the phenotype connected to TBPH silencing in muscles, in the different development stages of Drosophila, an RNA interference sequence formed by a long hairpin construct specific for TBPH (TBPH IR) and positioned under the control of UAS sequences was expressed with two muscle-specific drivers: Myosin heavy chain-Gal4 (MHC-GAL4) and Myocyte enhancer factor 2-Gal4 (Mef2-GAL4).

Myosin heavy chain is a muscle-expressing protein. It is essential for muscle contraction through its ATP-dependent interaction with actin filaments (Sellers, 2000). Myocyte enhancing factor 2 is a transcriptional factor involved in muscle development. Its mRNA can be located in visceral, somatic, and heart muscles (Nguyen et al., 1994; Sandmann et al., 2006). Therefore, their promoters are active mainly in muscles.

Our first observations focused on possible alterations of larval movements as a consequence of TBPH silencing in muscles. In a wild type background for TBPH, we expressed its RNAi with the MHC-GAL4 driver, and only by increasing the temperature at 29°C to enhance the expression of the RNAi we managed to detect the impairment in larval motility (Figure 24). Larvae with silenced TBPH performed significantly worse than the wildtype. While the number of peristaltic waves for the wildtype reached

an average of 95 peristaltic waves in a time interval of two minutes, the peristaltic waves in TBPH-silenced larvae dropped to 80.

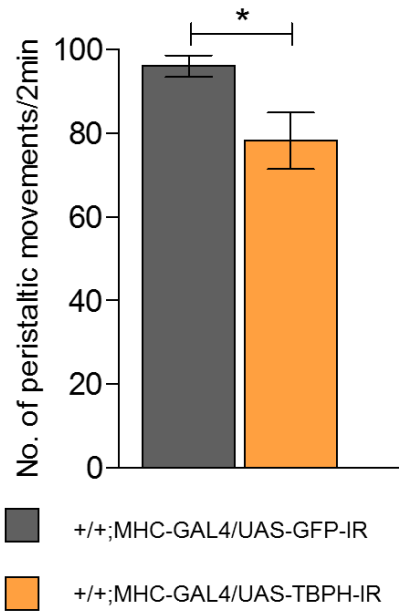

Figure 24: ***Larval movement was significantly impaired when TBPH in muscles was silenced.*** *Counting peristaltic waves significantly dropped in larvae expressing UAS-TBPH-IR comparing to larvae expressing UAS-GFP-IR. *p<0.05 calculated by T-test, error bars SEM. N=20 larvae per genotype.*

We wondered if the statistical significance would have been more considerable in a heterozygous background for TBPH, where one copy of TBPH is deleted. Since *tbph*$^{\Delta 23}$/+ flies do not manifest any phenotype of the null fly *tbph*$^{\Delta 23}$/- (Feiguin et al., 2009), we were sure that any phenotypical effect would be a consequence of silencing.

Also, in this analysis, crosses were kept at 29°C to enhance the expression of silencing RNA (UAS-TBPH-IR and UAS-GFP-IR), and we

compared them versus the previous experiment performed in wild type background. The quantification of the peristaltic waves showed a stronger statistical difference between control and silencing (Figure 25). Moreover, we observed behaviour for TBi (*tbph*$^{\Delta 23}$/+; MHC-GAL4/UAS-TBPH-IR) larvae, very similar to the *tbph*$^{\Delta 23}$/- larvae. While controls moved straight forward with little or no stops, silenced larvae stopped frequently, searched the surroundings, and remained mainly in the same position on the plate because of frequent turnings.

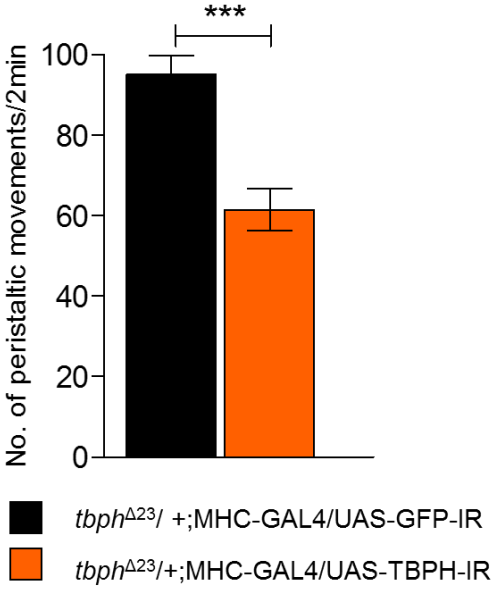

Figure 25: ***Larval motility was impaired in animals with silenced TBPH.*** *Counting peristaltic waves significantly dropped in larvae expressing UAS-TBPH-IR comparing to larvae expressing UAS-GFP-IR. ***p<0.001 calculated by T-test, error bars SEM. N=20 larvae per genotype.*

The reduction of larval waves reached 35%, an average of 95 waves in two minutes for controls compared to the 61 waves of larvae with silenced TBPH. We could conclude that even if a phenotype is already detectable in larvae with wildtype background for TBPH, a much stronger effect can be seen in the heterozygous background.

However, to further confirm the results and to explore if a stronger phenotype could be obtained, we used another muscle-specific driver Mef2-GAL4. Also, with this driver, all crosses were set at 29°C. We followed the same pattern of experiments. First, we analysed the larval movement phenotype in a wildtype background for TBPH.

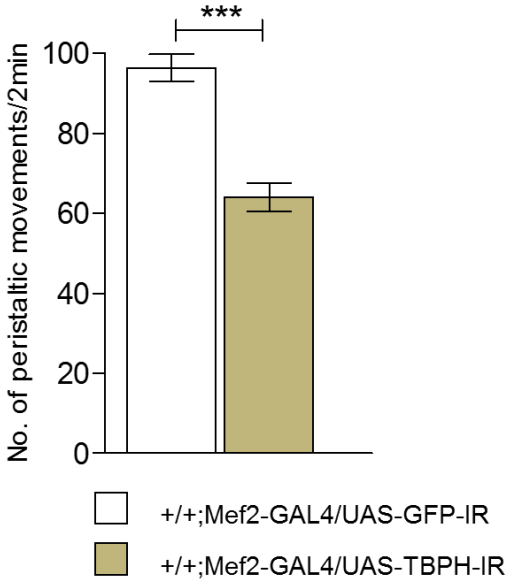

Figure 26: ***Larvae with silenced TBPH in wild type background performed worse than the control group.*** *Counting peristaltic waves significantly dropped in larvae expressing UAS-TBPH-IR comparing to larvae expressing UAS-GFP-IR. ***p<0.001 calculated by T-test, error bars SEM. N=20 larvae per genotype.*

A 33% reduction in larval waves was scored in TBi (+/+; Mef2-GAL4/UAS-TBPH-IR) larvae comparing to the control group (Figure 26), a result comparable to the one obtained using the MHC driver in heterozygous condition for TBPH, and also, in this case, the behaviour of larvae was very similar to the one of the null allele TBPH larvae, with very frequent stops and turning. We proceeded to test the effect of silencing in heterozygous conditions for TBPH with Mef2-GAL4, but the *tbph*$^{\Delta 23}$/+ background showed a phenotype comparable to the wild type background.

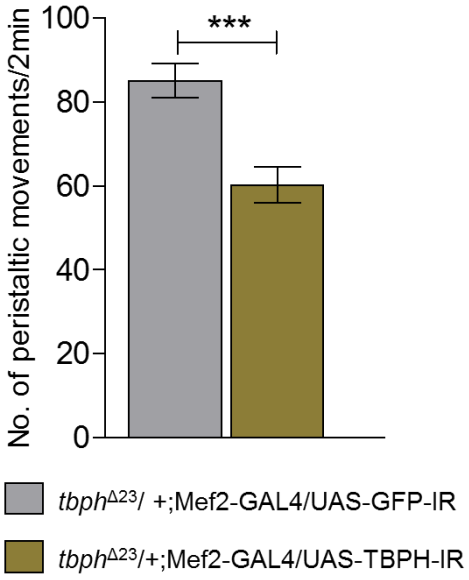

Figure 27: ***Larvae with TBPH silenced have impaired mobility.*** *Counting peristaltic waves significantly dropped in larvae expressing UAS-TBPH-IR comparing to larvae expressing UAS-GFP-IR. ***p<0.001 calculated by T-test, error bars SEM. N=20 larvae per genotype.*

The average number of larval waves was 31% lower than the control (Figure 27).

Our experiments performed both in wild type and heterozygous condition for TBPH confirmed that TBPH silencing in muscles affects larval mobility.

The phenotype seen in larvae rose the question whether it could also be observed in adult flies. We decided to test the phenotypes triggered by both drivers. Since the most robust larval phenotype using MHC-GAL4 was observed in heterozygous background *tbph*$^{\Delta 23}$/+, we decided to test adult flies only in this background. To keep it consistent, we used the same background also in flies where Mef2-GAL4 drove expression of TBPH-IR.

The temperature was fixed at 29°C. The phenotype in adult flies was characterised by performing a climbing assay and tracking days of survival. The TBPH silenced flies resulted in being impaired in their climbing ability, as well as their survival (Figure 28 and Figure 29).

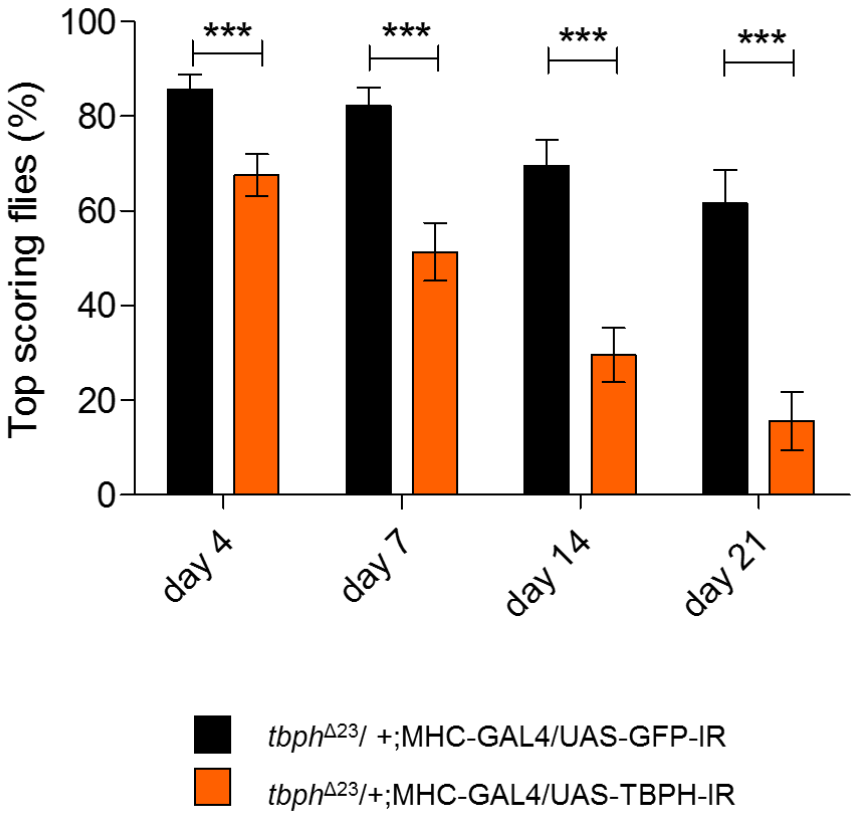

Figure 28: ***Flies' ability in climbing was impaired.*** *The percentage of flies that reached the top of the cylinder significantly dropped in flies expressing UAS-TBPH-IR comparing to flies expressing UAS-GFP-IR on day 4, 7 and 14. On day 21, the difference was not significant. ***p<0.001 calculated by two-way ANOVA, error bars SEM. N=200 flies per genotype.*

The climbing ability was measured at four time points: day 4, 7, 14, and 21. Even if silenced flies did not show the poor leg coordination observed for the *tbph*$^{\Delta 23}$/- flies and walked normally, their climbing resulted impaired. Silenced flies fell onto the bottom of the cylinder after trying to climb. Quantification of fly performance showed a significantly smaller percentage of TBPH-silenced flies being able to climb already on day 4.

With time the ability of climbing declined. At every time point less flies with silenced TBPH reached the top in comparison to wild type control (Figure 28).

In parallel with climbing, we also tracked days of survival. It must be underlined that 29°C temperature is already a stressor by itself and consequently, as expected, the heat shortened the lifespan to approximately 30 to 40 days when most wildtype flies die (Linford et al., 2013).

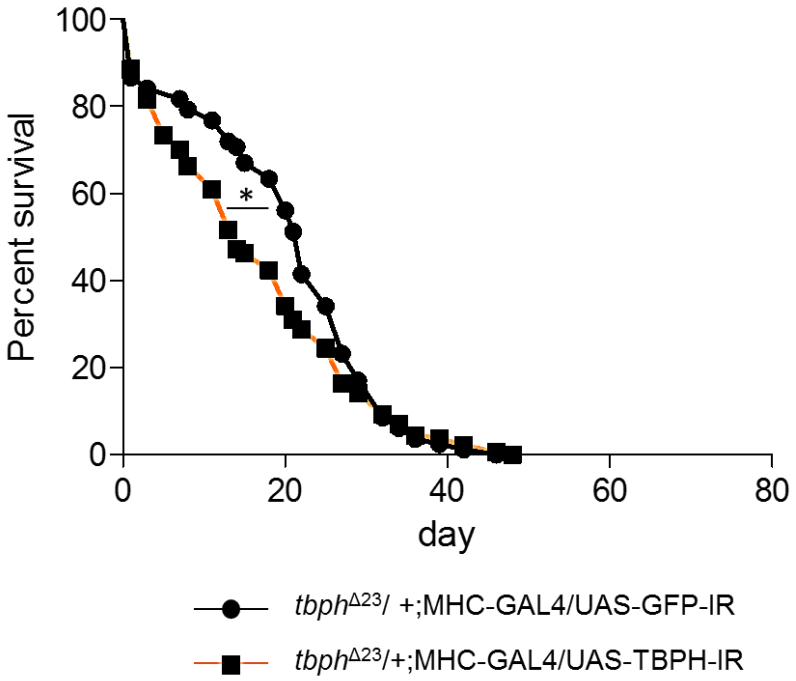

Figure 29: ***Flies had a significantly shorter lifespan when TBPH in muscles was silenced in early time points****. The percentage of death events in silencing flies compared to their control was higher at the beginning of the*

*measurement. The statistical difference was calculated by the Gehan-Breslow-Wilcoxon test, *p<0.05. N=200 flies per genotype.*

The comparison of the survival curves calculated by Log-rank test that takes into account the whole follow up period (Bland and Altman, 2004) was not significant, while the Gehan-Breslow-Wilcoxon test that gives more weight to early time points (Martinez and Naranjo, 2010) defined the two samples significantly different. To sum up, in the beginning, more flies with silenced TBPH died compared to the wildtype control (Figure 29).

Following the flow of larval phenotypisation, we decided to determine the phenotype of adult flies also using Mef2-GAL4 driver. As mentioned above, only *tbph*$^{\Delta 23}$/+ background was used, and crosses were set at 29°C. Unfortunately, even if larvae pupated, they did not hatch. A detailed inspection of pupae confirmed that they remained intact and no breaks nor opening on the shell was noticed. Keeping in mind that from our previous experiments done on the larva, the Mef2-GAL4 driver resulted much stronger, we concluded that the RNAi expression was too robust at 29°C, so crosses were moved at 25°C. With the lower temperature, even if some flies remained trapped in the pupa shell, we could collect a decent number of flies for further tests.

The stronger effect of Mef2-GAL4 driver forced us to adapt the time points for testing climbing abilities slightly. Since half of the collected flies died within the first days, we evaluate climbing ability on day 1, 4, 7, and 14. The measurement of day 21 was not possible, because only control group survived up to that day.

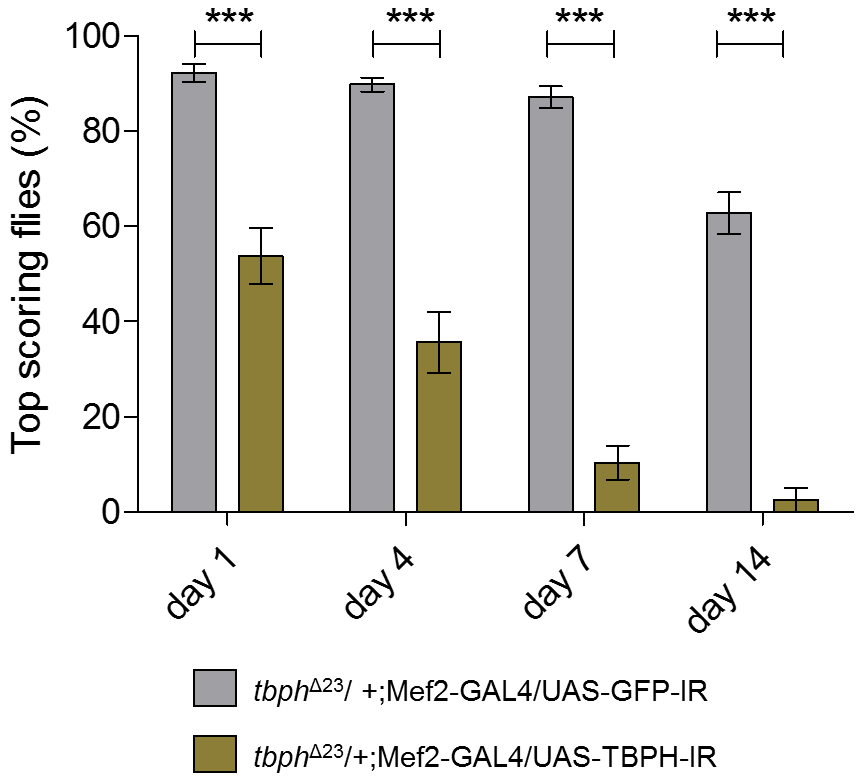

Figure 30: ***Flies climbed significantly less when TBPH in muscles was silenced.*** *The percentage of flies that reached the top of the cylinder significantly dropped in flies expressing UAS-TBPH-IR comparing to flies expressing UAS-GFP-IR on day 1, 4, 7 and 14. **p<0.01 and ***p<0.001 calculated by two-way ANOVA, error bars SEM. N=200 flies per genotype.*

Similarly to what was observed for the MHC-GAL4 driver, flies with silenced TBPH in muscles did not show any abnormality in leg coordination, but they were just not strong enough to climb. Even if they started to climb, a lot of them fell onto the bottom of the cylinder. We statistically evaluated the percentage of flies that reached the top of the cylinder in the fixed two-minute time period. Flies with silenced TBPH in muscles performed statistically worse than the control group, and this unfitness was observed already on day 1; however, it was clear that their climbing ability worsened over time also on day 4, 7 and 14, when silenced flies performed worse than the wildtype control (Figure 30).

In parallel with the climbing assay, the same set of flies were observed to characterise their lifespan and evaluate any possible difference.

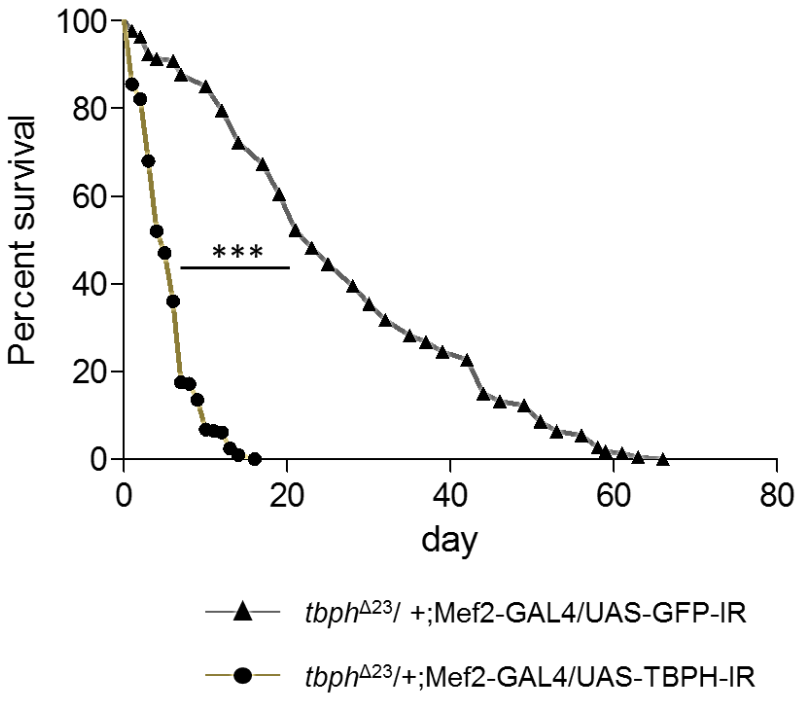

Figure 31: ***Flies lived a significantly shorter time when TBPH in muscles was silenced.*** *Silencing of TBPH affects the overall life span (log-rank test), including with early events evaluation (Gehan-Breslow-Wilcoxon test). ***p<0.001. N=200 flies per genotype.*

With Mef2-gal4 driver both, log-rank test (the overall statistical difference) and Gehan-Breslow-Wilcoxon test (statistical difference at the beginning of the tracking), showed a statistically significant difference between silenced flies and the control group. As mentioned above, 50% of the flies died in the first four days, and the survived flies did not reach 20 days (Figure 31).

To sum up, flies with silenced TBPH in muscles show significant phenotype described by larval movement, adult climbing ability, and

survival. The observed differences in larvae allowed us to test whether there might be any changes in the structure of the neuromuscular junction (NMJ). We decided to take the genotype that showed the most robust phenotype. Therefore, we compared and statistically evaluated all larval movement data from larvae with silenced TBPH. We used one-way ANOVA with Bonferroni correction to analyse the results and focused mainly on the differences between the silencing and the corresponding control.

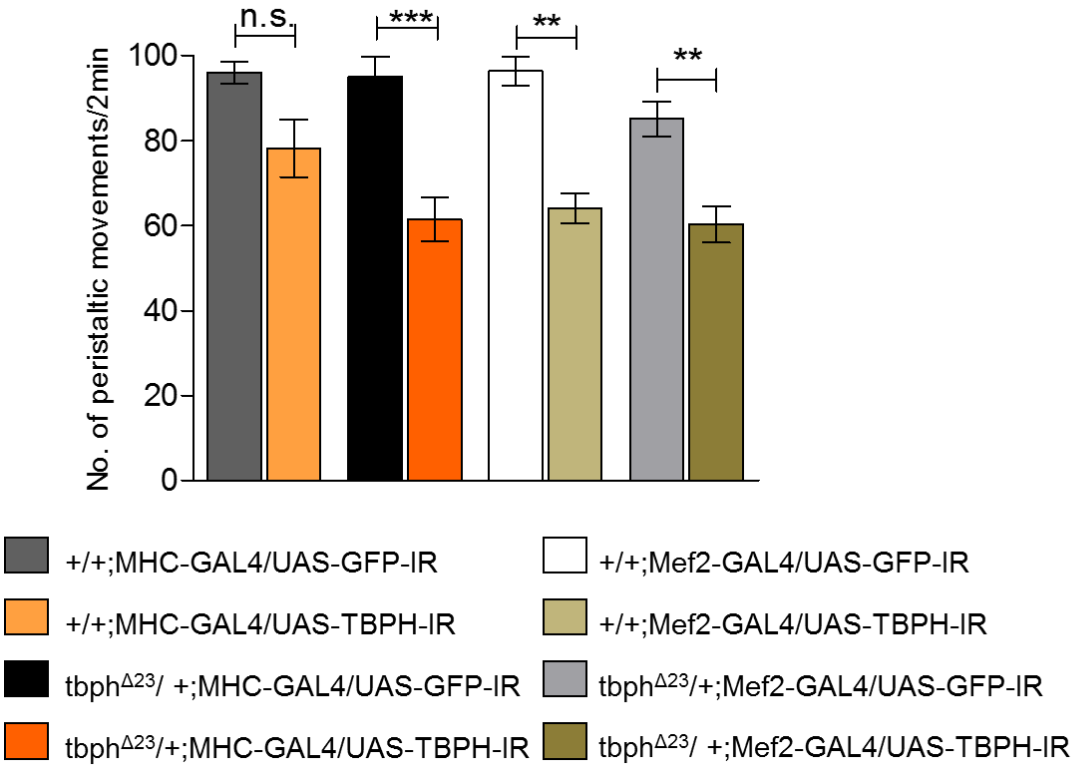

Figure 32: ***With one-way ANOVA test statistically the strongest difference show TBPH silencing with MHC-GAL4 in heterozygous background.*** *ns = not significant **p<0.01 and ***p<0.001 calculated by one-way ANOVA. Error bars SEM. N=20 larvae per genotype.*

With this statistical approach, we obtained different strengths of statistical difference. The genotype with MHC-GAL4 driver in *tbph*$^{\Delta 23}$/+ background showed the most robust difference. We used this genotype for subsequent analysis on NMJs.

3.1.2. Boutons are misshaped, and Futsch level drops with TBPH silencing in muscles

We wanted to see whether the NMJs are somehow affected when TBPH was silenced in the muscle.

NMJ consists of a presynaptic part, a synaptic cleft, and a postsynaptic part. The presynaptic part is represented by the axon of a neuronal cell, while the postsynaptic one is represented by the muscle (Slater, 2017). It has already been published that *tbph*$^{\Delta 23}$/- flies have deprived growth of NMJ (Feiguin et al., 2009). The objective was to check whether silencing TBPH in muscles could trigger the same or similar phenotype. To address this question, we stained larval carcasses with αHRP antibody, which labels glycoproteins present in the neuronal membrane explicitly. We quantified the number of branches of the NMJs innervating muscles 6 and 7 located in the second segment of the larval body.

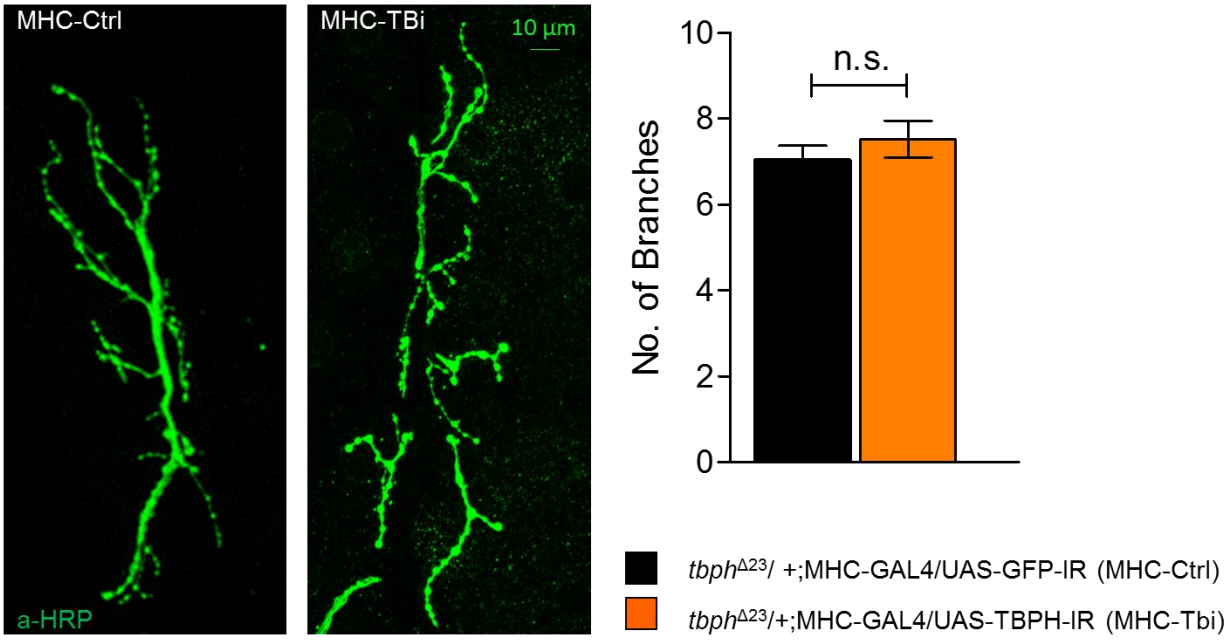

Figure 33: ***In larvae with silenced TBPH in muscles number of branches did not significantly change***. Confocal images of the third instar NMJ terminals in muscle 6 / 7, second segment stained with anti-HRP (in green) are represented. The representative terminals are shown, together with the quantification. ns= not significant, calculated by T-test, error bars SEM. N = 20 larvae per genotype.

Silencing of TBPH in muscles did not affect the neuromuscular growth. NMJs of silenced larvae were comparable to the wildtype control, and the branches quantification showed TBi larvae with a slightly higher number of branches on average, but not statistically significant, with approximately seven branches per neuromuscular junction for both, control and TBi larvae (Figure 33).

A hallmark of the synapsis of the null allele *tbph*$^{\Delta 23}$/- larvae was the misshaped boutons. In mutants, a higher percentage of irregular boutons

and consequently lower percentage of the regular ones were detected compared to the W^{1118} genetic background (Feiguin et al., 2009).

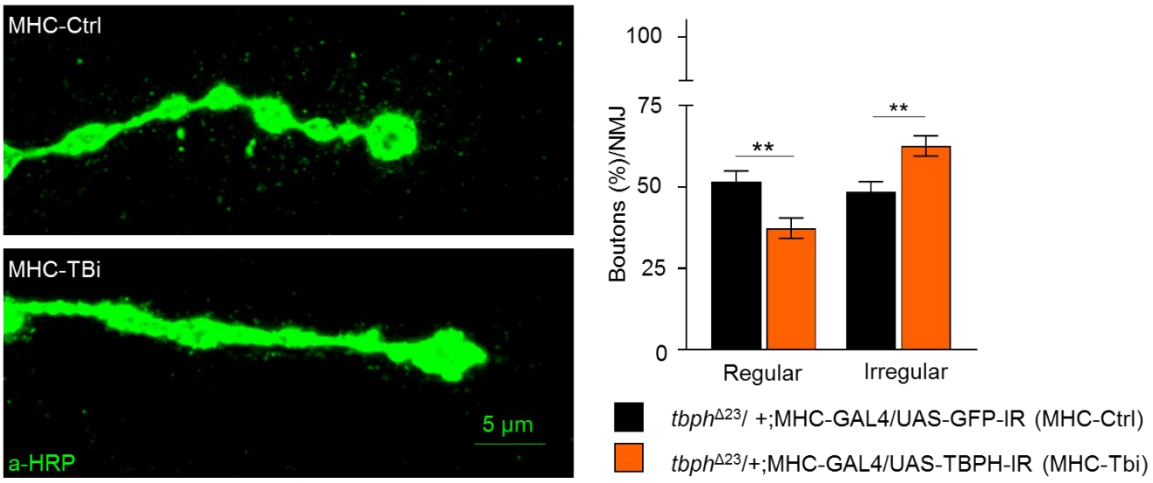

Figure 34: ***Silencing TBPH in muscles affected the bouton shape.*** Confocal images of the third instar NMJ terminals in muscle 6 / 7, second segment stained with anti-HRP (in green). The representative bouton shapes are shown, together with the quantification. **p<0.01, calculated by T-test, error bars SEM. N = 20 larvae per genotype.

Similarly, silencing TBPH in muscles caused alteration in bouton shape. Boutons were wrinkled and, in some cases, fused. The quantification showed a significant difference in the percentage of two groups: the percentage of regular boutons was lower in TBPH silenced larvae, and in parallel, the percentage of irregular boutons was higher than control (Figure 34).

An increased percentage of irregular boutons implies an alteration in the process of bouton forming, and one of the proteins known to be involved in this process is Futsch (Roos et al., 2000). Since it has been already reported that in *tbph*$^{\Delta 23}$/-, flies possess a downregulation of Futsch (Godena et al., 2011), we decided to check Futsch levels also in larvae with silenced TBPH in muscles.

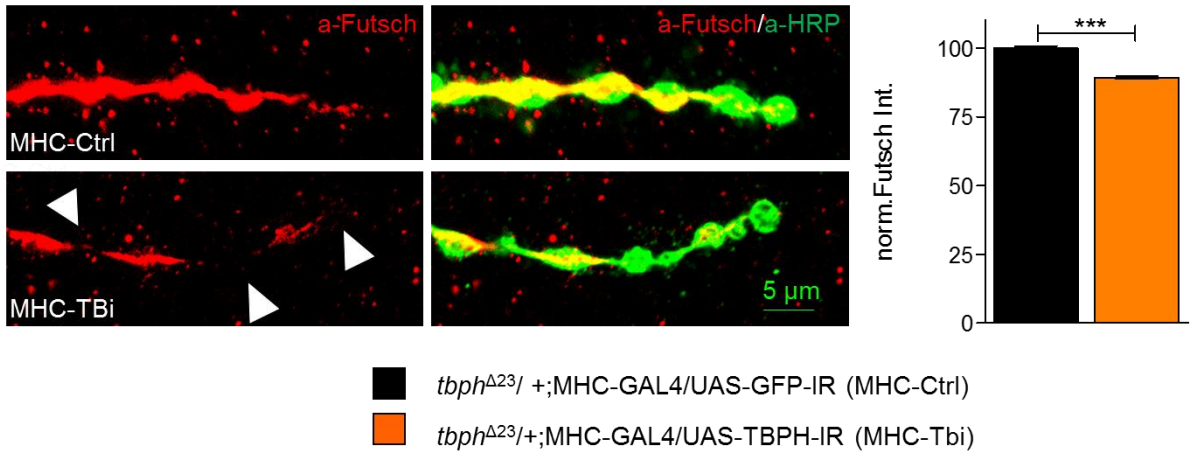

Figure 35: ***Futsch was significantly reduced in flies with silenced TBPH in muscles.*** *Confocal images of third instar NMJ terminals in muscle 6 / 7 second segment stained with anti-HRP (in green) and anti-Futsch (in red) in MHC-Ctrl (tbph$^{\Delta 23}$/ +; MHC-GAL4/UAS-GFP-IR) and MHC-TBi (tbph$^{\Delta 23}$/+; MHC-GAL4/UAS-TBPH-IR). Arrows show boutons with reduced levels or absence of Futsch in boutons. Quantification of Futsch intensity was normalised on control.* ***p<0.001, calculated by T-test, Error bars SEM. N=20 larvae per genotype.

We observed deficiency of Futsch protein both in terminal and middle boutons, and a precise quantification revealed a reduction of Futsch level

for approximately 15%, which was statistically different from the control sample (Figure 35).

3.1.3. Dlg and glutamate receptors are downregulated

Observing the alteration in the presynaptic structures of NJM by TBPH silencing, we decided to investigate the organisation of the postsynaptic structures in NMJ, represented by muscles. Several proteins are required to ensure a functional neuronal transmission, among which Dlg and glutamate receptors (GluRIIA) are essential. The levels of these postsynaptic proteins have been already well characterised in *tbph*$^{\Delta 23}$/- flies, and significant downregulation of Dlg and GluRIIA was recorded (Romano et al., 2014). These experiments aimed to verify if silencing TBPH in muscles affected Dlg and GluRIIA levels.

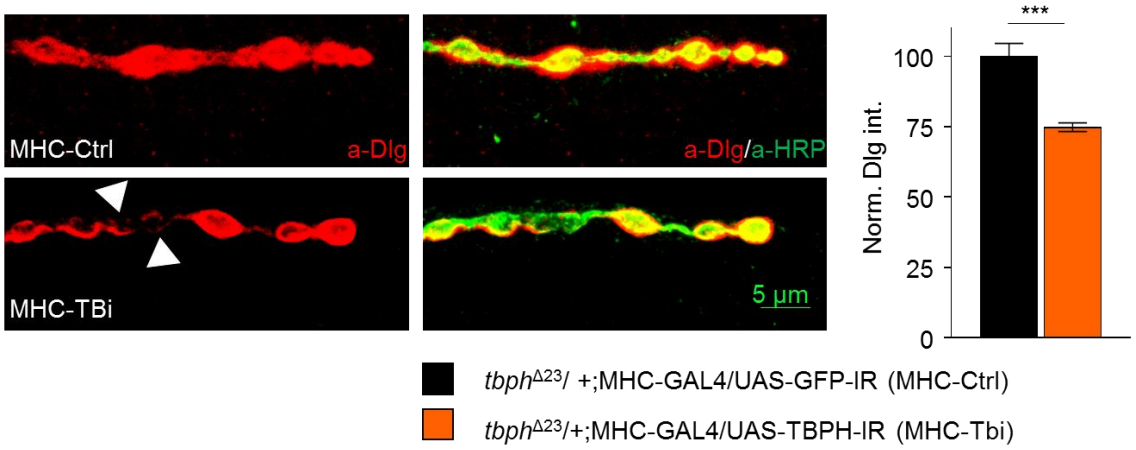

Figure 36: ***Dlg protein level was reduced by TBPH silencing in muscles.*** *Confocal images of the third instar NMJ terminals in muscle 6 / 7 second segment stained with anti-HRP (in green) and anti-Dlg (in red) in MHC-Ctrl*

($tbph^{\Delta 23}$/ +; MHC-GAL4/UAS-GFP-IR) and MHC-TBi ($tbph^{\Delta 23}$/+; MHC-GAL4/UAS-TBPH-IR) together with the quantification of Dlg intensity normalised on ctrl. Arrows point to the absence of the protein in the postsynaptic part of NMJ. ***p<0.001, calculated by T-test, Error bars SEM. *N=20 larvae per genotype.*

The wildtype control's boutons, marked with HRP (in green), are surrounded with the signal of the Dlg protein (in red) shaped like a circle, and not discontinued in any part of the synapsis. On the contrary, larvae expressing TBPH-IR revealed an altered protein distribution. We noticed that formed circles were discontinued, and most of the disruptions were located around the boutons lying in the middle of the branch (Figure 36). Moreover, Dlg signal quantification showed a reduction of about 25% on average in TBPH silenced larvae.

The other protein located in the postsynaptic part of the NMJ that we checked was the glutamate receptor, specifically the subunit A (GluRIIA). In the wildtype control, we could detect clusters of receptors (in red) forming a circle of the size of boutons (in green). In the TBi larvae, the glutamate receptor clusters were visibly reduced and, in some cases, even absent (Figure 37). By confocal microscopy quantification, the intensity of GluRIIA dropped by 30% in TBi larvae.

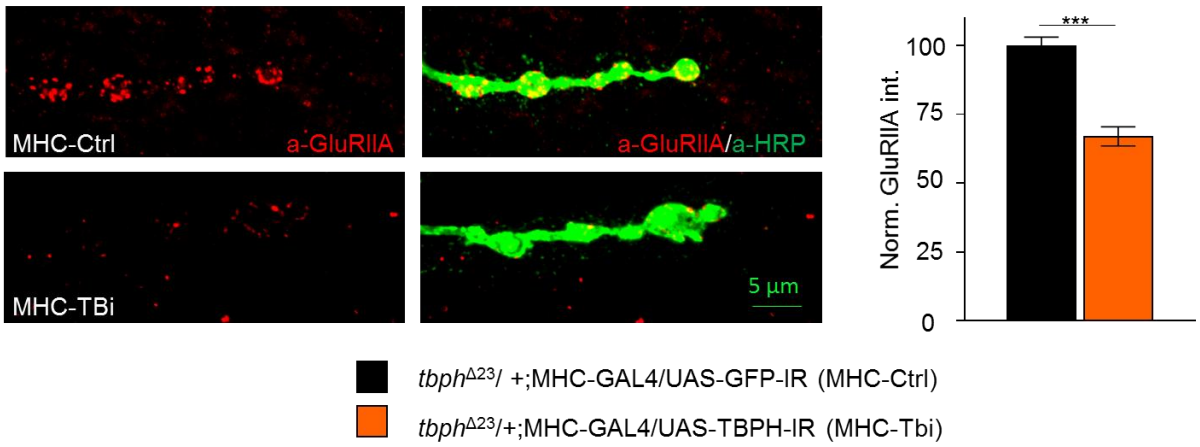

Figure 37: ***Glutamate receptors (subunit GluRIIA) are downregulated by TBPH silencing in muscles****. Confocal images of the third instar NMJ terminals in muscle 6 / 7 second segment stained with anti-HRP (in green) and anti-GluRIIA (in red) in MHC-Ctrl (tbph$^{\Delta 23}$/ +; MHC-GAL4/UAS-GFP-IR) and MHC-TBi (tbph$^{\Delta 23}$/+; MHC-GAL4/UAS-TBPH-IR) together with the quantification of GluRIIA intensity normalised on ctrl.* ***p<0.001, calculated by T-test, Error bars SEM. *N=20 larvae per genotype.*

3.2. TBPH rescue in *tbph*$^{\Delta 23}$/- flies

To confirm the previously described results and to get new insights into the role of TBPH in muscles, we decided to express TBPH protein in the muscles of *tbph*$^{\Delta 23}$/- flies and characterise both, the phenotype and the NMJ of these animals. My thesis work focused on the characterisation of the expression of UAS-TBPH with the Mef2-GAL4 driver in order to implement some preliminary data previously done with the MHC-GAL4 driver in our laboratory.

A crucial step was to verify a possible toxic effect due to the combination of Mef2-GAL4 driver and UAS-TBPH. Since the combination of Mef2-GAL4 and UAS-TBPH at 25°C resulted in being lethal (all progeny died in the stage of the first instar larva), we required reducing the protein expression level and took advantage of the co-expression of a regulatory protein, GAL80^{ts}, which blocks the expression of GAL4 protein at lower temperatures (19°C). Therefore, the protein is expressed in lower quantities, when the animals are exposed to 25°C. Thanks to GAL80^{ts}, it was possible to achieve full development, and the progeny fully developed reached adulthood at 25°C.

The peristaltic movements of larvae expressing both the Drosophila TBPH or the human TDP-43 did not show a significant difference, compared to UAS-GFP as the wild-type control. With that examined, we confirmed that

GAL80^{ts} co-expression and the 25°C temperature are conditions that ensure no toxicity at all in a gain of function and can therefore be used for rescuing a TBPH null phenotype larva (Figure 38).

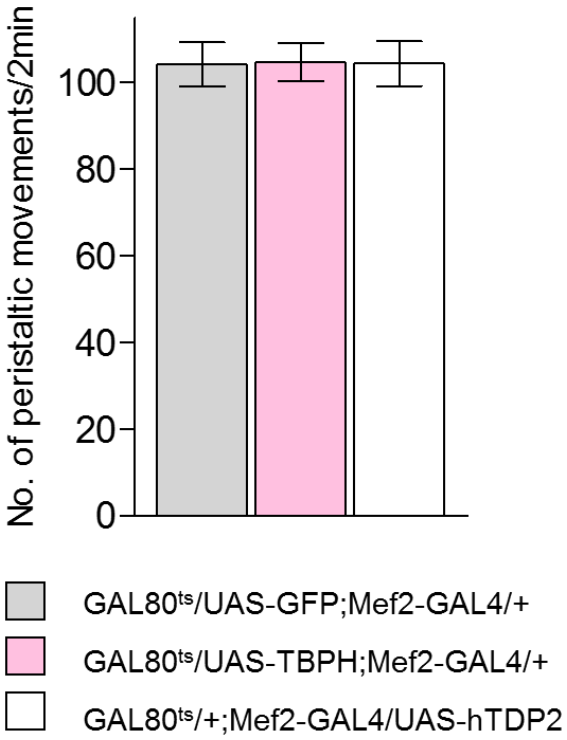

Figure 38: ***TBPH and hTDP expression with co-expression of GAL80^{ts} did not affect larval phenotype at 25°C.*** *Calculated by one-way ANOVA with Bonferroni correction, error bars SEM. N=20 larvae per genotype.*

3.2.1. The motility in larvae but not in adult flies is recovered

With the conditions set, we characterised both the larval and adult flies' phenotype. In all experiments, we had as control animals with *tbph*$^{\Delta 23}$/+ background, GAL80^{ts}, and Mef2-GAL4 driver. For rescuing the *tbph*$^{\Delta 23}$/-

background, GAL80^{ts} and Mef2-GAL4 driver were used to express the UAS-GFP as the negative control and UAS-TBPH or UAS-TDP-43 as crosses of interest.

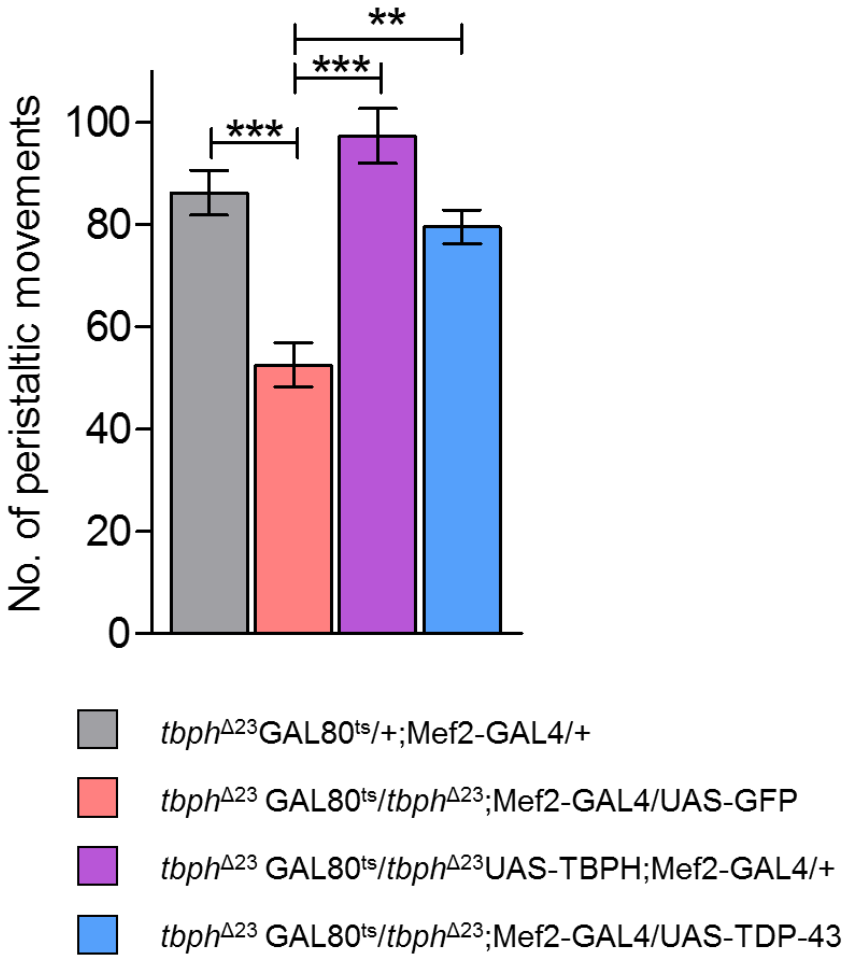

Figure 39: ***Larval motility was recovered by expressing TBPH or hTDP2 in muscles****. The number of peristaltic waves significantly raised in larvae expressing UAS-TBPH and UAS-TDP-43. **p<0.01, ***p<0.001 calculated by one-way ANOVA with Bonferroni correction, error bars SEM. N=20 larvae per genotype.*

While wild-type larvae reached an average of 90 peristaltic waves in two minutes, larvae with null alleles for TBPH presented a reduced number of peristaltic waves of approximately 50%. The expression of UAS-TBPH exclusively in muscles rose up the number of peristaltic waves to the level of wild-type control rescuing the *tbph*$^{\Delta 23}$/- background (Figure 39, purple column).

Moreover, human TDP-43 statistically recovered larval mobility compared to GFP. Human TDP-43-expressing larvae exhibited motility like the wild type control. The result implies that both proteins, TBPH, and human TDP-43, present the molecular features that allow larval movement recovery when expressed in muscles.

The larval movement recovery was apparent, because larvae expressing TBPH and TDP-43 never stopped or searched the surroundings like a *tbph*$^{\Delta 23}$/- larvae expressing GFP. They moved straight forward, with very little or no stops.

Even if both rescued genotypes, TBPH and TDP-43, reached the adult stage, they did not reveal a significant recovery. They resembled the phenotype showed by the null allele *tbph*$^{\Delta 23}$/-. The leg coordination was weak, and only a few flies walked normally. Moreover, their climbing performance was not outstanding.

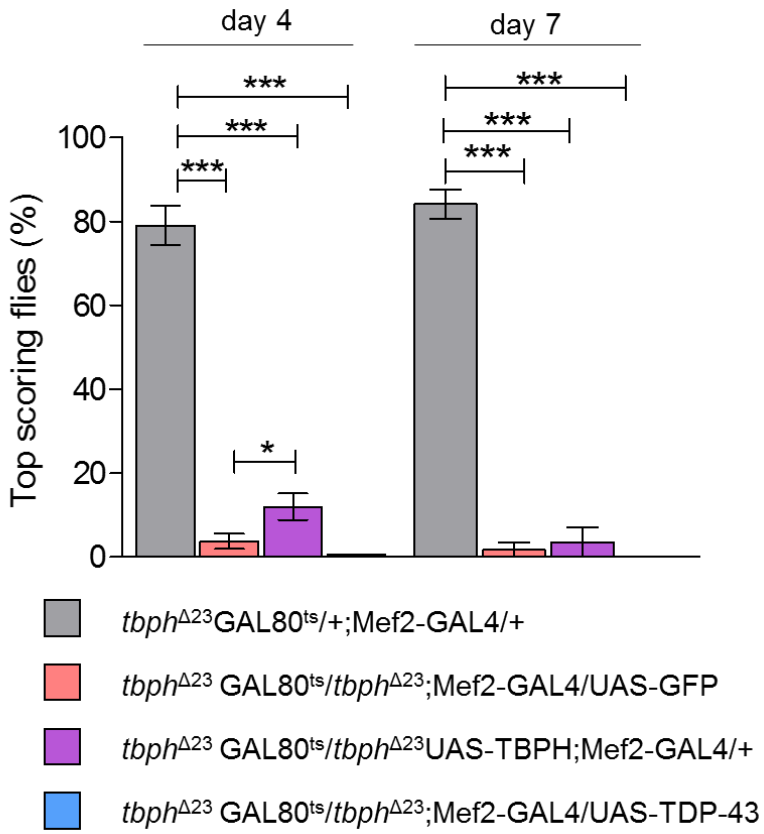

Figure 40: ***TBPH and TDP-43 expressing in muscles do not improve the climbing ability.*** *The percentage of flies that reached the top of the cylinder was not significantly higher in flies expressing UAS-TBPH or UAS-TDP-43 comparing to the negative control group (UAS-GFP) on day 4 and 7. *p<0.05 and ***p<0.001 calculated by one-way ANOVA with a Bonferroni correction, error bars SEM. N=200 flies per genotype.*

Although on day 4 of the climbing assay, flies expressing TBPH in muscles climbed significantly better than the ones expressing GFP (Figure 40), on day 7, TBPH-expressing flies were too weak to climb. Moreover, human TDP-43 did not rescue climbing ability at all.

Thinking that a walking assay may be less demanding than a climbing one, we challenged rescued flies to perform a walking assay. Flies with TBPH

expression in muscles performed significantly better (Figure 41), they walked almost 9 cm, whereas the negative control reached a maximum length of 2 cm.

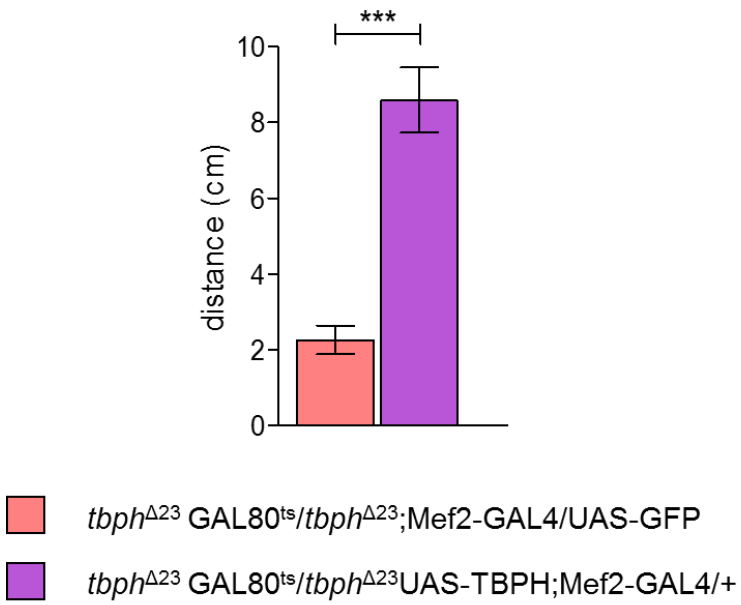

Figure 41: ***Flies expressing TBPH in muscles walked a greater distance.*** *Walking assay analysis of flies expressing UAS-GFP and UAS-TBPH using Mef2-GAL4 at day 2. ***p<0.001 calculated by t-test, error bars SEM. N = 50 flies per genotype.*

Even though the expression of TBPH or TDP-43 respectively rescued the climbing ability of the adult flies only partially or not at all, we tracked the events of deaths. We aimed to evaluate whether a prolong life span can be seen – neither the muscular expression of TBPH nor the one of TDP-43 prolonged the lifespan (Figure 42).

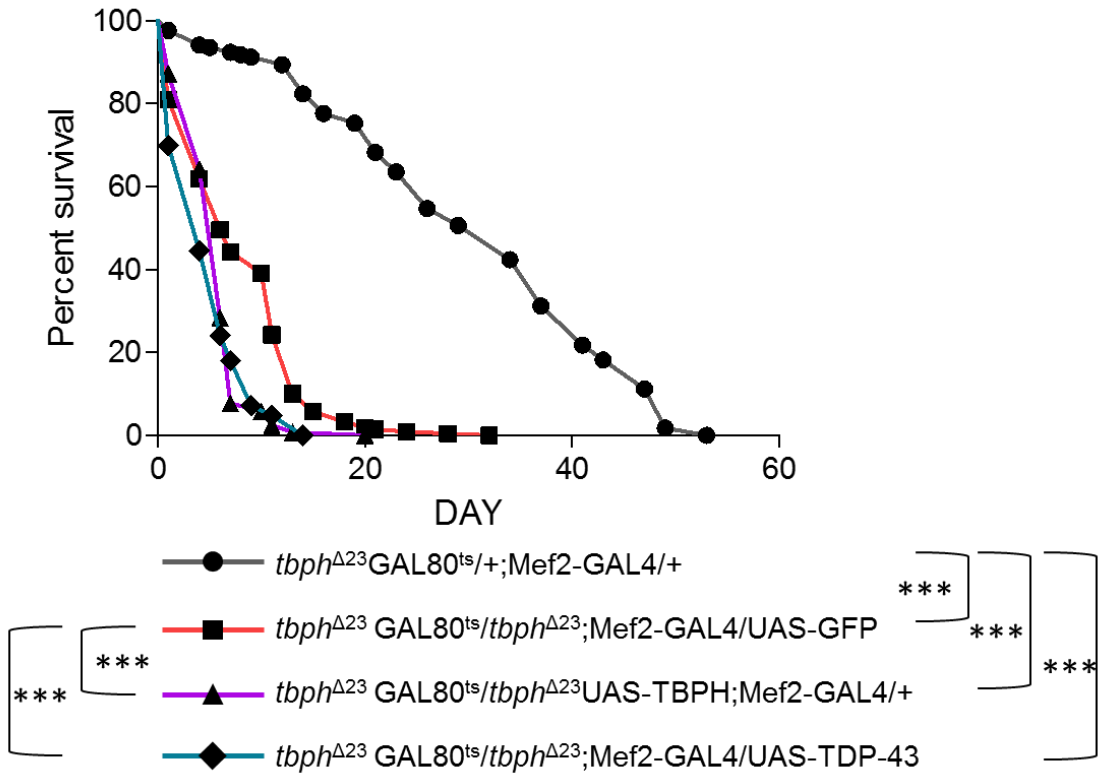

Figure 42: ***TBPH and TDP-43 expression in muscles did not rescue the phenotype.*** *The lifespan of flies expressing TBPH, TDP-43, and GFP. Statistical analysis was calculated with the log-rank test. ***p<0.001. N=200 flies per genotype.*

All the three genotypes in *tbph*$^{\Delta 23}$/- background, expressing any of the UAS-gene (UAS-GFP, UAS-TBPH or UAS-TDP-43), lived significantly shorter than the wild-type control. The statistics were done with Log-rank test for overall survival and Gehan-Breslow-Wilcoxon test for early death events. In both cases, the p-value was less than 0.001.

Intriguing, we also found a significant difference between flies expressing GFP and flies expressing TBPH or TDP-43. Accordingly to the Log-rank

test, with a p-value less than 0.001, the expression of both TBPH or TDP-43 shorten the lifespan overall, which implies a toxic effect of both proteins when expressed in adult phase (Figure 42 red, purple, and blue lines). To check this hypothesis, we overexpressed TBPH and TDP-43 in wild-type background for TBPH, using Mef2-GAL4 as a driver and $GAL80^{ts}$ at 25°C, evaluating whether the expression of proteins by itself caused shorter lifespan and reduced climbing activity.

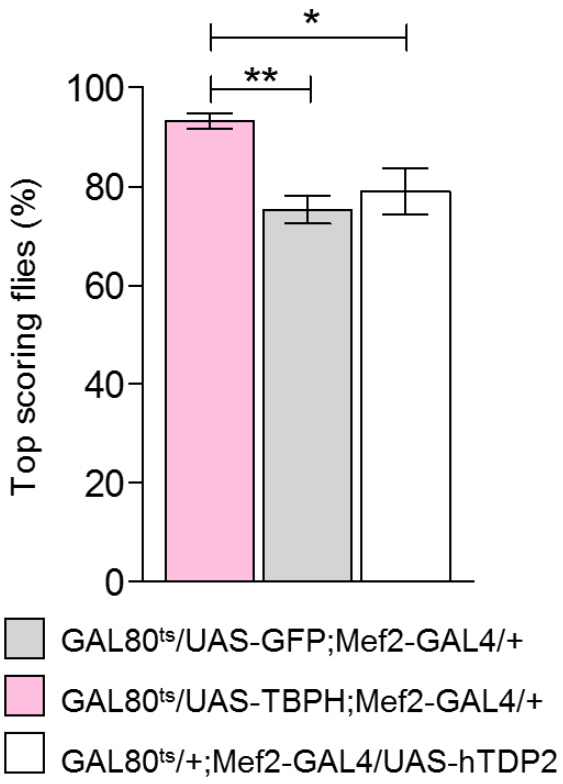

Figure 43: ***Flies expressing TBPH or TDP-43 climbed worse than the wild type.*** *The percentage of flies that reached the top of the cylinder is significantly lower in flies expressing UAS-TBPH or UAS-TDP-43 comparing to a positive control group (UAS-GFP) on day 4. *p<0.05 and **p<0.01 calculated by one-way ANOVA with a Bonferroni correction, error bars SEM. N=200 flies per genotype.*

The climbing assay performed on day 4, had already shown defects in climbing performance of flies that, in wild type background, expressed TBPH and TDP-43 in muscles. A reduction of approximately 15% and 20%, for flies expressing TDP-43 and TBPH, respectively, was observed (Figure 43). Climbing results showed a slightly higher level of toxicity for TBPH compared to TDP-43, and the toxicity was much more evident comparing the lifespan of adult flies expressing TBPH and TDP-43 in muscles.

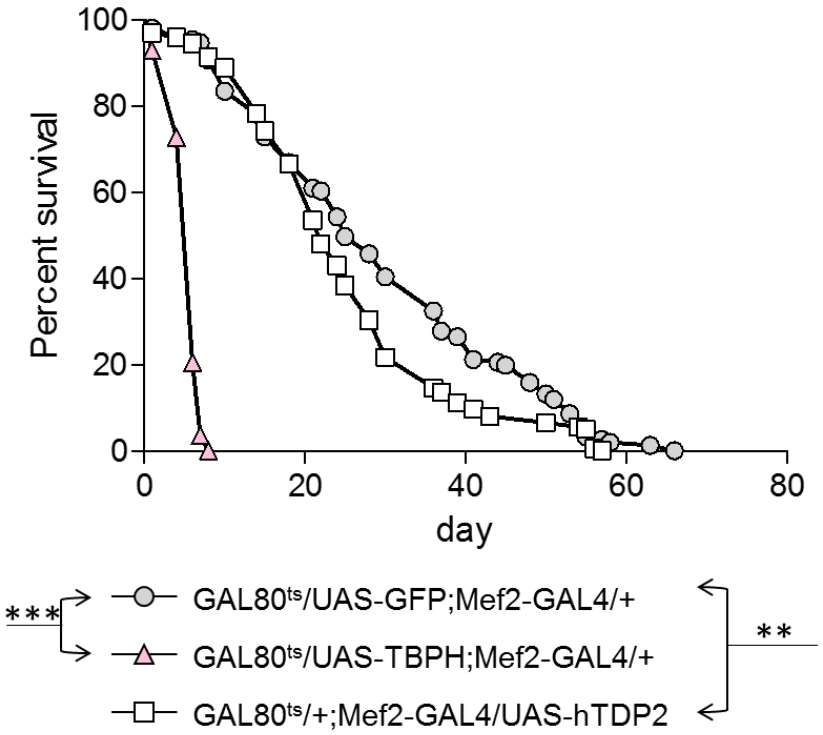

Figure 44: ***Lifespan was significantly shorter in flies expressing TBPH and TDP-43 in muscles.*** *The lifespan of flies expressing TBPH, TDP-43, and GFP in a wild-type background. Statistical analysis was calculated with the log-rank test. **p<0.01 and ***p<0.001. N=200 flies per genotype.*

Calculated by both statistical tests, log-rank test, and Gehan-Breslow-Wilcoxon test, the difference was significant between TBPH and TDP-43 versus GFP expression, but also between TBPH and TDP43 (Figure 44).

In conclusion, impaired climbing in adult flies allowed us to deduce the toxicity of TBPH or TDP-43 expression in adult muscles. However, the level of toxicity was not as high as to explain the missed rescue of TBPH null adult flies expressing either TBPH or TDP-43 in muscles. Consequently, since TBPH expression in larvae did not induce any toxicity and, moreover, the TBPH null phenotype was rescued, we decided to further investigate the mechanism of rescue by immunostainings of NMJs in larvae.

3.2.2. NMJ growth and shape are recovered

Our previous experiments revealed some aspects of TBPH role in muscles. Its silencing-induced impairment of larval movements and alterations at the NMJ level, as summarised in Table 2. Thus, we were wondering if the rescue of the peristaltic waves obtained by the TBPH expression in muscles could be explained by a recovery of NMJ features like the number of branches, bouton shapes or Dlg and GluIIRA distribution.

Table 2: ***Characterisation of larvae with silenced TBPH****. While the number of branches remained unmodified, the percentage of regular boutons dropped, and thus Dlg and GluRIIA levels.*

CHARACTERISTICS	TBPH silencing in muscles
Number of terminal branches	=
Bouton shape	↓
Dlg levels	↓
GluRIIA levels	↓

We characterised NMJ growth by counting branches marked with αHRP antibodies. We compared wild-type larvae to *tbph*$^{\Delta 23}$/- flies expressing or UAS-TBPH, for rescuing, or UAS-GFP, as a negative control, in muscles. Statistical analysis of confocal images showed significant recovery in the number of branches when expressing TBPH (Figure 45). We obtained eight branches on average, as in the wild-type control, while *tbph*$^{\Delta 23}$/- larvae expressing GFP had a reduced number of branches matching the previously reported number for mutants (Feiguin et al., 2009).

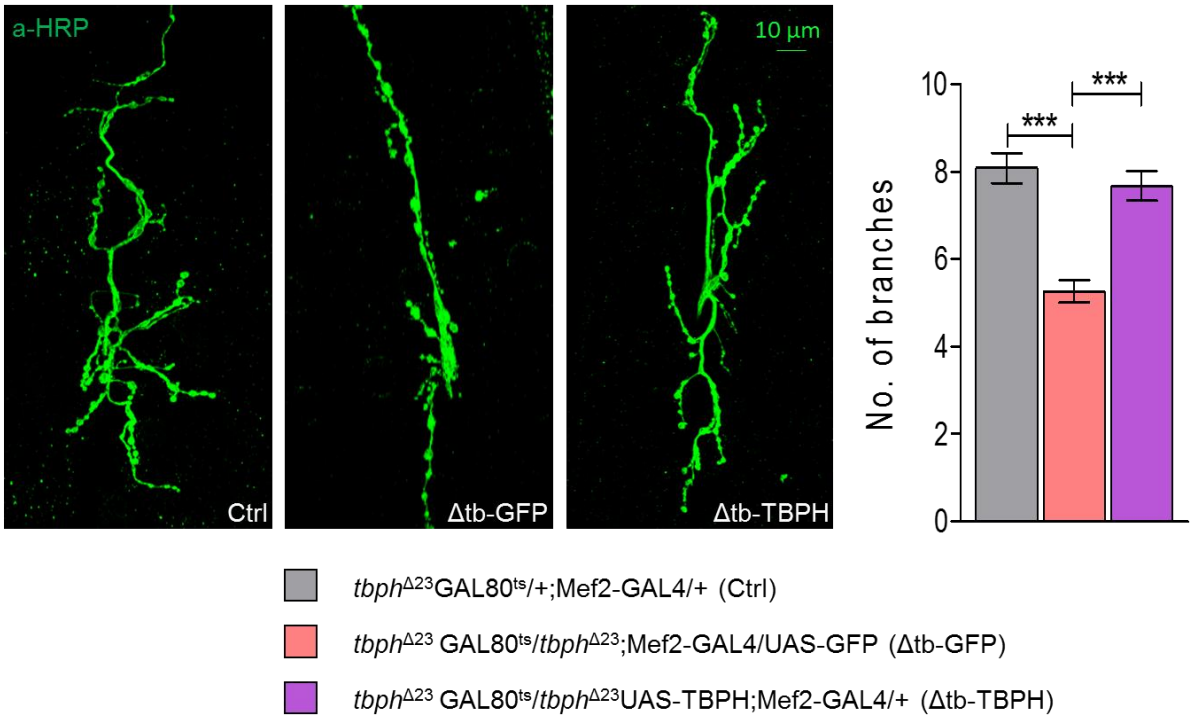

Figure 45: ***The number of branches was recovered in larvae expressing TBPH in muscles.*** Confocal images of the third instar NMJ terminals in muscle 6 / 7, second segment stained with anti-HRP (in green). The representative terminals are shown, together with the quantification. ***p<0.001, calculated by one-way ANOVA with Bonferroni correction, error bars SEM. N = 20 larvae per genotype.

On the same samples, on which branching was evaluated, we performed quantification and characterisation of bouton shape. Even if a small number of irregular boutons could be detected in wild type larvae, the percentage of misshaped boutons significantly increased in TBPH null larvae (Figure 46). The NMJ of mutant larvae presented about 40% more irregular boutons in comparison to the wild type control. The regular ones that are around 70% of all boutons in wild-type larvae reach only to 30% in the case of the TBPH null larvae.

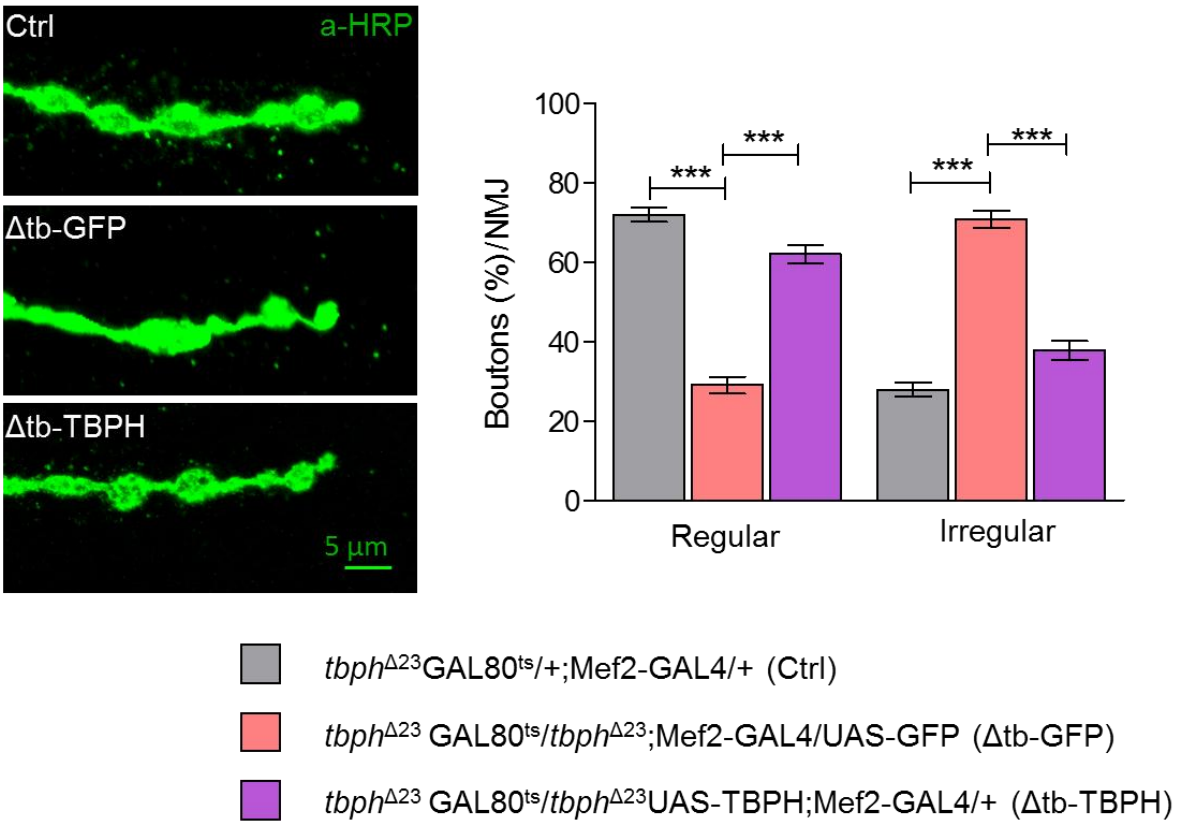

Figure 46: ***The percentage of regular boutons increases when TBPH was expressed in larval muscles.*** Confocal images of the third instar NMJ terminals in muscle 6 / 7, second segment stained with anti-HRP (in green). The representative bouton shapes are shown, together with the quantification. ***p<0.001, calculated by one-way ANOVA, error bars SEM. N = 20 larvae per genotype.

In the case of muscular rescue with TBPH in null larvae, the percentage of regular boutons almost matched the wild-type control. Therefore, a significant recovery in terms of the number of regular boutons was achieved.

Therefore, even if the silencing of TBPH in muscles did not alter the branches of NMJ and made us believe that the TBPH level present in

muscles did not control NMJ branching, the rescue performed in muscles demonstrates the opposite. TBPH expressed in muscles may influence the branches of the synapsis.

3.2.3. Dlg and glutamate receptors are recovered, as well as NMJ function

In our previous results, we demonstrated, that TBPH silencing, exclusively in muscles, affected Dlg and glutamate receptors levels in the postsynaptic region of NMJ and the same was true for TBPH mutant larvae (Romano et al., 2014). We wondered whether muscular TBPH expression in mutant larvae could influence the levels of Dlg and GluRIIA and augment them. To characterise these synaptic markers, we double-stained NMJ with αHRP and antibodies αDlg or αGluRIIA.

The Dlg level in mutants expressing GFP was reduced for approximately 50% with an altered distribution compared to the wild-type ones. Gaps in the Dlg pattern were frequent, and moreover, some boutons did not present any Dlg signal. TBPH rescue in muscles induced a complete recovery of the signal pattern (Figure 47). The intensity of the quantified Dlg signal was statistically higher in the TBPH rescue compared to the GFP control reaching almost a wild-type level.

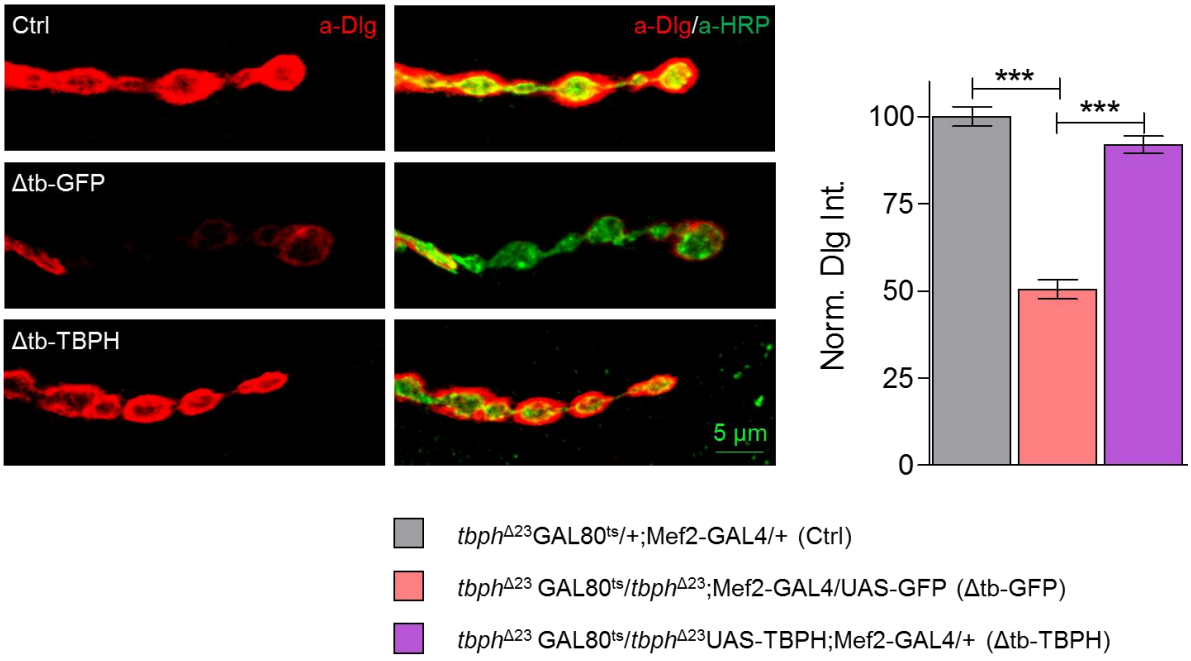

Figure 47: ***Dlg protein level was recovered after overexpression of TBPH in muscles.*** *Confocal images of the third instar NMJ terminals in muscle 6 / 7 second segment stained with anti-HRP (in green) and anti-Dlg (in red) in Ctrl ($tbph^{\Delta 23}GAL80^{ts}$/+; Mef2-GAL4/+), Δtb-GFP ($tbph^{\Delta 23}$ $GAL80^{ts}$/$tbph^{\Delta 23}$; Mef2-GAL4/UAS-GFP) and Δtb-TBPH ($tbph^{\Delta 23}$ $GAL80^{ts}$/$tbph^{\Delta 23}$UAS-TBPH; Mef2-GAL4/+), together with the quantification of Dlg intensity normalised on ctrl.* ***p<0.001, calculated by one-way ANOVA with Bonferroni correction, Error bars SEM. *N=20 larvae per genotype.*

Staining glutamate receptors in wild type synapsis showed clustered receptors (red signal) distributed as circles in the bouton area (green signal), while there was a significant drop of signal intensity in TBPH mutants, together with an alteration of the distribution with less or no clusters per bouton (Figure 48). Recover of the signal intensity and the distribution was observed in the larvae rescued with TBPH in muscles, compared to the GFP expressing ones. Nevertheless, the intensity of the GluIIRA signal was still statistically lower than the one of the wild-type controls.

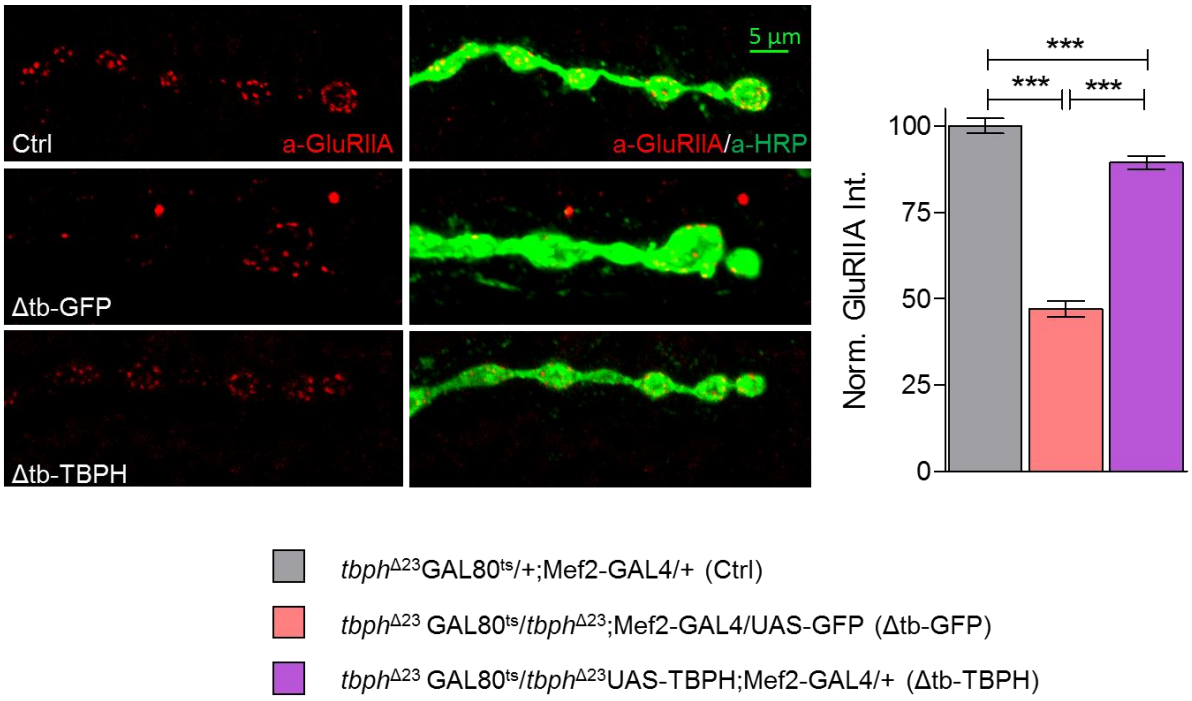

Figure 48: ***Level of glutamate receptors was recovered in mutant larvae expressing TBPH in muscles.*** *Confocal images of the third instar NMJ terminals in muscle 6 / 7 second segment stained with anti-HRP (in green) and anti-GluRIIA (in red) in Ctrl (tbph$^{\Delta 23}$GAL80^{ts}/+; Mef2-GAL4/+), Δtb-GFP (tbph$^{\Delta 23}$ GAL80^{ts}/tbph$^{\Delta 23}$; Mef2-GAL4/UAS-GFP) and Δtb-TBPH (tbph$^{\Delta 23}$ GAL80^{ts}/tbph$^{\Delta 23}$UAS-TBPH; Mef2-GAL4/+) together with the quantification of GluRIIA intensity normalised on ctrl.* ***p<0.001, calculated by one-way ANOVA with Bonferroni correction, Error bars SEM. *N=20 larvae per genotype.*

Overall, expressing TBPH in muscles of TBPH null mutants manifested in the phenotypic recovery of peristaltic waves, complete recovery of branching, regular bouton percentage, Dlg levels, and partial rescue of GluIIRA levels. Therefore, our interest moved to investigate whether the evoked junctional potential (EJP) was recovered in the rescued genetic background. All EJP experiments were done in collaboration with Aram

Megighian from University of Padova, Department of Biomedical Sciences.

The EJP of wild type larvae was about 40mV and dropped to 10mV in TBPH null larvae. The TBPH muscular rescue of mutant larvae effectively increased the EJP, but only partially. The average value did not reach wild type values. Partial recovery of EJP in the TBPH muscular rescue reached approximately 50% of the wild-type value (Figure 49). This could be explained by partial recovery of the GluIIRA, and this may be true also for other synaptic components causing a lower EJP in the rescued larvae.

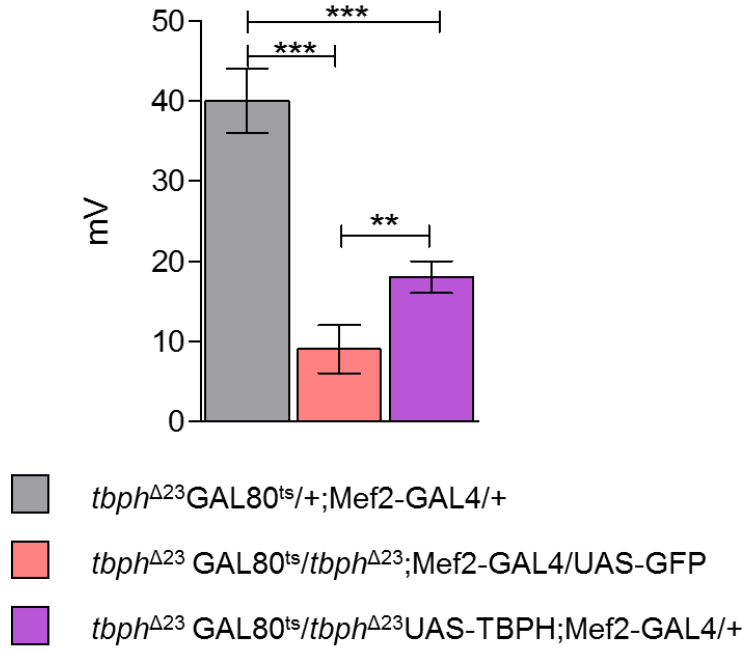

Figure 49: ***Evoked junctional potential in mutant larvae expressing TBPH was recovered****. Representative EJPs evoked by segmental nerve stimulation of Ctrl (tbph$^{\Delta 23}$GAL80^{ts}/+; Mef2-GAL4/+), Δtb-GFP (tbph$^{\Delta 23}$ GAL80^{ts}/tbph$^{\Delta 23}$; Mef2-GAL4/UAS-GFP) and Δtb-TBPH (tbph$^{\Delta 23}$ GAL80^{ts}/tbph$^{\Delta 23}$UAS-TBPH; Mef2-GAL4/+) in*

*muscle fibre 6 / 7 of A3 in third instar larvae. For each fibre 5, EPPs following 0.5Hz stimulation were considered. **p<0.01, ***p<0.001 calculated by one-way ANOVA with Bonferroni correction, error bars SEM. N = 10 larvae per each genotype.*

3.3. Dlg rescues *tbph*$^{\Delta 23}$/- flies

Alterations of Dlg levels in NMJs of both TBPH mutants and TBPH muscular silenced larvae have been observed in already published data (Romano et al., 2014) and the results previously presented here, respectively. Therefore, we wondered if the expression of Dlg exclusively in muscles might have influenced the neuromuscular growth. In order to proceed with this analysis, our first step was to check any possible toxicity related to UAS-DLG expression with Mef2-GAL4 driver in a wild type background.

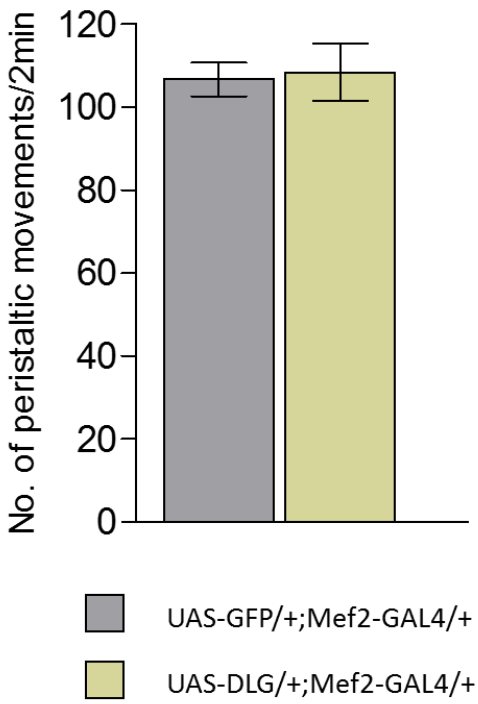

Figure 50: ***UAS-DLG expression with Mef2-GAL4 did not affect larval phenotype at 25°C.*** *Calculated by t-test, error bars SEM. N=20 larvae per genotype.*

Crosses were set at 25°C, and peristaltic movements of 20 third instar larvae per genotype were recorded. No differences in peristaltic movements were detected comparing to UAS-GFP expressing control. We concluded that there was no toxic effect expressing Dlg in muscles with Mef2-GAL4 driver at 25°C, which allowed us further rescue experiments (Figure 50).

3.3.1. Expression of Dlg in muscles rescues the phenotype in larvae, as well as in adult flies

After having confirmed the absence of toxicity for muscular expression of Dlg, we aimed to check whether a Dlg rescue in muscles could recover

the impaired phenotype of *tbph*$^{\Delta 23}$/- larvae and adult flies. Peristaltic waves of a positive (*tbph*$^{\Delta 23}$/+ larvae with driver Mef2-GAL4), a negative (*tbph*$^{\Delta 23}$/- larvae expressing UAS-GFP in muscles) control and an experimental genotype (*tbph*$^{\Delta 23}$/- larvae expressing UAS-DLG in muscles) were counted and it turned out that Dlg expressing larvae moved statistically faster in comparison with GFP expressing animals (Figure 51). Muscular Dlg expressing larvae moved steadily, with little or no stops and no searching of direction.

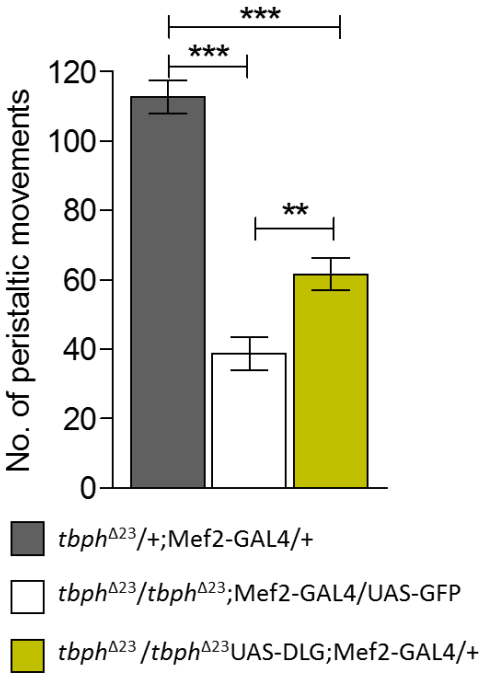

Figure 51: ***Dlg expression in muscles rescued the larval phenotype.*** *The number of peristaltic waves significantly raised in larvae expressing UAS-DLG comparing to larvae expressing UAS-GFP. **p<0.01, ***p<0.001 calculated by one-way ANOVA with Bonferroni correction, error bars SEM. N=20 larvae per genotype.*

Nevertheless, the total number of peristaltic movements was not comparable to the one detected in positive control. While a Dlg expressing larvae reached up to 70 peristaltic waves, the control moved about 110-times in two minutes (Figure 51).

Despite a partial rescue, we decided to characterise the phenotype in adult flies testing climbing ability and tracking the aging. Indeed, we managed to see the improvements in the climbing assay. The flies expressing Dlg protein performed better in climbing than control flies expressing GFP (Figure 29). We measured the climbing abilities at four different time points: day 4, 7, 14, and 21. At day 4, we obtained a statistically significant recovery in the climbing ability of Dlg expressing flies compared to GFP expression that just barely climbed and mainly remained at the bottom of the cylinder. The climbing ability of Dlg expressing flies reduced with aging; nevertheless, on day 21, 5% of flies managed to reach the top of the cylinder. However, it must be underlined that the climbing performance of Dlg rescued flies did not reach the wildtype control values even if we could observe the improvement of leg coordination, which in some cases was not different from the wild type.

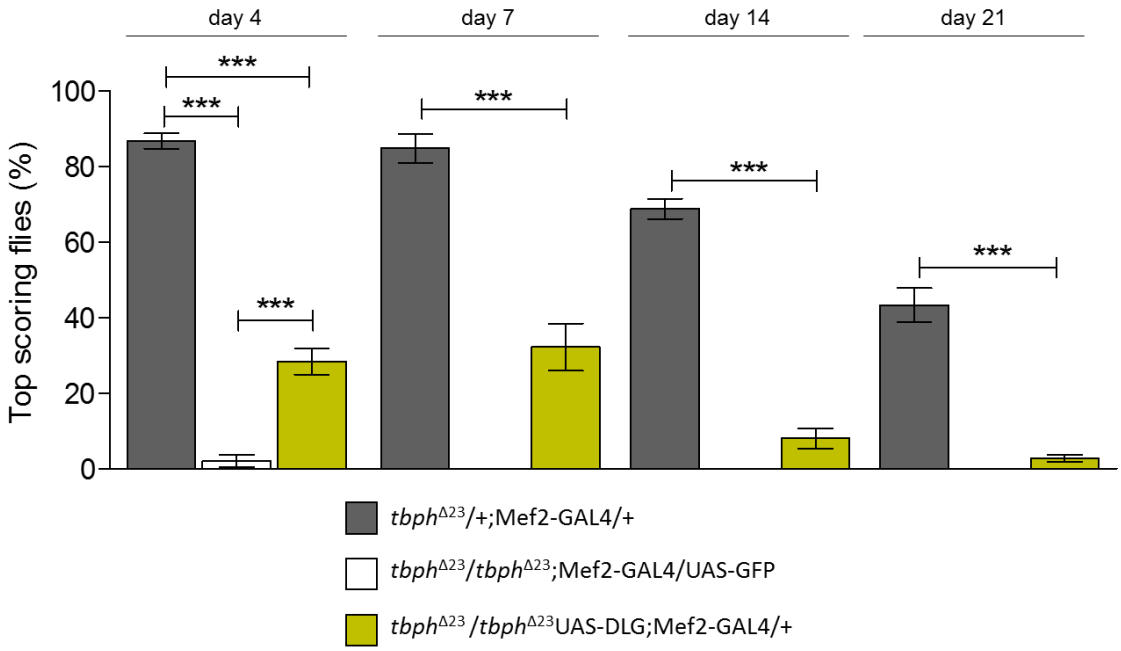

Figure 52: ***Climbing performance was significantly improved when Dlg was expressed in muscles****. The percentage of flies that reached the top of the cylinder was significantly higher in flies expressing UAS-DLG comparing to the negative control (UAS-GFP) on day 4. ***p<0.001 calculated by one-way ANOVA with a Bonferroni correction, error bars SEM. N=200 flies per genotype.*

In parallel with the climbing assay, we tracked the survival rate of all three genotypes. Wildtype control survived for approximately 60 days while flies expressing GFP lived for only 15 days. More than 50% of them died already within ten days. The flies in *tbph*$^{\Delta 23}$/- background rescued with Dlg lived significantly longer than the GFP control; yet, Dlg expressing flies lived significantly shorter (considering both statistical tests) than the wildtype control. They lived for 49 days in total. The statistical significance calculated by log-rank test and Gehan-Breslow-Wilcoxon test was in both cases with a p-value less than 0.001 (Figure 53).

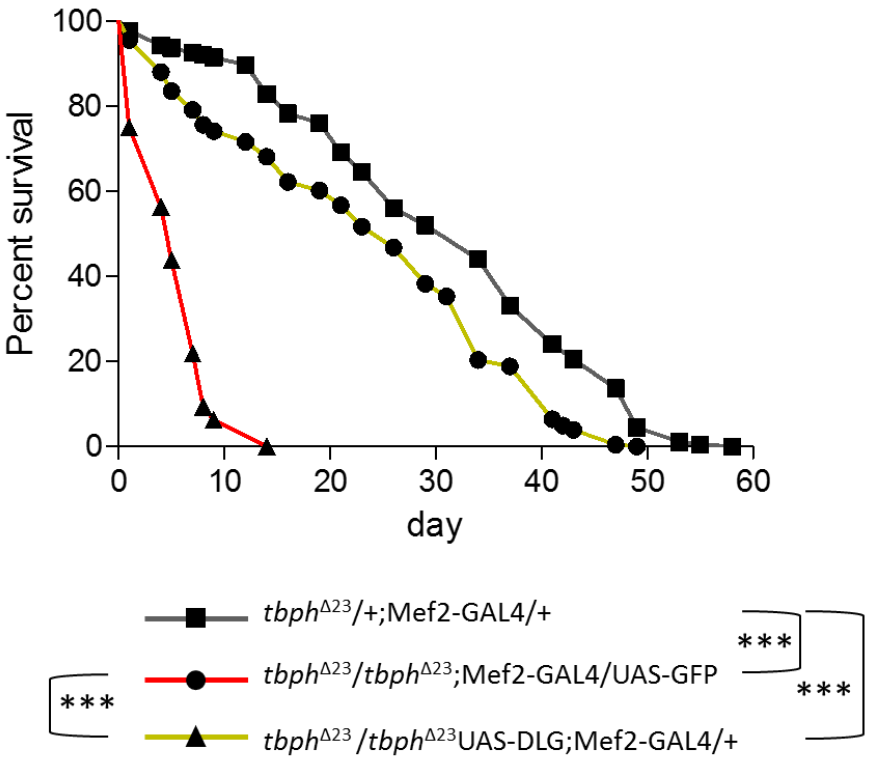

Figure 53: ***Flies expressing Dlg had a longer lifespan than mutant flies.*** *The lifespan of flies expressing only driver Mef2-GAL4, UAS-GFP and UAS-DLG. Statistical analysis was calculated with the log-rank test. ***p<0.001. N=200 flies per genotype.*

3.3.2. Expression of Dlg in muscles contributes to NMJ growth and function

The improved crawling ability of muscular Dlg rescued larvae induced us to perform immunostainings of NMJ to evaluate pre- and postsynaptic features of the NMJs of muscles 6 / 7 in the second segment. The branching and characterisation of bouton shape highlighted by HRP staining defined the organisation of the presynaptic part of the NMJ while the postsynaptic sector was characterised by glutamate receptor staining.

We counted seven to eight branches on average for each NMJ in a wild type control. The number significantly dropped to approximately four in the *tbph*$^{\Delta 23}$/- larvae expressing GFP. The *tbph*$^{\Delta 23}$/- larvae rescued in muscles by Dlg had branching recovered. We counted six to seven branches on average. Almost doubling the ones of the GFP expressing larvae and reaching a wild type level (Figure 54).

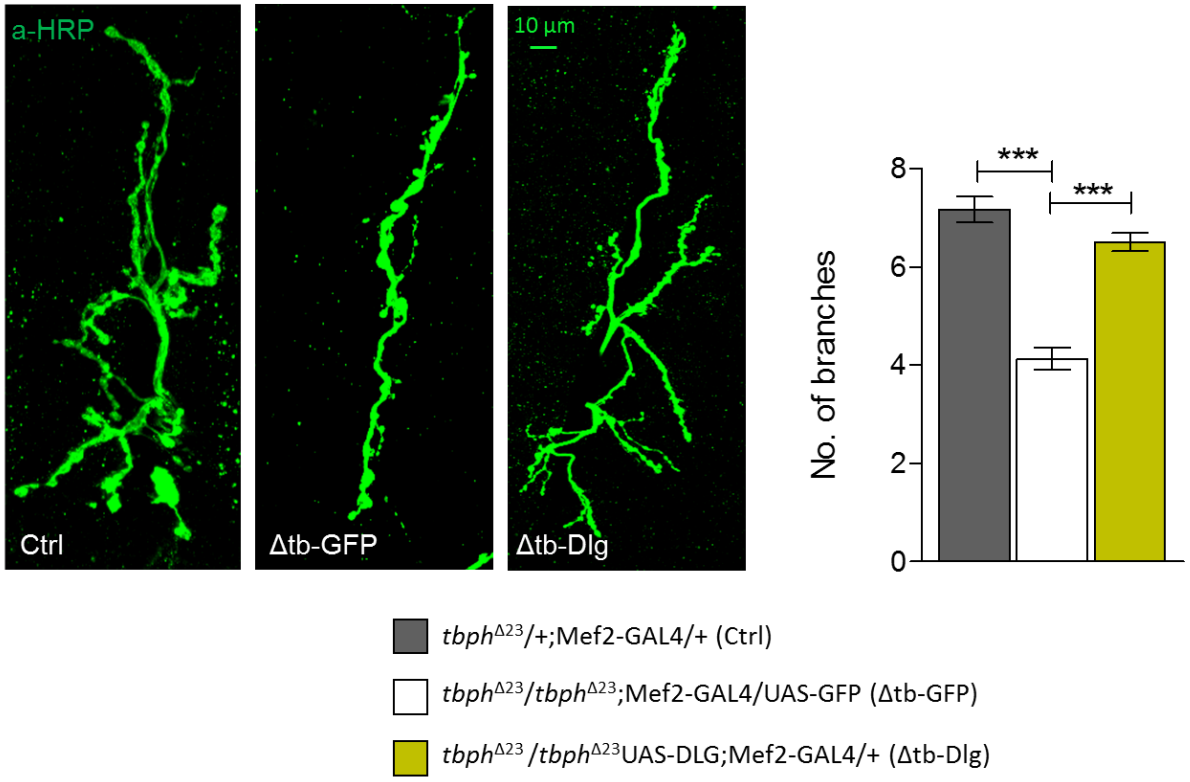

Figure 54: ***NMJ shape was recovered by Dlg expression.*** Confocal images of the third instar NMJ terminals in muscle 6 / 7, second segment stained with anti-HRP (in green). The representative terminals are shown, together with the quantification. ***p<0.001, calculated by one-way ANOVA with Bonferroni correction, error bars SEM. N = 20 larvae per genotype.

The same NMJs subjected to branch-counting were evaluated for bouton shape, to check whether Dlg might improve the percentage of adequately shaped boutons compared to *tbph*$^{\Delta 23}$/- larvae expressing GFP.

In wildtype larvae, we evaluated 70% of the boutons per NMJ as regular and 30% as irregular while the negative control (*tbph*$^{\Delta 23}$/- larvae expressing GFP) presented a reversed situation. More than 70% of NMJ boutons were classified as irregular and less than 30% as regular. Muscular expression of Dlg improved the percentage of regular and decreased the percentage of irregular boutons. On average, 50% of boutons resulted in being regular while the remaining 50% were irregularly shaped. Nevertheless, the outcome of regular boutons in Dlg-rescued larvae was still significantly lower than the wildtype control (Figure 55).

To complete the NMJ characterisation of larvae rescued with Dlg in muscle tissues, we evaluated the level of the GluIIRA in the postsynaptic compartment of NMJs at the second segment, muscles 6 / 7.

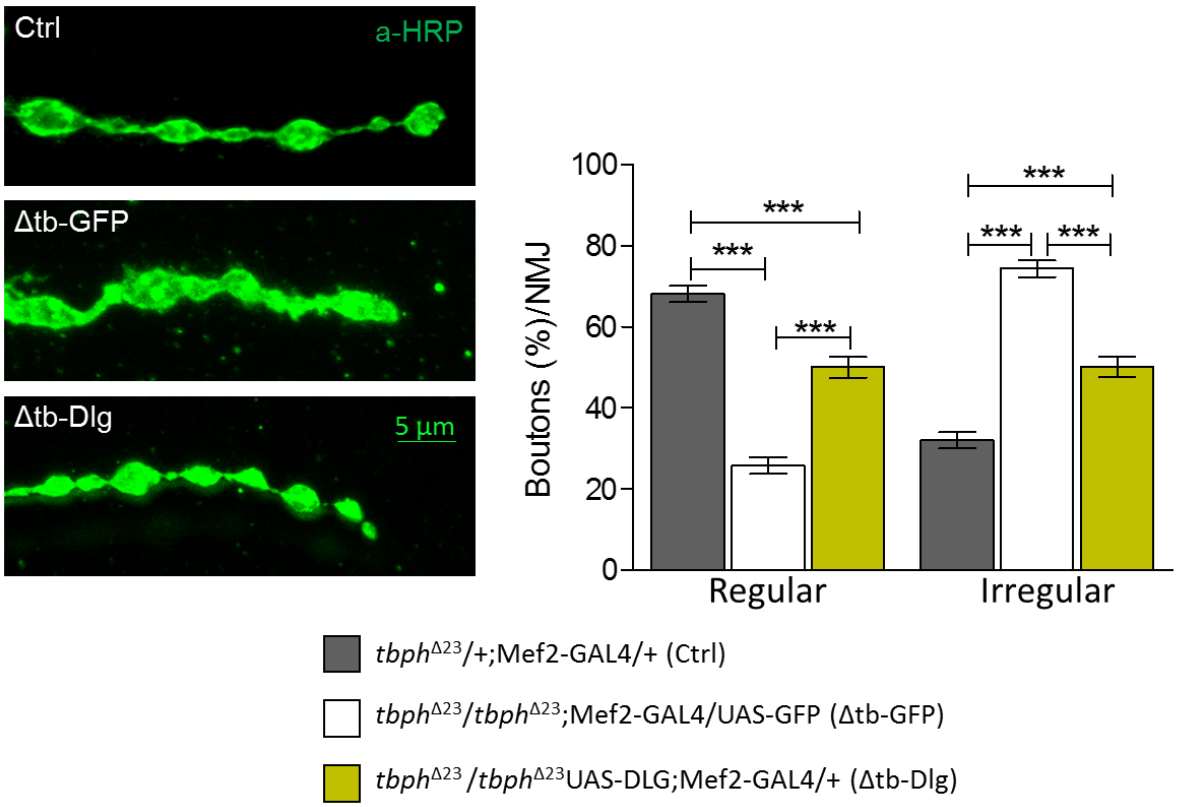

Figure 55: ***Larvae expressing Dlg had a higher percentage of regular boutons and a lower percentage of irregular ones***. Confocal images of the third instar NMJ terminals in muscle 6 / 7, second segment stained with anti-HRP (in green). The representative bouton shapes are shown, together with the quantification. ***p<0.001, calculated by one-way ANOVA, error bars SEM. N=20 larvae per genotype.

As previously reported, *tbph*$^{\Delta 23}$/- larvae manifest lower level of GluIIRA, and similarly, the muscular GFP rescued larvae appeared with significantly less glutamate receptors comparing to the wildtype control. In wild type background, glutamate receptors formed clusters right under boutons, yet, in mutants and, similarly in GFP rescued larvae, clustering of glutamate receptor was not so evident than in wild type control. The Dlg rescue in muscles resulted in statistically higher GluIIRA compared to the GFP

negative control, although it did not reach the intensity measured in wild type conditions (Figure 56).

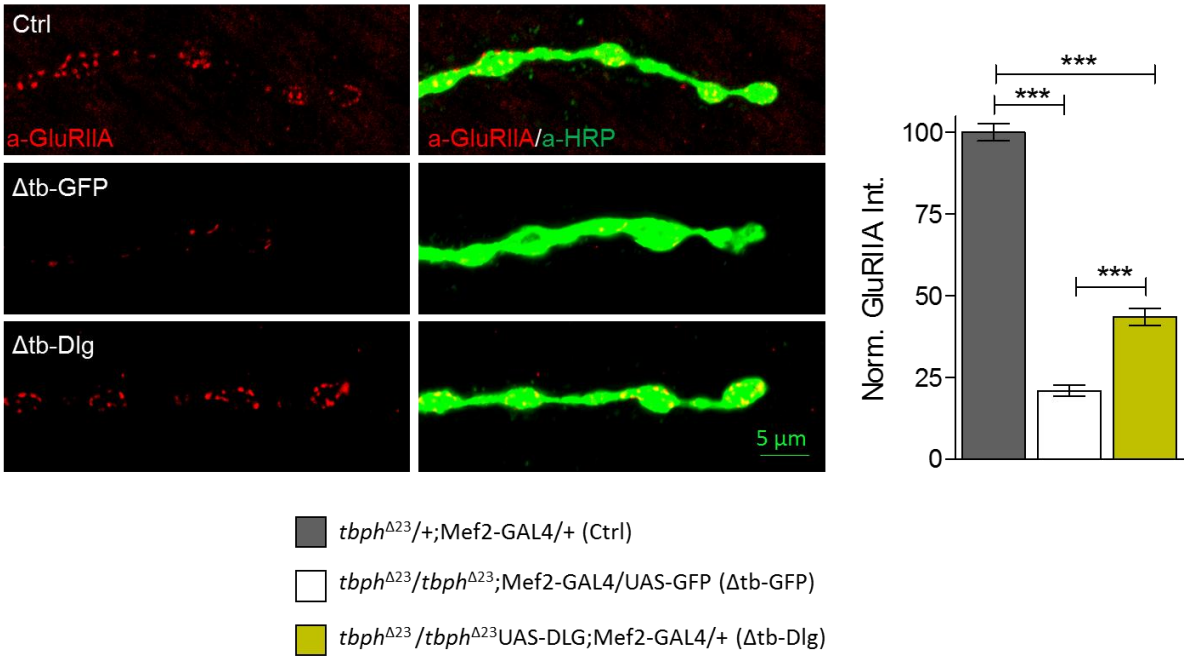

Figure 56: ***Dlg expression in muscles recovered the glutamate receptors level.*** *Confocal images of the third instar NMJ terminals in muscle 6 / 7 second segment stained with anti-HRP (in green) and anti-GluRIIA (in red) in Ctrl ($tbph^{\Delta 23}$/+; Mef2-GAL4/+), Δtb-GFP ($tbph^{\Delta 23}$/$tbph^{\Delta 23}$; Mef2-GAL4/UAS-GFP) and Δtb-Dlg ($tbph^{\Delta 23}$/$tbph^{\Delta 23}$UAS-DLG; Mef2-GAL4/+), together with the quantification of GluRIIA intensity normalised on ctrl.* ***p<0.001, calculated by one-way ANOVA with Bonferroni correction, Error bars SEM. *N=20 larvae per genotype.*

Consistent with this result, higher EJP was observed in larvae rescued with Dlg in muscles. Even if the rescued muscular Dlg larvae did not reach the 40 mV of the wild type control, they resulted in statistically higher values to one of the TBPH mutant larvae expressing GFP as control

(10mV) (Figure 57). Additionally, the Dlg rescue and TBPH rescue in muscles ended up with comparable EJP values (compare with Figure 49).

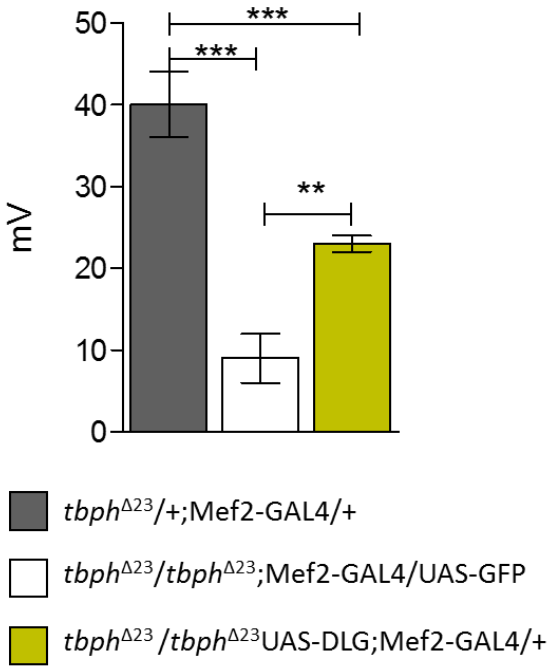

Figure 57: ***The evoked junctional potential was rescued when Dlg was expressed in muscles.*** *Representative EJPs evoked by segmental nerve stimulation of tbph$^{\Delta 23}$/+; Mef2-GAL4/+, tbph$^{\Delta 23}$/tbph$^{\Delta 23}$; Mef2-GAL4/UAS-GFP and tbph$^{\Delta 23}$ /tbph$^{\Delta 23}$UAS-DLG; Mef2-GAL4/+ in muscle fibre 6 / 7 of A3 in third instar larvae. For each fibre 5, EPPs following 0.5Hz stimulation were considered. **p<0.01, ***p<0.001 calculated by one-way ANOVA with Bonferroni correction, error bars SEM. N = 10 larvae per each genotype.*

3.3.3. Expression of Dlg in neurons improve the mobility of larvae

Since it is known that Dlg protein can be found in both muscles and neurons in Drosophila (Astorga et al., 2016), and additionally, our previous results of TBPH silencing in muscles demonstrated a direct correlation

with Dlg protein level, we tried to explore the interactions between TBPH and Dlg also in neurons. For this reason, we performed a western blot on adult heads of both TBPH null flies and a TBPH rescued flies performed with the pan-neural driver Elav-GAL4 (Figure 58).

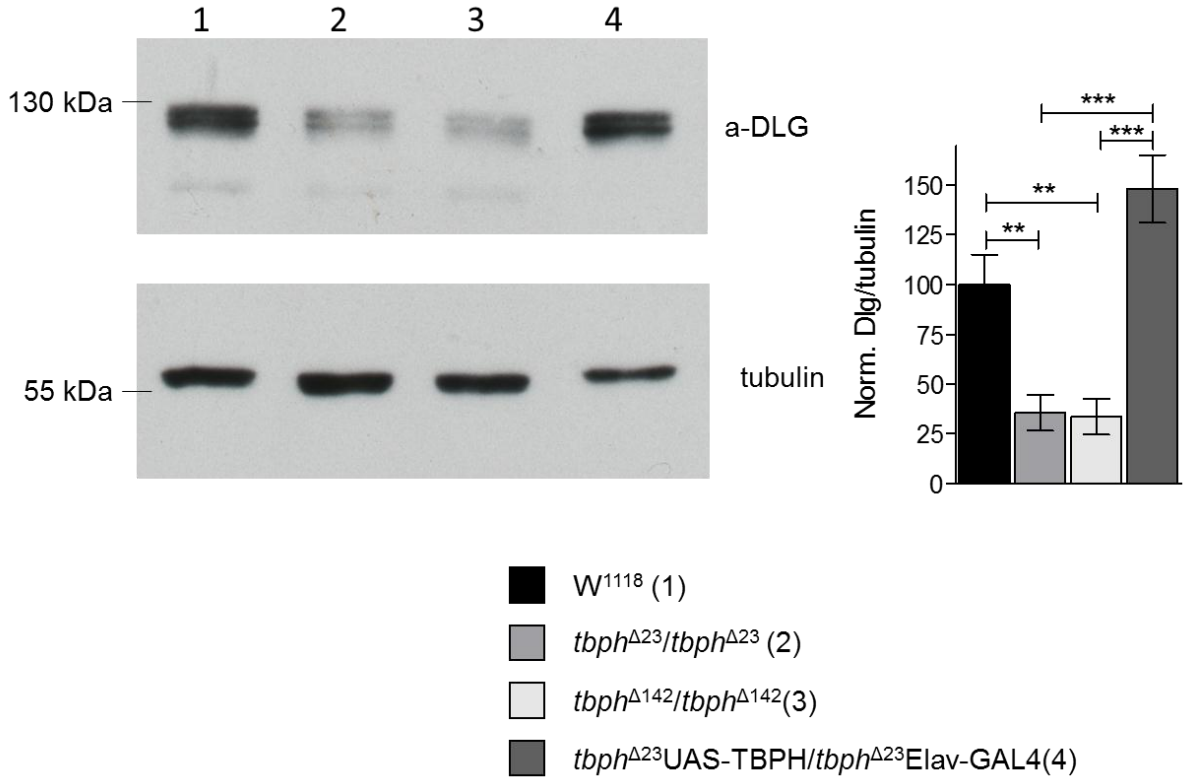

Figure 58: ***In TBPH mutants, Dlg levels were downregulated. Expression of TBPH recovered the intensity.*** *Western blot analysis of lane 1 (w^{1118}), lane 2 ($tbph^{\Delta 23}/tbph^{\Delta 23}$), lane 3 ($tbph^{\Delta 142}/tbph^{\Delta 142}$) and lane 4 ($tbph^{\Delta 23}$UAS-TBPH /$tbph^{\Delta 23}$ Elav-GAL4). Adult brains, one day old, were probed with anti-Dlg and alpha-tubulin antibodies. The same membrane was probed with the two antibodies, and the bands of interest were cropped. Quantification of normalised amounts was reported below each lane. n=3 (biological replicates).*

The level of Dlg in the adult brain of $TBPH^{-/-}$ flies dropped to less than 50% compared to W^{1118} flies, and the result was consistent for both TBPH mutants, $tbph^{\Delta 23}$/- (lane 2) and $tbph^{\Delta 142}$/- (lane 3). The difference with W^{1118} was significant. When TBPH was expressed in neurons with Elav-GAL4 driver, Dlg levels were significantly recovered to the level obtained at W^{1118} (Figure 58).

According to western blot results, we decided to express Dlg in neurons and examine the phenotype and some characteristics of NMJs in the third instar larvae.

We used a pan-neuronal driver nSyb-GAL4. Before we began with the experiment, we set the conditions. We set two experimental crosses. One progeny expressed GFP and the second Dlg, both with the driver mentioned above. The crosses were set at 25°C. To check the toxicity of the gene-driver combination, we performed the larval movement.

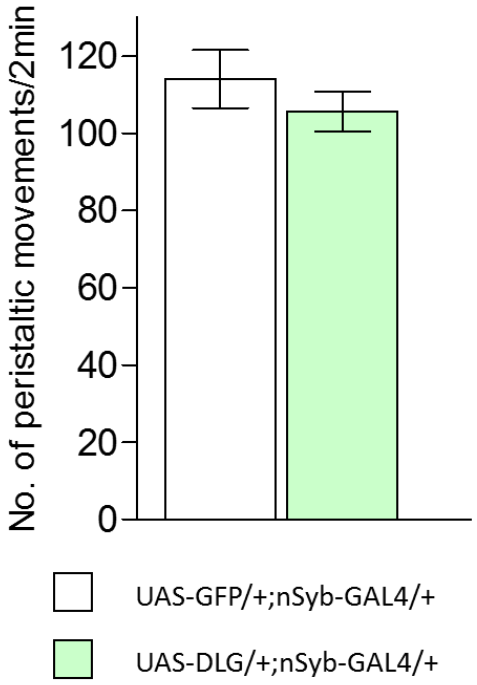

Figure 59: ***UAS-DLG gene expression with nSyb-GAL4 did not affect larval phenotype at 25°C.*** *Calculated by t-test, error bars SEM. N=20 larvae per genotype.*

By counting the peristaltic waves, we did not obtain any significant difference in the number of peristaltic waves when GFP or Dlg is expressed with nSyb-GAL4 driver (Figure 59). The average numbers were not significantly different. Therefore, we decided to use nSyb-GAL4 without regulatory protein GAL80^{ts} and to set all subsequent experiments at 25°C.

We aimed to check if the expression of Dlg protein might change the phenotype obtained in *tbph*$^{\Delta 23}$/- larvae. To begin with, we characterised larval phenotype by counting peristaltic waves.

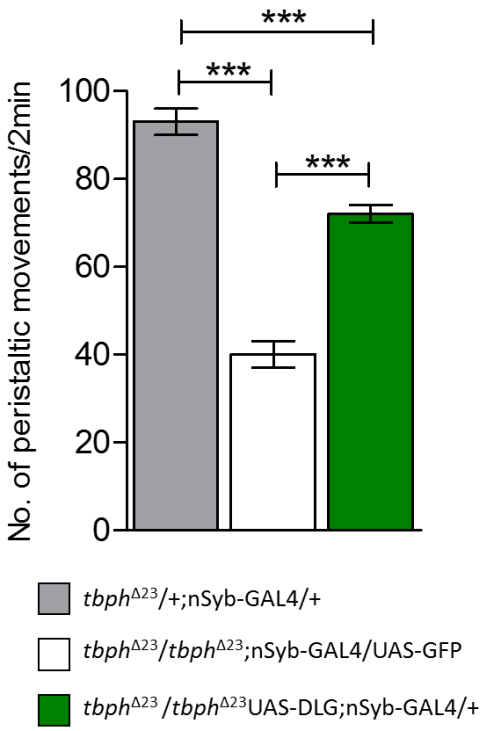

Figure 60: ***Dlg expression in neurons rescued the larval phenotype.*** *The number of peristaltic waves significantly raised in larvae expressing UAS-DLG comparing to larvae expressing UAS-GFP. ***p<0.001 calculated by one-way ANOVA with Bonferroni correction, error bars SEM. N=20 larvae per genotype.*

We tested three different genotypes, following the pattern used in muscle rescue. The positive control (wild type) had a heterozygous background (*tbph*$^{\Delta 23}$/+), expressing only the driver. Negative control had *tbph*$^{\Delta 23}$/- background, expressing UAS-GFP in neurons, and finally, the experimental genotype had *tbph*$^{\Delta 23}$/- background, expressing UAS-DLG gene. Wildtype larvae reached 90 peristaltic waves in two minutes. GFP expressing larvae performed 40 peristaltic waves on average. The

expression of Dlg improved mobility for around 30 peristaltic waves comparing to GFP expressing larvae and reached 70 peristaltic waves (Figure 60). The performance was statistically different. Thus, the values did not reach wildtype larvae result.

Laval movements of larvae expressing Dlg was different to the way negative control moved. The movements were fluent, without stopping and twisting to multiple directions. However, they moved slower as the wildtype.

The recovery of the phenotype led us to investigate the effect of Dlg on NMJ shape and structure. The first experiments were focused on the presynaptic part of NMJ of 6 / 7 muscle at the second segment (the third instar larvae). With the help of αHRP staining, we evaluated the number of branches per NMJ as a marker of NMJ growth.

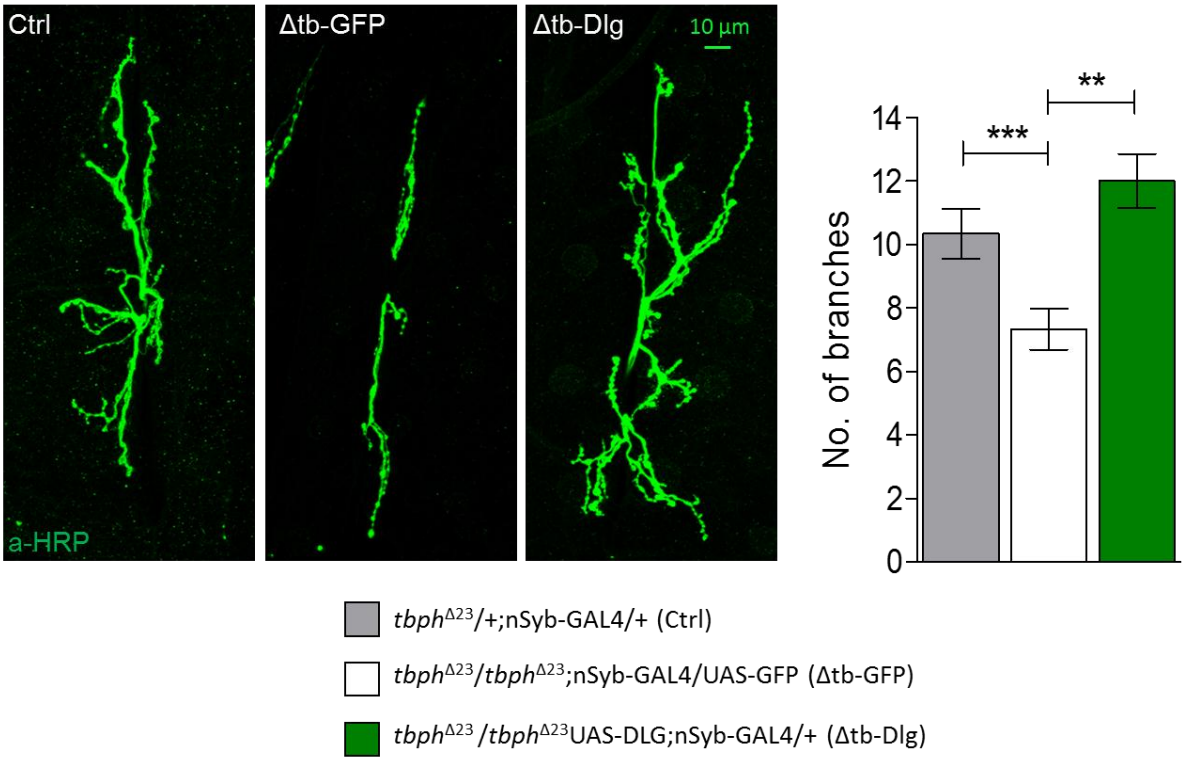

Figure 61: ***Dlg expressed in neurons recovered the number of branches****.* Confocal images of the third instar NMJ terminals in muscle 6 / 7, second segment stained with anti-HRP (in green). The representative terminals are shown, together with the quantification. **p<0.01 and ***p<0.001, calculated by one-way ANOVA with Bonferroni correction, error bars SEM. N = 20 larvae per genotype.

Ten branches on average were counted in wildtype control. Consistently, the number of branches in *tbph*$^{\Delta 23}$/- larvae, expressing GFP was significantly reduced, to seven branches per NMJ. We obtained a significantly higher number of branches in larvae expressing Dlg, comparing to the GFP control. Moreover, the recovery was complete. There was no significant difference between numbers of wild type larvae and larvae expressing Dlg (Figure 61).

To assess whether Dlg expression in neurons can also rescue some characteristics in the postsynaptic compartment of NMJ, we quantified the glutamate receptor levels.

The results were normalised on the wildtype control that represented the maximal intensity obtained in the experiment. In the negative control, we consistently observed a significant drop in intensity, for 65% on average, comparing to the wildtype control. Dlg expression elevated the glutamate receptor level for 20% in comparison to larvae expressing GFP (Figure 62). The clusters of glutamate receptors were downregulated or absent in the negative control. On the contrary, Dlg expressing larvae held visible clusters, yet, the signal was weaker than in the wildtype control.

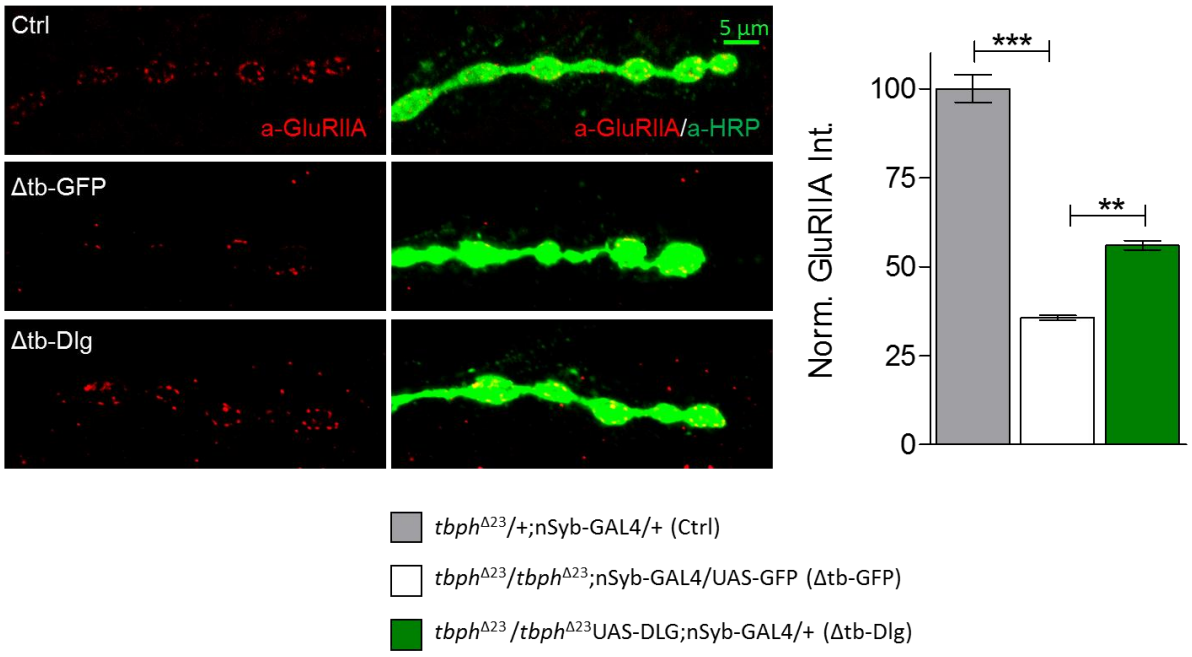

Figure 62: ***Glutamate receptor level was higher when expressing Dlg.*** *Confocal images of the third instar NMJ terminals in muscle 6 / 7 second segment stained with anti-HRP (in green) and anti-GluRIIA (in red) in Ctrl ($tbph^{\Delta 23}$/+;nSyb-GAL4/+), Δtb-GFP ($tbph^{\Delta 23}$/$tbph^{\Delta 23}$;nSyb-GAL4/UAS-GFP) and Δtb-Dlg ($tbph^{\Delta 23}$ /$tbph^{\Delta 23}$UAS-DLG;nSyb-GAL4/+), together with the quantification of GluRIIA intensity normalised on ctrl. **p<0.01 and* ***p<0.001, calculated by one-way ANOVA with Bonferroni correction, Error bars SEM. *N=20 larvae per genotype.*

3.4. TBPH directly binds *dlg* mRNA

We demonstrated that the TBPH alteration of TBPH caused alterations in Dlg levels. Regardless of the tissue, neuronal or muscular, when TBPH was missing, Dlg levels dropped and when TBPH was expressed, Dlg levels rose.

It has been reported that TBPH is RNA binding protein and binds with higher affinity to $(TG)_n$ repeats (Ratti and Buratti, 2016). *dlg* DNA sequence contains sequences that have three or more repeats of TG nucleotides. Based on our results and theoretical background, we wanted to see if TBPH could directly bind *dlg* mRNA. To address that question, we perform co-immunoprecipitation, followed by the real-time PCR. We compared levels of *dlg* mRNA in TBPH gain of function and $TBPH^{F/L}$ (TBPH with two modified amino acids in the RRM1 domain, Phe147 and Phe149 are mutated to Leu and the RNA binding ability is fully abrogated (Buratti and Baralle, 2001)) gain of function flies.

We used thoraces to study the binding of *dlg* mRNA to TBPH in muscles. As a housekeeping gene, we used *rpl11*, and as a positive control *hdac6*. In flies expressing TBPH$^{F/L}$, the levels of mRNAs of *dlg* were not elevated. On the contrary, TBPH expression highly enriched levels of *dlg* mRNA, indicating the binding of that mRNA to TBPH protein in muscles (Figure 63).

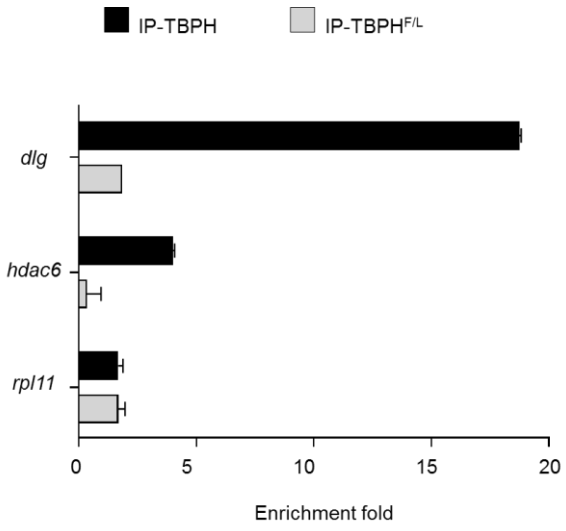

Figure 63: ***Dlg mRNA levels were enriched in flies' muscles overexpressing TBPH****. qRT-PCR analysis of mRNAs immunoprecipitated by Flag-tagged TBPH (UAS-TBPH/+; Mef2-GAL4/+, IP-TBPH) and its mutant variants TBPH$^{F/L}$ (+/+; UAS-TBPH $^{F/L}$/Mef2-GAL4, IP-TBPH$^{F/L}$) in adult thoraces. The dlg enrichment-folds was referred to as rpl-11 (negative control), hdac6 has been used as a positive control. n=3 (biological replicates).*

mRNA levels of *dlg* gene were also measured in adult's heads. The UAS-genes expressed were the same as in the case of thoraces (TBPH and its mutant TBPH$^{F/L}$), under control of Elav-GAL4 driver. As a housekeeping

gene, we used *rpl11*, and as a positive control *syntaxin*. *Syntaxin* mRNA was enriched around 9-times, and in the case of *dlg* mRNA, the enrichment reached to 25-fold in samples with TBPH overexpression. The enrichment was minimal for both mRNAs in brains with $TBPH^{F/L}$ overexpression (Figure 64).

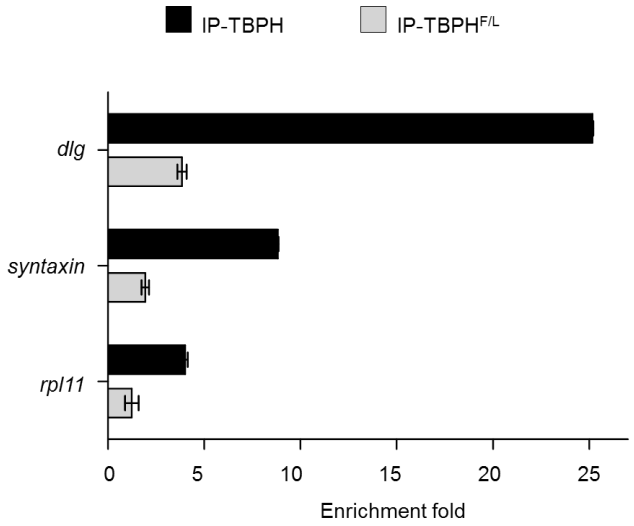

Figure 64: ***Dlg mRNA levels were enriched when TBPH was overexpressed in flies' neurons.*** *qRT-PCR analysis of mRNAs immunoprecipitated by Flag-tagged TBPH (Elav-GAL4/UAS-TBPH/+;+/+, IP-TBPH) and its mutant variants $TBPH^{F/L}$ (Elav-GAL4/+; UAS-TBPH $^{F/L}$/+, IP-$TBPH^{F/L}$) in adult heads. The dlg enrichment-folds was referred to rpl-11 (negative control), syntaxin has been used as a positive control. n=3 (biological replicates).*

The results showed that overexpression of TBPH results in increased levels of *dlg* mRNA in both, thoraces and brain, relative to housekeeping gene rpl11. Moreover, we showed that this enrichment requires the RNA binding domains of TBPH, seeing that $TBPH^{F/L}$ overexpression did not cause significant enrichment of *dlg* mRNA.

3.5. TDP-43 in human cells regulates Dlg levels

To extrapolate our discovery to humans, we aimed to investigate the influence of TDP-43 on the levels of Dlg in neuroblastoma cell line SHSYS5 and differentiated neuronal cells from ALS patients. We observed alterations in Dlg protein when TBPH is knockout, silenced, or overexpressed in flies. Therefore, we silenced TDP-43 and measured Dlg level by western blot in SHSYS5 cells.

Silencing of TDP-43 in cells was controlled with the silencing of GFP protein in the same cell line. The intensity of the band in TDP-43 silenced cells was 75% lower than the intensity obtained in the cells expressing siRNA against GFP. With that been observed, we could confirm that the silencing of TDP-43 was efficient (Figure 65A and C).

Further, we checked Dlg levels in the same cells. The intensity of Dlg band was reduced in the samples where TDP-43 was silenced, comparing to GFP silencing samples (Figure 65A). The intensities were weighed over GAPDH (loading control) and statistically analysed. On average, we obtained a 70% reduction of Dlg protein when TDP-43 is silenced, comparing to siGFP control (Figure 65B).

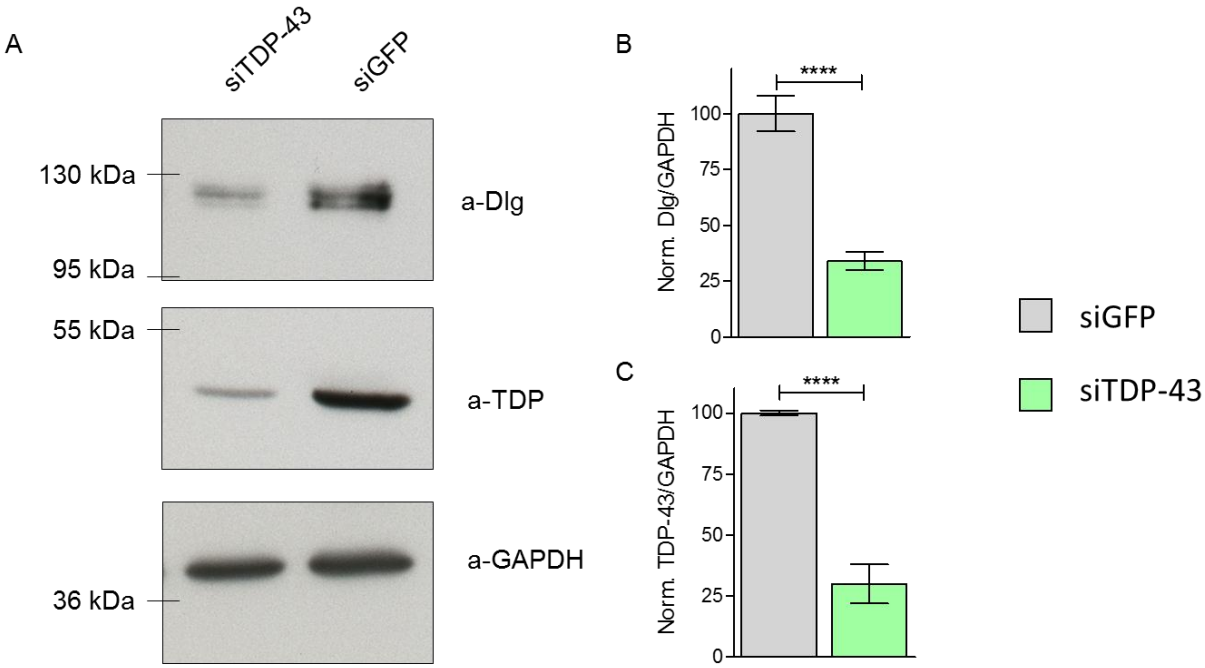

Figure 65: ***Dlg levels were downregulated when TDP-43 was silenced****. A) Western blot analysis on human neuroblastoma (SH-S5Y5) cell line probed for anti-Dlg, anti-GAPDH, and anti-TDP-43 in siGFP (GFP ctrl) and siTDP-43 (TDP-43 silenced). The same membrane was probed with the three antibodies, and the bands of interest were cropped. B) Quantification of normalised protein amount (Dlg). C) Quantification of normalised protein amount (TDP-43). ****p=0.0001, using t-test. n=3 (biological replicates).*

We eventually checked the relevance of Dlg levels in disease conditions, specifically in patient-derived neuronal cells. Differentiated iPSc cells were provided by Monica Nizzardo University of Milan, Dino Ferrari Centre. Cells were differentiated as described in (Ng et al., 2015). We examined cells of two patients with TDP-43 mutations (ALS #1 had G294V and ALS #2 had G376S mutation) and two healthy controls (not affected by any neurodegenerative disorder). The levels of Dlg were analysed by western blot.

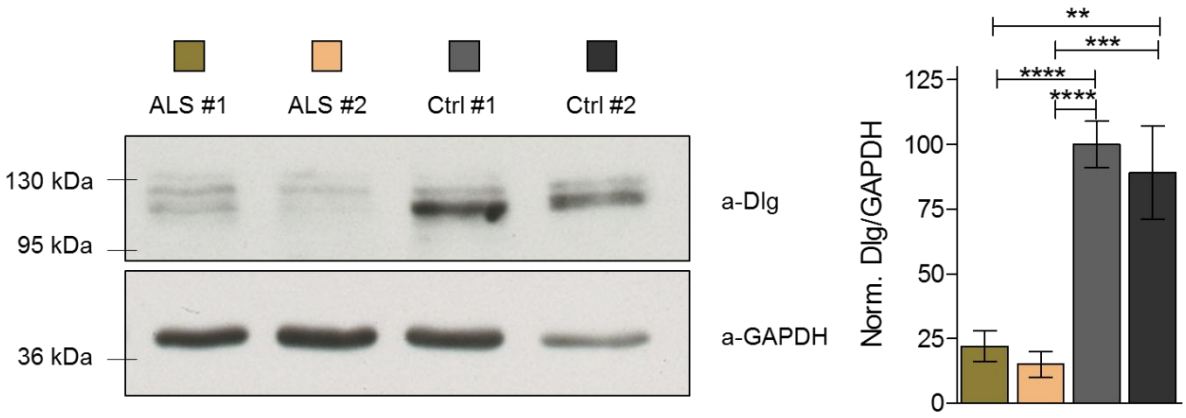

Figure 66: ***ALS patients have decreased levels of Dlg in differentiated neuronal cells.*** *Western blot analysis probed for anti-Dlg and anti-GAPDH on human differentiated motoneurons derived from iPSCs of an ALS patient (ALS patient #1 and ALS patient #2) and a non-ALS affected control (Ctrl #1 and Ctrl #2). The same membrane was probed with the two antibodies, and the bands of interest were cropped. Quantification of normalised protein amount was reported below each lane. **p<0.01, ***p<0.001, ****p< 0.0001 calculated by one-way ANOVA, error bars SEM.*

We observed a significant drop in the intensity of Dlg levels in both patients comparing to both controls. The reduction of measured intensities was more than 75% in both cases (ALS #1 and ALS #2) comparing to non-ALS controls.

These results presented the relevance of the alterations seen in flies. This gave additional credibility to our system and possibilities for further investigations and possible therapies.

4. DISCUSSION

4.1. Silencing of TBPH in muscles affects locomotion, life span, NMJ shape and function

Muscles are a part of NMJ. Therefore, we wanted to investigate whether TBPH somehow contributes to NMJ growth and function, and consequently, if the effect is shown as a specific phenotype. Moreover, we wanted to investigate whether the ALS-like symptoms that are evident in *tbph*$^{\Delta 23}$/- fly can be mimicked by silencing TBPH selectively in muscles. We silenced TBPH in muscles by RNA interference and observed impaired locomotion both in larvae and adult flies. Larvae resembled *tbph*$^{\Delta 23}$/- animals, although they moved slightly faster. In adult flies, the phenotype was more evident. Most of the flies did not hatch. For the ones that fully developed, the climbing assay had to be carried out on day 1, since most flies died on day 4. All flies were dead on day 14. While climbing, flies could control the movement of their legs, but they were not strong enough to climb. They started climbing and after some time fell onto the bottom of the cylinder. The cause of early death was not thoroughly investigated. It is likely that the absence of TBPH compromises some vital functions connected to muscles (heart muscle, smooth muscles, and skeletal muscles) and thus results in premature death. One published study already investigated the effect of silencing in muscles (Diaper et al., 2013). However, they did not describe anything more than the phenotype.

They observed impaired mobility like we did, but the lifespan was not affected. Indeed, they silenced TBPH with Mef2-GAL4. However, they investigated flies with wildtype background and not with *tbph*$^{\Delta 23}$/+ conditions like we did. The different background could contribute to slightly different results.

Since the phenotype was significantly different from the wild type control, NMJ shape and structure were investigated. A presynaptic and postsynaptic compartment of NMJ were characterised by immunostaining. From the neuronal point of view, there were no changes in the number of branches. However, the shape of the boutons was different. Observed NMJ had a higher proportion of irregularly shaped boutons. They were bigger than the wild type, without a defined shape, deformed with a wrinkled membrane.

The irregular bouton shape implies to disturbances in the cytoskeleton. We analysed protein Futsch, which is a structural protein involved in cytoskeleton organisation, dendritic, and axonal growth (Hummel et al., 2000). Reduced levels of Futsch protein were observed in *tbph*$^{\Delta 23}$/- flies (Godena et al., 2011), and thus in our model. The reduction was 15%, but significant and seemingly enough to affect the bouton shape, although not for branching.

Intact branches could be the consequence of the maternal contribution of TBPH. Therefore, despite the silencing, TBPH can remain in small quantities and execute its role. The second possible explanation why boutons but not branches were affected may be the backup pathways that compensate for the absence of muscular TBPH. In TBPH mutants, the protein was absent in all tissues, but in our case, surrounding tissues might partially rescue the phenotype.

Further, we investigated the postsynaptic part of NMJ. Past analysis in our laboratory showed that Dlg protein and glutamate receptors were downregulated in *tbph*$^{\Delta 23}$/- fly (Romano et al., 2014). Therefore, we decided to quantify the levels of these proteins in our model. Both proteins resulted in being downregulated, although at a different extent (25% and 50%, respectively).

Overall, the results indicated that TBPH in muscles plays a vital role in NMJ formation and function by regulating Dlg protein, glutamate receptors, and formation of the boutons. Alteration in NMJ is shown on a phenotypical level. The phenotype in adult flies is more prominent than in larvae. A possible explanation is above-mentioned maternal contribution of TBPH in larvae, and therefore, we do not see changes in branching but in the bouton shape. To confirm this, we should investigate NMJ in adult flies. The animals are dependent on their endogenous protein production, so

the silencing should be more efficient and the effect more significant. Still, we cannot exclude compensatory mechanisms. After all, we are dealing with the entire organism.

Interestingly, our experimental outcome can be compared to the results obtained in TBPH neuronal silencing. Lack of TBPH in neurons manifested in locomotion problems, shorter life span, higher percentage of irregularly shaped boutons, downregulation of Dlg protein and glutamate receptor levels (Feiguin et al., 2009; Romano et al., 2014). The comparison of the two tissues lead us to a hypothesis that there should be communication between neurons and muscles through NMJ. The two tissues might communicate through signalling pathways or physical connection between proteins from both sides. TBPH needs to be present in muscles and neurons so that the NMJ can develop and function properly.

4.2. Expression of TBPH in muscles rescues TBPH$^{-/-}$ phenotype, NMJ function, and structure

To confirm the results obtained by silencing TBPH in muscles and getting some new insights into the TBPH role, we decided to express the protein in *tbph*$^{\Delta 23}$/- flies exclusively in muscles. We mainly concentrated on the characteristics that were altered in silencing.

A significant difference was already evident at the phenotypical level. Larvae recovered the phenotype in contrast to GFP-expressing larvae with

tbph$^{\Delta 23}$/- background. TBPH-expressing larvae moved straight forward and fast without searching for a direction. The recovery in adult flies was less efficient than in larvae. During the first few days, they climbed better than *tbph*$^{\Delta 23}$/- flies but worse than wild type animals. We also performed a walking assay. Flies expressing TBPH in muscles moved more efficiently than mutants. However, the lifespan was not significantly longer.

We wanted to explain why adult fly's phenotype did not show a substantial improvement. To further investigate the TBPH-expression phenotype, we expressed TBPH in wild type background and saw no effect on larval movement, but a significantly lower climbing ability in adult flies. Moreover, flies reached a lower age compared to the control, GFP-expressing flies. Thus, we can conclude that excessive expression of TBPH in muscles is toxic for the organism, particularly at a late stage of the insect's development, which can be complemented with the study where researches observed TBPH inclusions in muscles while overexpressing the protein with Mef2-GAL4 driver. They also reported a shorter life span and locomotive problems (Diaper et al., 2013).

Nevertheless, we decided to investigate the effect at an anatomical level in the third instar larvae, because at that stage, the phenotype was completely recovered. Compared to the TBPH silencing model, we observed utterly opposite results that further extended our knowledge of

the protein's function in muscles. We observed a recovery of NMJ growth. Junctions recovered the number of branches, which were not reduced when we silenced TBPH selectively in muscles. The result indicates that TBPH in muscles is essential, but not the main factor responsible for NMJ growth. With that been observed, the hypothesis about compensatory mechanisms is more probable. In TBPH-expressing model, we do not have endogenous protein. The muscles are the only source of the protein. Nevertheless, NMJ grew, and the bouton shape was recovered.

In the postsynaptic compartment of NMJ, we measured levels of Dlg protein and glutamate receptors. We observed an opposite effect compared to the silencing model. The Dlg level was fully recovered, and the glutamate receptors level was improved only partially. The outcome of the experiments implies a closer relationship between TBPH and Dlg than between TBPH and glutamate receptors. A probable explanation would be that the levels of glutamate receptors are not strictly dependent on processes taking place in muscles. Furthermore, we suspect that neurons are partially responsible for full development and proper location of receptors at the postsynaptic site. It has been demonstrated that when TBPH is silenced in neurons, syntaxin (responsible for the regulation of neurotransmitter release (Wu et al., 1999)), Dlg and glutamate receptors are downregulated. The rescue of *tbph*$^{\Delta 23}$/- larvae with neuronal

expression of syntaxin, only partially rescued Dlg level, but fully recuperated glutamate receptor level (Romano et al., 2014). Joining the results, it is evident that glutamate receptors are not regulated only from muscles. In this case, muscles cannot replace neuronal contribution.

We proceed our investigation with the measuring of excitatory junctional potential. It has been reported that the neurotransmission was impaired in ALS patients (Maselli et al., 1993). We observed the same in *tbph*$^{\Delta 23}$/- larvae. Muscular expression of TBPH partially recovered the EJP. The result matches the previous results, showing partial recovery of glutamate receptors. We cannot exclude other mechanisms that do not depend on glutamate receptor levels being responsible for the recovery of EJP.

Collectively, TBPH expression in muscles can rescue the phenotype of TBPH mutants at the level of the entire organism, as well as at the level of NMJ structure and function.

4.3. Dlg protein regulates NMJ shape and function

Dlg is expressed pre- and postsynaptically (Lahey et al., 1994) and for the proper function, it is required on both sides (Budnik et al., 1996). Therefore, we decided to check whether overexpression in one of the two compartments at least partially rescues the *tbph*$^{\Delta 23}$/- phenotype. Expressing Dlg in muscles or neurons partially recovered larval motility. When expressed in the presynaptic part, all measurements tended to be

improved at a greater extent, although we could not detect a significant difference between the two tissues. Expression of Dlg in muscles was further characterised in adult flies, by a climbing assay and tracking the survival of animals. The climbing abilities of adults were partially recovered, and the survival rate was significantly improved comparing to *tbph*$^{\Delta 23}$/- flies expressing GFP, which confirms a significant contribution of the protein to the function of the organism in general. Furthermore, we confirmed the effect of Dlg on NMJ shape and function by characterising the branching and bouton shape. It is known that Dlg is a scaffold protein and clusters glutamate receptors (Chen and Featherstone, 2005), so the idea was to see whether this effect can also be seen in *tbph*$^{\Delta 23}$/- animals. Dlg expression partially rescued the glutamate receptors level. Partial recovery was obtained in both tissues. The results suggest that Dlg is essential in both tissues for full functioning. Either muscular or neuronal expression can fully recover NMJ shape, but not the function. The EJP was recovered partially. Interestingly, when we compared results of EJP in larvae expressing TBPH versus larvae expressing Dlg, the recovery was not significantly different (data are not shown). Based on that, we could claim that TBPH in muscles regulates Dlg.

Finally, we checked if TBPH in muscles or neurons directly binds the *dlg* mRNA, since its DNA sequence contains several $(TG)_n$ repeats that might

mediate the binding to TBPH protein (Buratti and Baralle, 2001). Indeed, by the immunoprecipitation, we observed a high enrichment of *dlg* mRNA compared to housekeeping genes. TBPH binds to *dlg* mRNA and may regulate its expression at the level of mRNA metabolism. It controls the proper amount of Dlg protein in the cellular compartment where the protein must exert its function. To determine the exact role of TBPH in *dlg* mRNA metabolism, some additional investigations need to be done.

4.4. Dlg1 (SAP79) is downregulated in SH-SY5Y cells and ALS patients

The majority of glutamatergic synapses are located in the central nervous system. They are involved in sensory processing and cognitive function (Volk et al., 2015). Glutamate receptors (AMPA and NMDA) are located in the postsynaptic compartment of the synapse stabilised by postsynaptic density (PSD) (Howard et al., 2010; Muller et al., 1995). The major PSD components are proteins belonging to the MAGUK family. The four main representatives are PSD-95/SAP90, PSD-93/Chapsyn-110, SAP102, and SAP97 (Howard et al., 2010; Muller et al., 1995; Woods and Bryant, 1991). SAP97 is an ortholog of Drosophila Dlg (Figure 67). They share 44% identity and 58% similarity (https://www.uniprot.org/). Studies report that SAP97 binds AMPA receptors and promotes dendrite growth (Goodman et al., 2017; Howard et al., 2010; Zhou et al., 2008).

Figure 67: The alignment of D. melanogaster Dlg and human Dlg1. Equal amino acids (*) and similar amino acids (:) are marked (Source: https://www.uniprot.org/)

In our studies, we used two different models to check SAP97/Dlg1 levels – a cell line SH-SY5Y and iPS cells differentiated into neurons from ALS patients and healthy (non-ALS affected) donors. We saw that Dlg1 levels

are indeed downregulated in neuroblastoma cells when TDP-43 was silenced. What is even more striking, the same result was observed in samples from ALS patients. Not that we have just confirmed the relevance of our studies and model, but also discovered a new protein that is dysregulated. Dlg1 downregulation in neuroblastoma cell is connected to TDP-43 silencing, because we measured levels of both proteins in the same samples. However, we cannot claim that for the iPSCs, because we did not check the levels of TDP-43.

One of the reasons for impaired dendrite growth in ALS may be connected to the downregulation of SAP97.

4.5. Conclusions and future perspective

Animals with silenced TBPH in muscles had problems with mobility and shorter life span, which is also observed in TBPH knockout flies. Moreover, they had changes in neuromuscular junction shape and levels of the proteins. Most of the characteristics were recovered when TBPH was expressed exclusively in muscles of *tbph*$^{\Delta 23}$/- flies.

When TBPH levels were altered, the alteration of Dlg protein was observed. We showed that TBPH directly bound *dlg* mRNA. Additionally, we checked whether Dlg expression could recover the phenotype observed in *tbph*$^{\Delta 23}$/- flies. Indeed, it recovered regardless of the tissue where the protein was expressed (either neurons or muscles). The results

imply a physical connection between the two compartments of NMJ necessary for proper function.

Based on our research, we hypothesise that TBPH is responsible for the formation of Dlg protein. Dlg is located at the NMJ where it clusters the proteins and physically connects both compartments of NMJ (Figure 68). When the connection is formed, NMJ develops, grows, and partially contributes to the function. However, we cannot claim that this is the only mechanism needed in the process of NMJ formation and function.

We proved that Dlg could recover the phenotype of *tbph*$^{\Delta 23}$/- larvae regardless of where it is expressed (in muscles or neurons). We propose the explanation that overexpression of the protein in one of the tissues (muscular or neuronal) is adequate to attract and to anchor the residues of Dlg on the other side and so the execution of Dlg roles is possible. Nevertheless, one needs to keep in mind that in *tbph*$^{\Delta 23}$/- animals Dlg protein in NMJ is not entirely erased. However, its levels are too low to function in mutant background.

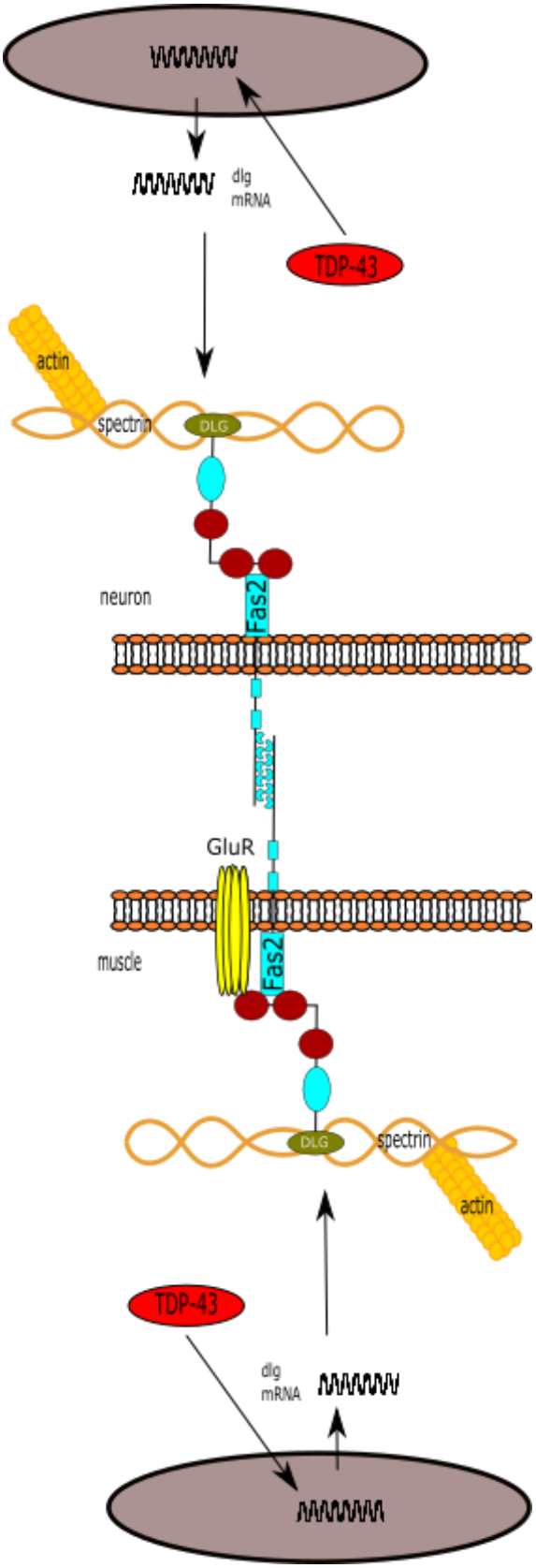

Figure 68: ***The model of TBPH function*** *in NMJ. TBPH in muscles and neurons binds dlg mRNA and regulates mRNA metabolism. Dlg is expressed and located in NMJ, whereby to-Dlg-bound proteins anchor the Dlg protein on the other side of NMJ, and so their functions can be executed.*

In the future, we would like to determine the mechanism through which presynaptic and postsynaptic compartments are communicating and affecting one another. Additionally, we would like to determine the role of TBPH in *dlg* mRNA metabolism. Perhaps, TBPH has any other roles in NMJ formation and controls other pathways. Manipulation of these pathways could also present a potential target for the ALS therapies.

Translational potential for patients

For long years it has been believed, that ALS is a neuronal disease. However, the involvement of surrounding tissues in disease progression is now considered. Our studies show the potential involvement of muscular tissue in ALS development and progression. We show, that NMJ can be manipulated via expression of certain proteins in muscles. Therefore, one can predict, that muscles are potential target in receiving a therapy for the disease. The advantage of this type of treatment is accessibility of muscles. Drug delivery to muscles is easier and less invasive than to neurons.

5. MATERIAL AND METHODS

5.1. Fly strains

The following genotypes were used:

w[1118] (Feiguin et al., 2009)

w[1118]; TBPH$^{\Delta 23}$/Cyo-GFP (Feiguin et al., 2009)

w[1118]; TBPH$^{\Delta 142}$/Cyo-GFP (Feiguin et al., 2009)

w[1118]; Mef2-GAL4/TM3-Sb (#27390, BDSC)

w[1118]; MHC-GAL4/TM3-Sb (#55133, BDSC)

w[1118]; UAS-mCD8::GFP/Cyo (#5137, BDSC)

w[1118]; UAS-TBPH/Cyo (Feiguin et al., 2009)

w[1118]; UAS-TBPH$^{F/L}$/TM3-Sb (Romano et al., 2014)

w[1118]; UAS-hTDP/TM3-Sb (Feiguin et al., 2009)

w[1118]; UAS-DLG(egfp)/UAS-DLG(egfp) (Budnik et al., 1996)

w[1118]; UAS-TBPH RNAi (#ID38377, VDRC)

w[1118]; UAS-GFP RNAi (#9330, BDSC)

w[1118]; UAS-GFP RNAi (#9331, BDSC)

w[1118]; Dicer(X) (#60009, VDRC)

Table 3: Primary antibodies used in experiments.

Primary Antibodies			
Name (supplier)	**Host**	**Dilution (NMJ)**	**Dilution (WB)**
αGFP (#A11122, Invitrogen)	rabbit	1 : 200	-
αHRP (#323-005-021 Jackson)	rabbit	1 : 150	-
αDlg (#4F3c, DSHB)	mouse	1 : 250	1 : 10,000
αGluRIIA (#8B4D2c, DSHB)	mouse	1 : 15	-
αFutsch (#22C10s, DSHB)	mouse	1 : 50	-
αTBPH (home-made)	rabbit	-	1 : 4,000
Atubulin DM1A (#CP06, Calbiochem)	mouse	-	1 : 4,000
αTDP-43 (#10782-2-AP, Proteintech)	rabbit	-	1 : 4,000
αDlg (#2D11, Santa Cruz)	mouse	-	1 : 1,000
αGAPDH (#47724 SC, Santa Cruz)	mouse	-	1 : 2,000

Table 4: Secondary antibodies used in experiments.

Secondary Antibodies			
Name (supplier)	**Host**	**Dilution (NMJ)**	**Dilution (WB)**
Alexa Fluor® 488 αmouse (#A11001) or αrabbit (#A11008), (Life Technologies)	goat	1 : 500	-
Alexa Fluor® 555 αmouse (#A21422) or αrabbit (#A21428), (Life Technologies)	goat	1 : 500	-
Alexa Fluor® 647 αmouse (#A21241, Life Technologies)	chicken	1 : 500	-
αmouse-HRP (#32430, Pierce)	goat	-	1 : 30,000(flies) 1 : 10,000(cells)
αrabbit-HRP (#32460, Pierce)	goat	-	1 : 10,000

5.2. Drosophila techniques

5.2.1. Fly stocks and crosses

Drosophila stocks were purchased from the Bloomington Drosophila Stock Center (Indiana; https//bdsc.indiana.edu/), the Drosophila Genetic Resource Center (Kyoto; https://kyotofly.kit.jp/cgi-bin/stocks/index.cgi), and Drosophila Stock Center (Vienna; https://stockcenter.vdrc.at/control/main). Additional stocks were kindly provided by colleagues and other laboratories or were generated as part of this project. Stocks were stored at room temperature or at 18°C and were flipped into new tubes, weekly or every 14 – 21 days, depending on the temperature settled. Experimental crosses were maintained in an incubator with controlled conditions (60% humidity, 25°C, 12 hours light and 12 hours dark cycles). Flies were grown in small tubes filled with fly food, prepared as reported in Table 5.

Table 5: Fly food ingredients and the quantity for the preparation

Ingredients of fly food	**Quantity**
yeast	1,000g
agar	100g
cornflour	466g
sugar	666g
propionic acid	66ml
water	17l

5.2.2. Phenotypic analysis in *Drosophila*

- LARVAL MOVEMENT

Wandering third instar larvae (about 120 hours old) were picked from tubes and washed in a drop of demineralised water (DEMI water). If necessary, they were selected against different markers such as tubby or CyoGFP and placed into 6cm diameter dishes, filled with 0.7% agar. A single larva at the time was transferred into a 10cm diameter dish, filled with 0.7% agar. After 30s of adaption period, the number of peristaltic waves was counted for two minutes. The tested larvae were subsequently transferred to a fresh fly tube to check them, both for hatching (after three to four days) and correct genotype selection. Generally, 20 – 25 larvae per genotype were tested.

- SURVIVAL RATE

One- to two-day-old adult flies were collected from the fly tube of an experimental cross in a 1 : 1 proportion of female and male, transferred to a fresh fly tube and stored in the incubator under controlled conditions (suitable temperature and humidity, 12h light and 12h night). Every second-day flies were transferred into a fresh fly tube without anaesthesia, and the number of deaths was scored. Approximately 200 flies per genotype were tested.

- CLIMBING ASSAY

One- to two-day-old adult flies were collected from the fly tube of an experimental cross in a 1 : 1 proportion of female and male, transferred into a fresh fly tube and maintained in an incubator as previously described. The day of the setting of the experiment was counted as day 0. Flies were tested on day 4, 7, 14, and 21. A 50ml glass cylinder was divided into three parts, as the bottom, middle and top (5cm each part) (Figure 69), and flies were carefully flipped into the cylinder from the fly tube without any anaesthesia and gently dropped to the bottom. After 30s of adaptation period, flies were dropped onto the bottom of the cylinder again, and after a time interval of 15s, the number of flies present in each part of the cylinder were scored. For each genotype, three trials per each tube were done, and the average of the scored fly numbers was

considered the final score. A minimum of 200 flies was tested for each genotype.

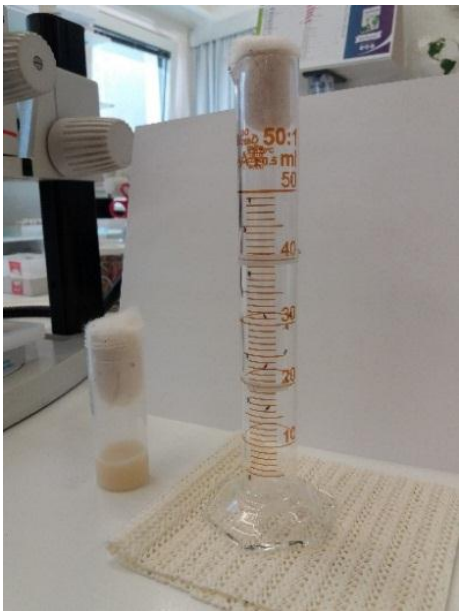

Figure 69: Divided glass cylinder prepared for the climbing assay.

- WALKING ASSAY

Young flies, two- to three-day old, were tested for walking ability. A 145mm dish was used. The bottom surface was divided into a grid of 1cm x 1cm squares (Figure 70) to facilitate the measuring of the distance walked by the flies. The fly without any anaesthesia was placed in the middle of the dish, and after 30s of adaptation to the environment, the distance covered by the fly was recorded for 30s, counting the number of squares. A minimum of 50 flies was individually tested for each genotype.

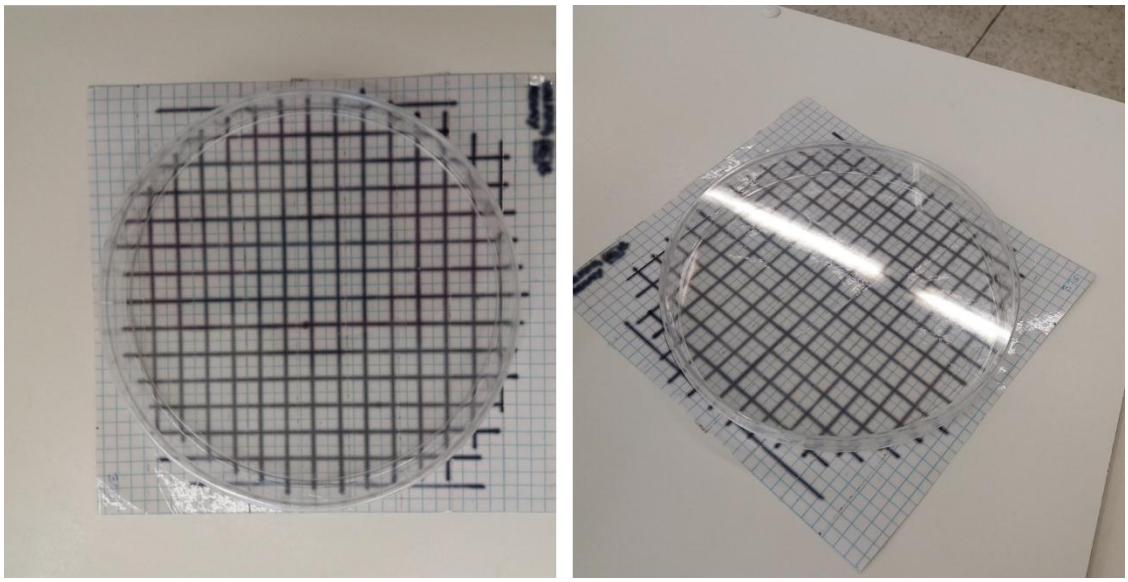

Figure 70: Walking assay plate with the 1cm x 1cm grid beneath it.

5.2.3. Immunohistochemistry studies

- LARVAL NMJ IMMUNOHISTOCHEMISTRY

Wandering third instar larvae were picked from a fly tube, in a drop of demineralised water, selected for the genotype and maintained during the time of dissection in a 6cm diameter dish filled with 0.7% agarose dissolved in water. Individually picked larva was dissected on Sylgard plates, in Dissection Solution (128mM NaCl, 2mM KCl, 4mM $MgCl_2$, 0.1mM $CaCl_2$, 35.5mM Sucrose and 5mM Hepes (pH 7.2)). Larvae were pinned at both ends with minute pins (Austerlic Insect Pins 0.1mm diameter, Fine Science Tools, Germany) and opened on the dorsal site with Spring scissors (Fine Science Tools, Germany). Once larva was opened, internal organs were removed, and the interior was extensively washed with Dissection Solution leaving muscle wall opened, pinned flat

on the surface. The subsequent step was a fixation, generally done with 4% PFA in PBS for 20min; however, in the case of glutamate receptors staining, a methanol fixation of 5min at -20°C was performed. Fixation solution was removed with three washes in PBS-T (PBS 1x supplemented with 0.1% (v/v) Tween20) for 5min each. After a blocking step of 30 min in blocking solution (5% NGS (Normal Goat Serum, Chemicon in PBS-T buffer), larvae were incubated overnight at 4°C in primary antibodies (Table 3) diluted in blocking solution. The day after, the primary antibody was removed with three washes of 10min each with PBS-T and a further blocking step of 30min was performed before adding secondary antibodies (Alexa Fluor® Secondary antibodies, Life Technologies) (Table 3). All secondary antibodies were diluted in blocking solution. An incubation was 2h long, performed at the room temperature (RT). Antibody excess was removed by three subsequent washes of 20 minutes each in PBS-T. Finally, dissected-stained larvae were incubated overnight at 4°C in Slowfade®Gold antifade (Life Technologies) reagent, before being mounted on a glass slide and scanned with a confocal microscope (Carl Zeiss LSM 510 Meta).

- <u>BOUTON SHAPE</u>

Boutons were stained with an anti-HRP antibody that recognises five glycoproteins located in the neuronal membrane (Jan and Jan, 1982). The

shape of boutons was evaluated as regular if they were round and with a smooth surface, with an equal diameter on both axes (Figure 71). On the other hand, boutons were considered as irregular if the shape was not round, the membrane was wrinkled, and the diameter of one axe was different compared to the other one (Figure 71).

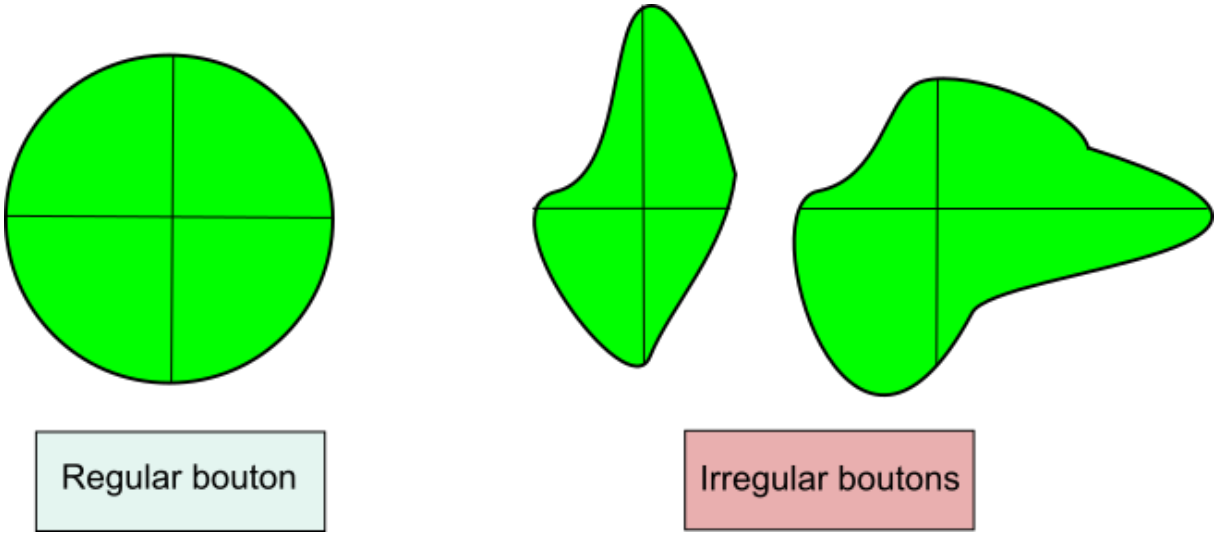

Figure 71: When an equal diameter on both axes of the bouton is observed, the bouton is considered regular. Irregular boutons come in different sizes and shapes, with a different diameter on both axes.

- NUMBER OF BRANCHES

The protocol of processing larvae used for this analysis was immunohistochemistry. Images of an anti-HRP antibody stained branches were acquired with the same settings. All branches were counted together (primary, secondary, tertiary) (Figure 72).

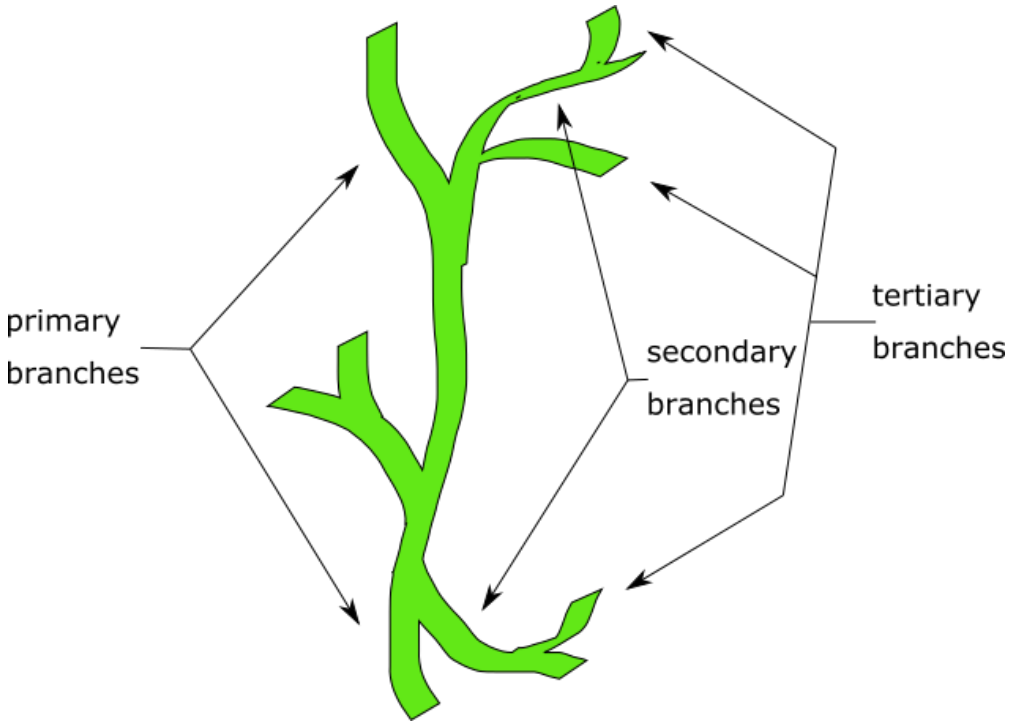

Figure 72: Scheme of branches in NMJ and their hierarchy.

- QUANTIFICATION OF PRE- AND POSTSYNAPTIC MARKERS

Larvae were processed with the protocol for immunohistochemistry. Double labelled samples with anti-HRP and antibodies against pre- and postsynaptic proteins were analysed on the confocal microscope and acquired under the constant settings. Images were further processed with ImageJ software and boutons from NMJs of the 2nd larval segment, muscles 6 and 7, were quantified. Both the HRP and the pre- or postsynaptic markers intensity were quantified. The obtained signal of the synaptic markers was normalised on HRP intensity. Results were statistically analysed by the Prism Graphpad software.

5.2.4. Electrophysiology on NMJ of the third instar larva preparation

Larval body wall preparations were dissected out in Ca2+-free HL3 solution from third instar larvae pinned on Sylgard coated Petri dishes. The central nervous system was excised by cutting segmental nerves roots. After replacing Ca2+ free HL3 solution with Ca2+ 1 mM HL3, postsynaptic potentials at the neuromuscular junction of fibre 6 / 7 of abdominal segments A3 / A4 were intracellularly recorded, at room temperature in current-clamp condition, using an intracellular microelectrode (tip diameter 0.5µm, 15MΩ resistance). The recorded signal was amplified by a current-clamp amplifier (SEC 05, NPI, Tamm, Germany), digitised at 10kHz sampling rate using an A / D interface (National Instruments, Austin, TX, USA) and fed to a computer for display and storage using an appropriate software (Win EDR, Strathclyde University, Glasgow, UK).

Fibres with a resting membrane potential below -60mV were considered for the experiment. In these fibres, membrane potential was set at -70mV throughout the experiment by injecting current through the intracellular electrode. Evoked postsynaptic potentials (EPSPs or Excitatory Junctional Potentials or EJPs) were recorded by stimulating at 0.1Hz (pulse duration 0.4ms; 1.5 threshold voltage) the segmental nerve using a suction electrode (tip diameter ~10µm) connected to a stimulator (S88, Grass, Pleasanton, CA, USA) (Figure 73) through a stimulus isolation unit (SIU5, Grass, Pleasanton, CA, USA). Intracellular recordings were analysed

offline using pClamp software (pClamp, Axon, Sunnyvale, CA, USA). Statistical comparisons and graphs were made using the Graphpad software (Graphpad, La Jolla, CA, USA) or MATLAB (Matworks, Natick, MA, USA).

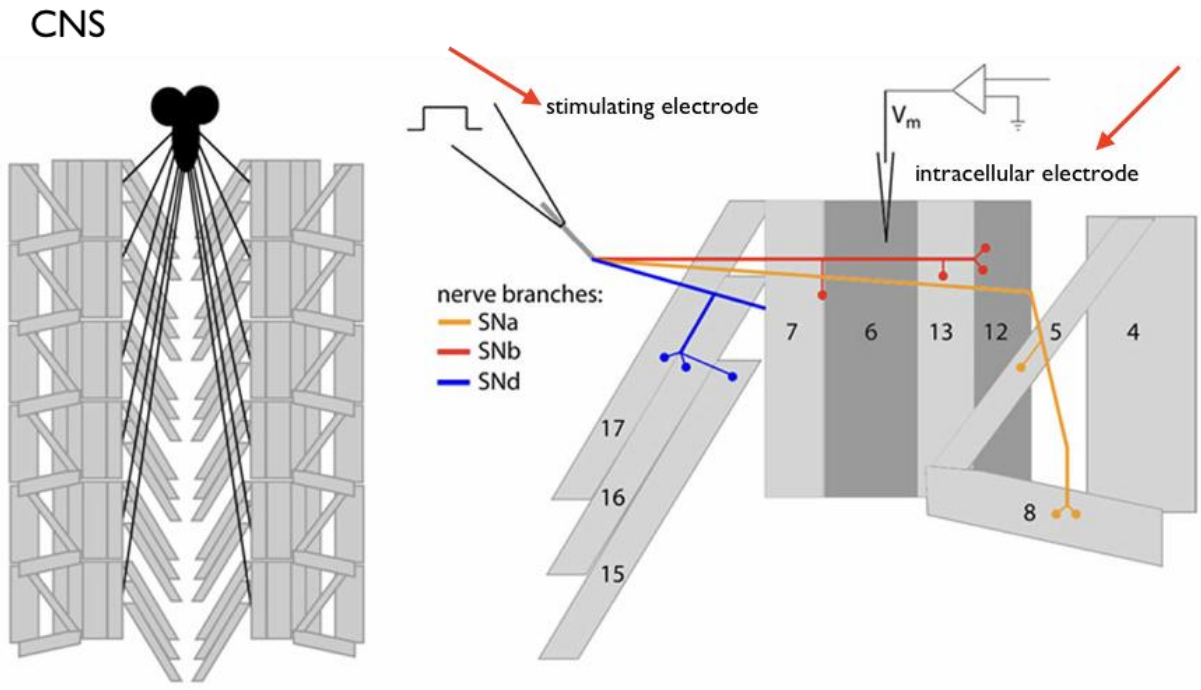

Figure 73: The scheme of measuring the EJPs.

5.3. Biochemical techniques

5.3.1. Immunoprecipitation

Protein G magnetic beads (Invitrogen) were washed two times, with PBS+0.02% Tween and coated with anti-FLAG M2 monoclonal antibody (Sigma). Thoraces or heads of adult flies were cut and stored in lysis buffer containing 20mM Hepes, 150mM NaCl, 0.5mM EDTA, 10% Glycerol, 0.1% Triton X-100, 1mM DTT, and protease inhibitor. Samples were homogenised with a Dounce homogeniser, and major debris was removed

by centrifugation step of 5 min at 0.4g at 8°C. The pretreated beads and tissue extracts were mixed and incubated for 30min at 4°C. After this binding step, beads were washed five times with washing buffer (20mM Hepes, 150mM NaCl, 0.5mM EDTA, 10% Glycerol, 0.1% Triton X-100, 1mM DTT, protease inhibitor, 0.2% DOC, 0.5M Urea) using DynaMagTM-Spin (Invitrogen). RNA transcripts bound by TBPH-Flag-tagged were extracted. The beads were treated with Trizol (Ambion) and precipitated with isopropanol adding glycogen (Thermo scientific). Retro-transcription with Superscript III First-Strand Synthesis (Invitrogen #18080051) was performed with Oligo-dT primers on resuspended RNA. Real-time PCR was carried out with gene-specific primers, the sequences of which are listed below.

rpl11

fw 5’-CCATCGGTATCTATGGTCTGGA-3’

rev 5’-CATCGTATTTCTGCTGGAACCA-3’

syntaxin

fw 5’-TGTTCACGCAGGGCATCATC-3’

rev 5’-GCCGTCTGCACATAGTCCATAG-3’

hdac-6

fw 5’-CGAGCGGCTGAAGGAGAC-3’

rev 5’-ACCAGATGGTCCACCAATTCG-3’

dlg:

fw 5’-ACTGGGCTTCTCAATTGCCG-3’

rev 5’-CCAGTTCGTGCGTTACGTTC-3’

In order to calculate the enrichment fold, initially, all data were normalised to the respective inputs. The signal was represented by how many more fold increase was measured compared to the control signal. The enrichment was calculated according to the following equation:

$$enrichment = 2^{-\Delta\Delta C_t}$$

$$\Delta\Delta C_t = \frac{\Delta C_t\,(TBPH)}{\Delta C_t\,(TBPH^{F/L})} = \frac{C_t\,(IP\ TBPH) - C_t\,(input\ TBPH)}{C_t\,(IP\ TBPH^{F/L}) - C_t\,(input\ TBPH^{F/L})}$$

The results were derived from three independent immunoprecipitation experiments.

5.3.2. Protein extraction

To collect adult heads, flies were flash-frozen in liquid nitrogen for 10 seconds and immediately vortexed to easily detach heads from bodies. Heads were subsequently transferred into Lysis buffer (150mM Tris, 5mM EDTA, 10% glycerol, 5mM EGTA, 50mM NaF, 4M urea, 5mM DTT and protease inhibitors). After a squeezing step, performed both manually and mechanically, the homogenised samples were gotten rid of major debris by centrifugation at 0.5 x g for 6 min on 4°C. The protein concentration of the collected supernatant was quantified with Quant-iT^{TM} Protein Assay Kit (Invitrogen), following supplier protocol.

Transfected neuroblastoma cell line SH-SY-5Y were resuspended in iced RIPA buffer added of Protease Inhibitors (Roche) and subjected to sonication (Biorupture sonication system, Diagenode).

Lysates were quantified (BCA Protein kit #23225 Thermo Scientific), following supplier protocol.

5.3.3. SDS-PAGE

Protein samples were diluted in 1x Laemmli buffer (the composition of 5x: 0.3M Tris-HCl pH 6.8, 50% glycerol, 10% SDS, 25% β-mercaptoethanol, 0.05% bromophenol blue) to reach the same concentration among all and

then boiled at 95°C for 5min. Afterwards, they were loaded on a polyacrylamide gel (Table 6).

Table 6: The ingredients and the concentrations of gels used in SDS-PAGE.

Preparation		
Ingredients	**Resolving gel**	**Stacking gel**
Acrylamide M-BIS 40%	4% – 10% (v/v)	5% (v/v)
Tris-HCl pH 8.8	0.37M	-
Tris-HCl pH 6.8	-	0.125M
Ammonium persulphate	0.1% (w/v)	0.1% (w/v)
SDS	0.1% (w/v)	0.1% (w/v)
TEMED	0.02% (v/v)	0.02% (v/v)

The loaded gel was placed into the chamber with 1x running buffer (10x running buffer: 30.28g Tris, 114.13g Glycine, 10g SDS in 1l water). The conditions set were 25mA per gel.

5.3.4. Western blot

When the electrophoresis separated proteins, they were transferred to a nitrocellulose membrane Amersham™ Protran™ 0.2µm NC (GE Healthcare, Life Science). The western blot sandwich was put into the chamber, filled with transfer buffer 1x containing 20% methanol (transfer

buffer 10x: 30g Tris, 144g glycine in 1l water). The transfer lasted 1 hour at 350mA.

The membrane was incubated with a solution of 5% milk in 1x TBS 0.01% Tween (TBS-T) for 30min at room temperature on a shaker (TBS buffer 10x: 24.2g Tris, 80g NaCl in 1l water, pH 7.6). After blocking, the membrane was set into dilution of antibodies with TBS-T with 5% milk. It was placed at 4°C overnight.

When the incubation with primary antibodies was over, five washes with TBS-T followed for 5min each. Next, the membrane was incubated with the secondary antibody diluted in TBS-T with 5% milk for 1hour at room temperature. The protein detection was performed with SuperSignal®West Femto Maximum Sensitivity Substrate (ThermoFisher Scientific).

5.4. Cell culture techniques

5.4.1. Cell culture and RNA interference

SH-SY-5Y neuroblastoma cell line was cultured in standard conditions in DMEM-Glutamax (Thermo Fisher Scientific) supplemented 10% fetal bovine serum and 1X antibiotic-antimycotic solution (Sigma). RNA interference of TDP-43 was achieved using HiPerfect Transfection Reagent (Qiagen) and siRNA specific for human TDP43 (5'-GCAAAGCCAAGAUGAGCCU-3'); as control siRNA for GFP was used

(5’-GCACCAUCUUCUUCAAGGA-3’; Sigma). Immediately before transfection, 2-4x10^5 cells were seeded in 6-well plates in 1.4ml of medium containing 10% fetal serum. A volume of 3µl of each siRNA (40µM solution in water) was added to 91µl of Opti-MEM I reduced serum medium (Thermo Fisher Scientific); after a 5-minute incubation at room temperature, 6µl of HiPerfect Transfection Reagent was added. The mixture was drop-wise poured onto the cells after a 10-minute room temperature incubation to allow the formation of the complexes. The silencing procedure was performed again after 24 hours, for a total of two rounds of silencing.

5.5. Statistical analysis

All statistical analysis was performed with Prism (GraphPad, USA) version 5.1. One-way ANOVA with Bonferroni correction, two-way ANOVA or t-test with Man-Whitney correction was applied as a statistical test. In all figures, all the values were presented as the mean and the standard error of the mean (SEM). Statistical significance was portrayed as *$p<0.05$, **$p<0.01$, ***$p<0.001$.

REFERENCES

Alami, N.H., Smith, R.B., Carrasco, M.A., Williams, L.A., Winborn, C.S., Han, S.S.W., Kiskinis, E., Winborn, B., Freibaum, B.D., Kanagaraj, A., et al. (2014). Axonal transport of TDP-43 mRNA granules is impaired by ALS-causing mutations. Neuron *81*, 536–543.

Ambegaokar, S.S., Roy, B., and Jackson, G.R. (2010). Neurodegenerative models in Drosophila: polyglutamine disorders, Parkinson disease, and amyotrophic lateral sclerosis. Neurobiol. Dis. *40*, 29–39.

Andersen, P.M., Nilsson, P., Keränen, M.L., Forsgren, L., Hägglund, J., Karlsborg, M., Ronnevi, L.O., Gredal, O., and Marklund, S.L. (1997). Phenotypic heterogeneity in motor neuron disease patients with CuZn-superoxide dismutase mutations in Scandinavia. Brain *120 (Pt 10)*, 1723–1737.

Andersen, P.M., Borasio, G.D., Dengler, R., Hardiman, O., Kollewe, K., Leigh, P.N., Pradat, P.-F., Silani, V., and Tomik, B. (2005). EFNS task force on management of amyotrophic lateral sclerosis: guidelines for diagnosing and clinical care of patients and relatives. European Journal of Neurology *12*, 921–938.

Anthony J.F. Griffiths, U. of B.C.S.R.W., University of California, Riverside; Sean B. Carroll, Howard Hughes Medical Institute, University of Wisconsin--Madison; John Doebley, University of Wisconsin--Madison (2015). Introduction to genetic analysis (Eleventh edition. New York, NY : W.H. Freeman & Company, [2015] ©2015).

Arai, T., Hasegawa, M., Akiyama, H., Ikeda, K., Nonaka, T., Mori, H., Mann, D., Tsuchiya, K., Yoshida, M., Hashizume, Y., et al. (2006). TDP-43 is a component of ubiquitin-positive tau-negative inclusions in frontotemporal lobar degeneration and amyotrophic lateral sclerosis. Biochem. Biophys. Res. Commun. *351*, 602–611.

Astorga, C., Jorquera, R.A., Ramírez, M., Kohler, A., López, E., Delgado, R., Córdova, A., Olguín, P., and Sierralta, J. (2016). Presynaptic DLG regulates synaptic function through the localization of voltage-activated Ca^{2+} Channels. Scientific Reports *6*, 32132.

Ayala, Y.M., Pantano, S., D'Ambrogio, A., Buratti, E., Brindisi, A., Marchetti, C., Romano, M., and Baralle, F.E. (2005). Human, Drosophila, and C.elegans TDP43: nucleic acid binding properties and splicing regulatory function. J. Mol. Biol. *348*, 575–588.

Ayala, Y.M., De Conti, L., Avendaño-Vázquez, S.E., Dhir, A., Romano, M., D'Ambrogio, A., Tollervey, J., Ule, J., Baralle, M., Buratti, E., et al. (2011). TDP-43 regulates its mRNA levels through a negative feedback loop. EMBO J. *30*, 277–288.

Balendra, R., and Isaacs, A.M. (2018). C9orf72 -mediated ALS and FTD: multiple pathways to disease. Nature Reviews Neurology *14*, 544.

Banks, G.T., Kuta, A., Isaacs, A.M., and Fisher, E.M.C. (2008). TDP-43 is a culprit in human neurodegeneration, and not just an innocent bystander. Mamm. Genome *19*, 299–305.

Becker, L.A., and Gitler, A.D. (2018). A neurodegenerative-disease protein forms beneficial aggregates in healthy muscle. Nature *563*, 477.

Berger, J., Suzuki, T., Senti, K.A., Stubbs, J., Schaffner, G., and Dickson, B.J. (2001). Genetic mapping with SNP markers in Drosophila. Nat. Genet. *29*, 475–481.

Bhandari, R., Kuhad, A., and Kuhad, A. (2018). Edaravone: a new hope for deadly amyotrophic lateral sclerosis. Drugs Today *54*, 349–360.

Bier, E. (2005). Drosophila, the golden bug, emerges as a tool for human genetics. Nat. Rev. Genet. *6*, 9–23.

Bland, J.M., and Altman, D.G. (2004). The logrank test. BMJ *328*, 1073.

Bourke, S.C., Tomlinson, M., Williams, T.L., Bullock, R.E., Shaw, P.J., and Gibson, G.J. (2006). Effects of non-invasive ventilation on survival and quality of life in patients with amyotrophic lateral sclerosis: a randomised controlled trial. Lancet Neurol *5*, 140–147.

Brand, A.H., and Perrimon, N. (1993). Targeted gene expression as a means of altering cell fates and generating dominant phenotypes. Development *118*, 401–415.

Brooks, B.R., Miller, R.G., Swash, M., Munsat, T.L., and World Federation of Neurology Research Group on Motor Neuron Diseases (2000). El Escorial revisited: revised criteria for the diagnosis of amyotrophic lateral sclerosis. Amyotroph. Lateral Scler. Other Motor Neuron Disord. *1*, 293–299.

Bruneteau, G., Simonet, T., Bauché, S., Mandjee, N., Malfatti, E., Girard, E., Tanguy, M.-L., Behin, A., Khiami, F., Sariali, E., et al. (2013). Muscle histone deacetylase 4 upregulation in amyotrophic lateral sclerosis:

potential role in reinnervation ability and disease progression. Brain *136*, 2359–2368.

Budini, M., Romano, V., Quadri, Z., Buratti, E., and Baralle, F.E. (2015). TDP-43 loss of cellular function through aggregation requires additional structural determinants beyond its C-terminal Q/N prion-like domain. Hum Mol Genet *24*, 9–20.

Budini, M., Buratti, E., Morselli, E., and Criollo, A. (2017). Autophagy and Its Impact on Neurodegenerative Diseases: New Roles for TDP-43 and C9orf72. Front. Mol. Neurosci. *10*.

Budnik, V., Koh, Y.H., Guan, B., Hartmann, B., Hough, C., Woods, D., and Gorczyca, M. (1996). Regulation of synapse structure and function by the Drosophila tumor suppressor gene dlg. Neuron *17*, 627–640.

Buratti, E., and Baralle, F.E. (2001). Characterization and functional implications of the RNA binding properties of nuclear factor TDP-43, a novel splicing regulator of CFTR exon 9. J. Biol. Chem. *276*, 36337–36343.

Buratti, E., Dörk, T., Zuccato, E., Pagani, F., Romano, M., and Baralle, F.E. (2001). Nuclear factor TDP-43 and SR proteins promote in vitro and in vivo CFTR exon 9 skipping. EMBO J. *20*, 1774–1784.

Buratti, E., Brindisi, A., Giombi, M., Tisminetzky, S., Ayala, Y.M., and Baralle, F.E. (2005). TDP-43 binds heterogeneous nuclear ribonucleoprotein A/B through its C-terminal tail: an important region for the inhibition of cystic fibrosis transmembrane conductance regulator exon 9 splicing. J. Biol. Chem. *280*, 37572–37584.

Castro, J.P., and Carareto, C.M.A. (2004). Drosophila melanogaster P Transposable Elements: Mechanisms of Transposition and Regulation. Genetica *121*, 107–118.

Chen, K., and Featherstone, D.E. (2005). Discs-large (DLG) is clustered by presynaptic innervation and regulates postsynaptic glutamate receptor subunit composition in Drosophila. BMC Biol. *3*, 1.

Chiang, P.-M., Ling, J., Jeong, Y.H., Price, D.L., Aja, S.M., and Wong, P.C. (2010). Deletion of TDP-43 down-regulates Tbc1d1, a gene linked to obesity, and alters body fat metabolism. Proc. Natl. Acad. Sci. U.S.A. *107*, 16320–16324.

Cohen, T.J., Lee, V.M.Y., and Trojanowski, J.Q. (2011). TDP-43 functions and pathogenic mechanisms implicated in TDP-43 proteinopathies. Trends in Molecular Medicine *17*, 659–667.

Colombrita, C., Onesto, E., Megiorni, F., Pizzuti, A., Baralle, F.E., Buratti, E., Silani, V., and Ratti, A. (2012). TDP-43 and FUS RNA-binding proteins bind distinct sets of cytoplasmic messenger RNAs and differently regulate their post-transcriptional fate in motoneuron-like cells. J. Biol. Chem. *287*, 15635–15647.

Corcia, P., Valdmanis, P., Millecamps, S., Lionnet, C., Blasco, H., Mouzat, K., Daoud, H., Belzil, V., Morales, R., Pageot, N., et al. (2012). Phenotype and genotype analysis in amyotrophic lateral sclerosis with TARDBP gene mutations. Neurology *78*, 1519–1526.

Cykowski, M.D., Powell, S.Z., Appel, J.W., Arumanayagam, A.S., Rivera, A.L., and Appel, S.H. (2018). Phosphorylated TDP-43 (pTDP-43) aggregates in the axial skeletal muscle of patients with sporadic and familial amyotrophic lateral sclerosis. Acta Neuropathologica Communications *6*, 28.

D'Ambrogio, A., Buratti, E., Stuani, C., Guarnaccia, C., Romano, M., Ayala, Y.M., and Baralle, F.E. (2009). Functional mapping of the interaction between TDP-43 and hnRNP A2 in vivo. Nucleic Acids Res. *37*, 4116–4126.

De Conti, L., Akinyi, M.V., Mendoza-Maldonado, R., Romano, M., Baralle, M., and Buratti, E. (2015). TDP-43 affects splicing profiles and isoform production of genes involved in the apoptotic and mitotic cellular pathways. Nucleic Acids Res. *43*, 8990–9005.

DeJesus-Hernandez, M., Mackenzie, I.R., Boeve, B.F., Boxer, A.L., Baker, M., Rutherford, N.J., Nicholson, A.M., Finch, N.A., Flynn, H., Adamson, J., et al. (2011). Expanded GGGGCC hexanucleotide repeat in noncoding region of C9ORF72 causes chromosome 9p-linked FTD and ALS. Neuron *72*, 245–256.

Dewey, C.M., Cenik, B., Sephton, C.F., Johnson, B.A., Herz, J., and Yu, G. (2012). TDP-43 aggregation in neurodegeneration: Are stress granules the key? Brain Research *1462*, 16–25.

Di Carlo, V., Grossi, E., Laneve, P., Morlando, M., Dini Modigliani, S., Ballarino, M., Bozzoni, I., and Caffarelli, E. (2013). TDP-43 regulates the microprocessor complex activity during in vitro neuronal differentiation. Mol. Neurobiol. *48*, 952–963.

Di Pietro, L., Lattanzi, W., and Bernardini, C. (2018). Skeletal Muscle MicroRNAs as Key Players in the Pathogenesis of Amyotrophic Lateral Sclerosis. International Journal of Molecular Sciences *19*, 1534.

DiAntonio, A. (2006). Glutamate receptors at the Drosophila neuromuscular junction. Int. Rev. Neurobiol. *75*, 165–179.

DiAntonio, A., Petersen, S.A., Heckmann, M., and Goodman, C.S. (1999). Glutamate receptor expression regulates quantal size and quantal content at the Drosophila neuromuscular junction. J. Neurosci. *19*, 3023–3032.

Diaper, D.C., Adachi, Y., Lazarou, L., Greenstein, M., Simoes, F.A., Di Domenico, A., Solomon, D.A., Lowe, S., Alsubaie, R., Cheng, D., et al. (2013). Drosophila TDP-43 dysfunction in glia and muscle cells cause cytological and behavioural phenotypes that characterize ALS and FTLD. Hum. Mol. Genet. *22*, 3883–3893.

Ehrhardt, J., and Morgan, J. (2005). Regenerative capacity of skeletal muscle. Curr. Opin. Neurol. *18*, 548–553.

van Es, M.A., Hardiman, O., Chio, A., Al-Chalabi, A., Pasterkamp, R.J., Veldink, J.H., and van den Berg, L.H. (2017). Amyotrophic lateral sclerosis. The Lancet *390*, 2084–2098.

Fallini, C., Bassell, G.J., and Rossoll, W. (2012). The ALS disease protein TDP-43 is actively transported in motor neuron axons and regulates axon outgrowth. Hum. Mol. Genet. *21*, 3703–3718.

Feiguin, F., Godena, V.K., Romano, G., D'Ambrogio, A., Klima, R., and Baralle, F.E. (2009). Depletion of TDP-43 affects Drosophila motoneurons terminal synapsis and locomotive behavior. FEBS Letters *583*, 1586–1592.

Fiesel, F.C., Weber, S.S., Supper, J., Zell, A., and Kahle, P.J. (2012). TDP-43 regulates global translational yield by splicing of exon junction complex component SKAR. Nucleic Acids Res *40*, 2668–2682.

Fomin, V., Richard, P., Hoque, M., Li, C., Gu, Z., Fissore-O'Leary, M., Tian, B., Prives, C., and Manley, J.L. (2018). The C9ORF72 Gene, Implicated in Amyotrophic Lateral Sclerosis and Frontotemporal Dementia, Encodes a Protein That Functions in Control of Endothelin and Glutamate Signaling. Mol. Cell. Biol. *38*.

Fortini, M.E., Skupski, M.P., Boguski, M.S., and Hariharan, I.K. (2000). A Survey of Human Disease Gene Counterparts in the Drosophila Genome. The Journal of Cell Biology *150*, F23–F30.

Fujii, R., and Takumi, T. (2005). TLS facilitates transport of mRNA encoding an actin-stabilizing protein to dendritic spines. Journal of Cell Science *118*, 5755–5765.

Fujii, R., Okabe, S., Urushido, T., Inoue, K., Yoshimura, A., Tachibana, T., Nishikawa, T., Hicks, G.G., and Takumi, T. (2005). The RNA binding protein TLS is translocated to dendritic spines by mGluR5 activation and regulates spine morphology. Curr. Biol. *15*, 587–593.

Gao, J., Wang, L., Huntley, M.L., Perry, G., and Wang, X. (2018). Pathomechanisms of TDP-43 in neurodegeneration. J. Neurochem.

Gao, J., Wang, L., Huntley, M.L., Perry, G., and Wang, X. Pathomechanisms of TDP-43 in neurodegeneration. Journal of Neurochemistry *146*, 7–20.

Gerstberger, S., Hafner, M., Ascano, M., and Tuschl, T. (2014). Evolutionary conservation and expression of human RNA-binding proteins and their role in human genetic disease. Adv. Exp. Med. Biol. *825*, 1–55.

Godena, V.K., Romano, G., Romano, M., Appocher, C., Klima, R., Buratti, E., Baralle, F.E., and Feiguin, F. (2011). TDP-43 regulates Drosophila neuromuscular junctions growth by modulating Futsch/MAP1B levels and synaptic microtubules organization. PLoS ONE *6*, e17808.

Goodman, L., Baddeley, D., Ambroziak, W., Waites, C.L., Garner, C.C., Soeller, C., and Montgomery, J.M. (2017). N-terminal SAP97 isoforms differentially regulate synaptic structure and postsynaptic surface pools of AMPA receptors. Hippocampus *27*, 668–682.

Gorczyca, M., Augart, C., and Budnik, V. (1993). Insulin-like Receptor and Insulin-like Peptide Are Localized at Neuromuscular Junctions in Drosophila. J Neurosci *13*, 3692–3704.

Gramates, L.S., and Budnik, V. (1999). Assembly and maturation of the Drosophila larval neuromuscular junction. Int. Rev. Neurobiol. *43*, 93–117.

Gregory, R.I., Yan, K.-P., Amuthan, G., Chendrimada, T., Doratotaj, B., Cooch, N., and Shiekhattar, R. (2004). The Microprocessor complex mediates the genesis of microRNAs. Nature *432*, 235–240.

Guan, B., Hartmann, B., Kho, Y.H., Gorczyca, M., and Budnik, V. (1996). The Drosophila tumor suppressor gene, dlg, is involved in structural plasticity at a glutamatergic synapse. Curr. Biol. *6*, 695–706.

Harraz, M.M., Marden, J.J., Zhou, W., Zhang, Y., Williams, A., Sharov, V.S., Nelson, K., Luo, M., Paulson, H., Schöneich, C., et al. (2008). SOD1 mutations disrupt redox-sensitive Rac regulation of NADPH oxidase in a familial ALS model. J. Clin. Invest. *118*, 659–670.

Hayashi, Y., Homma, K., and Ichijo, H. (2016). SOD1 in neurotoxicity and its controversial roles in SOD1 mutation-negative ALS. Adv Biol Regul *60*, 95–104.

Hoang, B., and Chiba, A. (2001). Single-cell analysis of Drosophila larval neuromuscular synapses. Dev. Biol. *229*, 55–70.

Howard, M.A., Elias, G.M., Elias, L.A.B., Swat, W., and Nicoll, R.A. (2010). The role of SAP97 in synaptic glutamate receptor dynamics. PNAS *107*, 3805–3810.

Hummel, T., Krukkert, K., Roos, J., Davis, G., and Klämbt, C. (2000). Drosophila Futsch/22C10 is a MAP1B-like protein required for dendritic and axonal development. Neuron *26*, 357–370.

Ishigaki, S., and Sobue, G. (2018). Importance of Functional Loss of FUS in FTLD/ALS. Front Mol Biosci *5*.

Jan, L.Y., and Jan, Y.N. (1982). Antibodies to horseradish peroxidase as specific neuronal markers in Drosophila and in grasshopper embryos. Proc. Natl. Acad. Sci. U.S.A. *79*, 2700–2704.

Johansen, J., Halpern, M.E., and Keshishian, H. (1989). Axonal guidance and the development of muscle fiber-specific innervation in Drosophila embryos. J. Neurosci. *9*, 4318–4332.

Johnson, B.S., McCaffery, J.M., Lindquist, S., and Gitler, A.D. (2008). A yeast TDP-43 proteinopathy model: Exploring the molecular determinants of TDP-43 aggregation and cellular toxicity. Proc. Natl. Acad. Sci. U.S.A. *105*, 6439–6444.

Johnson, B.S., Snead, D., Lee, J.J., McCaffery, J.M., Shorter, J., and Gitler, A.D. (2009). TDP-43 is intrinsically aggregation-prone, and amyotrophic lateral sclerosis-linked mutations accelerate aggregation and increase toxicity. J. Biol. Chem. *284*, 20329–20339.

Johnston, D.S. (2002). The art and design of genetic screens: Drosophila melanogaster. Nature Reviews Genetics *3*, 176.

Kabashi, E., Valdmanis, P.N., Dion, P., Spiegelman, D., McConkey, B.J., Vande Velde, C., Bouchard, J.-P., Lacomblez, L., Pochigaeva, K.,

Salachas, F., et al. (2008). TARDBP mutations in individuals with sporadic and familial amyotrophic lateral sclerosis. Nat. Genet. *40*, 572–574.

Keshishian, H., and Chiba, A. (1993). Neuromuscular development in Drosophila: insights from single neurons and single genes. Trends Neurosci. *16*, 278–283.

King, I.N., Yartseva, V., Salas, D., Kumar, A., Heidersbach, A., Ando, D.M., Stallings, N.R., Elliott, J.L., Srivastava, D., and Ivey, K.N. (2014). The RNA-binding protein TDP-43 selectively disrupts microRNA-1/206 incorporation into the RNA-induced silencing complex. J. Biol. Chem. *289*, 14263–14271.

Koh, Y.H., Gramates, L.S., and Budnik, V. (2000). Drosophila larval neuromuscular junction: molecular components and mechanisms underlying synaptic plasticity. Microsc. Res. Tech. *49*, 14–25.

Kwiatkowski, T.J., Bosco, D.A., Leclerc, A.L., Tamrazian, E., Vanderburg, C.R., Russ, C., Davis, A., Gilchrist, J., Kasarskis, E.J., Munsat, T., et al. (2009). Mutations in the FUS/TLS gene on chromosome 16 cause familial amyotrophic lateral sclerosis. Science *323*, 1205–1208.

Lahey, T., Gorczyca, M., Jia, X.-X., and Budnik, V. (1994). The Drosophila Tumor Suppressor Gene dlg Is Required for Normal Synaptic Bouton Structure. Neuron *13*, 823–835.

Lee, T., and Luo, L. (1999). Mosaic Analysis with a Repressible Cell Marker for Studies of Gene Function in Neuronal Morphogenesis. Neuron *22*, 451–461.

Linford, N.J., Bilgir, C., Ro, J., and Pletcher, S.D. (2013). Measurement of Lifespan in Drosophila melanogaster. J Vis Exp.

Littleton, J.T., and Ganetzky, B. (2000). Ion channels and synaptic organization: analysis of the Drosophila genome. Neuron *26*, 35–43.

Ma, J., and Ptashne, M. (1987). The carboxy-terminal 30 amino acids of GAL4 are recognized by GAL80. Cell *50*, 137–142.

Mackenzie, I.R.A., and Rademakers, R. (2008). The role of TDP-43 in amyotrophic lateral sclerosis and frontotemporal dementia. Curr Opin Neurol *21*, 693–700.

Manzano, R., Toivonen, J.M., Calvo, A.C., Oliván, S., Zaragoza, P., Muñoz, M.J., Montarras, D., and Osta, R. (2012). Quantity and activation

of myofiber-associated satellite cells in a mouse model of amyotrophic lateral sclerosis. Stem Cell Rev *8*, 279–287.

Manzano, R., Toivonen, J.M., Calvo, A.C., Oliván, S., Zaragoza, P., Rodellar, C., Montarras, D., and Osta, R. (2013). Altered in vitro proliferation of mouse SOD1-G93A skeletal muscle satellite cells. Neurodegener Dis *11*, 153–164.

Marrus, S.B., Portman, S.L., Allen, M.J., Moffat, K.G., and DiAntonio, A. (2004). Differential localization of glutamate receptor subunits at the Drosophila neuromuscular junction. J. Neurosci. *24*, 1406–1415.

Martinez, R.L.M.C., and Naranjo, J.D. (2010). A pretest for choosing between logrank and wilcoxon tests in the two-sample problem. METRON *68*, 111–125.

Maselli, R.A., Wollman, R.L., Leung, C., Distad, B., Palombi, S., Richman, D.P., Salazar-Grueso, E.F., and Roos, R.P. (1993). Neuromuscular transmission in amyotrophic lateral sclerosis. Muscle & Nerve *16*, 1193–1203.

Mathis, S., Goizet, C., Soulages, A., Vallat, J.-M., and Masson, G.L. (2019). Genetics of amyotrophic lateral sclerosis: A review. Journal of the Neurological Sciences *399*, 217–226.

McGuire, S.E., Le, P.T., Osborn, A.J., Matsumoto, K., and Davis, R.L. (2003). Spatiotemporal rescue of memory dysfunction in Drosophila. Science *302*, 1765–1768.

Menon, K.P., Carrillo, R.A., and Zinn, K. (2013). Development and plasticity of the Drosophila larval neuromuscular junction. Wiley Interdiscip Rev Dev Biol *2*, 647–670.

Milanese, M., Zappettini, S., Onofri, F., Musazzi, L., Tardito, D., Bonifacino, T., Messa, M., Racagni, G., Usai, C., Benfenati, F., et al. (2011). Abnormal exocytotic release of glutamate in a mouse model of amyotrophic lateral sclerosis. J. Neurochem. *116*, 1028–1042.

Moloney, E.B., de Winter, F., and Verhaagen, J. (2014). ALS as a distal axonopathy: molecular mechanisms affecting neuromuscular junction stability in the presymptomatic stages of the disease. Front Neurosci *8*, 252.

Monastirioti, M., Gorczyca, M., Rapus, J., Eckert, M., White, K., and Budnik, V. (1995). Octopamine immunoreactivity in the fruit fly Drosophila melanogaster. J. Comp. Neurol. *356*, 275–287.

Morgan, T.H. (1910). Sex Limited Inheritance in Drosophila. Science *32*, 120–122.

Muller, B.M., Kistner, U., Veh, R.W., Cases-Langhoff, C., Becker, B., Gundelfinger, E.D., and Garner, C.C. (1995). Molecular characterization and spatial distribution of SAP97, a novel presynaptic protein homologous to SAP90 and the Drosophila discs-large tumor suppressor protein. J. Neurosci. *15*, 2354–2366.

Narayanan, R.K., Mangelsdorf, M., Panwar, A., Butler, T.J., Noakes, P.G., and Wallace, R.H. (2013). Identification of RNA bound to the TDP-43 ribonucleoprotein complex in the adult mouse brain. Amyotroph Lateral Scler Frontotemporal Degener *14*, 252–260.

Neumann, M., Sampathu, D.M., Kwong, L.K., Truax, A.C., Micsenyi, M.C., Chou, T.T., Bruce, J., Schuck, T., Grossman, M., Clark, C.M., et al. (2006). Ubiquitinated TDP-43 in frontotemporal lobar degeneration and amyotrophic lateral sclerosis. Science *314*, 130–133.

Ng, L., Khan, F., Young, C.A., and Galea, M. (2017). Symptomatic treatments for amyotrophic lateral sclerosis/motor neuron disease. Cochrane Database of Systematic Reviews.

Ng, S.-Y., Soh, B.S., Rodriguez-Muela, N., Hendrickson, D.G., Price, F., Rinn, J.L., and Rubin, L.L. (2015). Genome-wide RNA-Seq of Human Motor Neurons Implicates Selective ER Stress Activation in Spinal Muscular Atrophy. Cell Stem Cell *17*, 569–584.

Nguyen, H.T., Bodmer, R., Abmayr, S.M., McDermott, J.C., and Spoerel, N.A. (1994). D-mef2: a Drosophila mesoderm-specific MADS box-containing gene with a biphasic expression profile during embryogenesis. PNAS *91*, 7520–7524.

Nie, M., Deng, Z.-L., Liu, J., and Wang, D.-Z. (2015). Noncoding RNAs, Emerging Regulators of Skeletal Muscle Development and Diseases.

O'Rourke, J.G., Bogdanik, L., Yáñez, A., Lall, D., Wolf, A.J., Muhammad, A.K.M.G., Ho, R., Carmona, S., Vit, J.P., Zarrow, J., et al. (2016). C9orf72 is required for proper macrophage and microglial function in mice. Science *351*, 1324–1329.

Pasinelli, P., and Brown, R.H. (2006). Molecular biology of amyotrophic lateral sclerosis: insights from genetics. Nat. Rev. Neurosci. *7*, 710–723.

Phukan, J., Pender, N.P., and Hardiman, O. (2007). Cognitive impairment in amyotrophic lateral sclerosis. Lancet Neurol *6*, 994–1003.

Pradat, P.-F., Barani, A., Wanschitz, J., Dubourg, O., Lombès, A., Bigot, A., Mouly, V., Bruneteau, G., Salachas, F., Lenglet, T., et al. (2011). Abnormalities of satellite cells function in amyotrophic lateral sclerosis. Amyotroph Lateral Scler *12*, 264–271.

Prasad, A., Bharathi, V., Sivalingam, V., Girdhar, A., and Patel, B.K. (2019). Molecular Mechanisms of TDP-43 Misfolding and Pathology in Amyotrophic Lateral Sclerosis. Front. Mol. Neurosci. *12*.

Prudencio, M., Jansen-West, K.R., Lee, W.C., Gendron, T.F., Zhang, Y.-J., Xu, Y.-F., Gass, J., Stuani, C., Stetler, C., Rademakers, R., et al. (2012). Misregulation of human sortilin splicing leads to the generation of a nonfunctional progranulin receptor. Proc. Natl. Acad. Sci. U.S.A. *109*, 21510–21515.

Ratti, A., and Buratti, E. (2016). Physiological functions and pathobiology of TDP-43 and FUS/TLS proteins. J. Neurochem. *138 Suppl 1*, 95–111.

Ratti, A., and Buratti, E. Physiological functions and pathobiology of TDP-43 and FUS/TLS proteins. Journal of Neurochemistry *138*, 95–111.

Reich-Slotky, R., Andrews, J., Cheng, B., Buchsbaum, R., Levy, D., Kaufmann, P., and Thompson, J.L.P. (2013). Body mass index (BMI) as predictor of ALSFRS-R score decline in ALS patients. Amyotroph Lateral Scler Frontotemporal Degener *14*, 212–216.

Renton, A.E., Majounie, E., Waite, A., Simón-Sánchez, J., Rollinson, S., Gibbs, J.R., Schymick, J.C., Laaksovirta, H., van Swieten, J.C., Myllykangas, L., et al. (2011). A Hexanucleotide Repeat Expansion in C9ORF72 Is the Cause of Chromosome 9p21-Linked ALS-FTD. Neuron *72*, 257–268.

Romano, G., Klima, R., Buratti, E., Verstreken, P., Baralle, F.E., and Feiguin, F. (2014). Chronological requirements of TDP-43 function in synaptic organization and locomotive control. Neurobiol. Dis. *71*, 95–109.

Romano, M., Feiguin, F., and Buratti, E. (2012). Drosophila Answers to TDP-43 Proteinopathies.

Roos, J., Hummel, T., Ng, N., Klämbt, C., and Davis, G.W. (2000). Drosophila Futsch Regulates Synaptic Microtubule Organization and Is Necessary for Synaptic Growth. Neuron *26*, 371–382.

Rosen, D.R., Siddique, T., Patterson, D., Figlewicz, D.A., Sapp, P., Hentati, A., Donaldson, D., Goto, J., O'Regan, J.P., and Deng, H.X.

(1993). Mutations in Cu/Zn superoxide dismutase gene are associated with familial amyotrophic lateral sclerosis. Nature *362*, 59–62.

Rowland, L.P., and Shneider, N.A. (2001). Amyotrophic lateral sclerosis. N. Engl. J. Med. *344*, 1688–1700.

Rubin, G.M., and Spradling, A.C. (1982). Genetic transformation of Drosophila with transposable element vectors. Science *218*, 348–353.

Russell, A.P., Wada, S., Vergani, L., Hock, M.B., Lamon, S., Léger, B., Ushida, T., Cartoni, R., Wadley, G.D., Hespel, P., et al. (2013). Disruption of skeletal muscle mitochondrial network genes and miRNAs in amyotrophic lateral sclerosis. Neurobiol. Dis. *49*, 107–117.

Sandmann, T., Jensen, L.J., Jakobsen, J.S., Karzynski, M.M., Eichenlaub, M.P., Bork, P., and Furlong, E.E.M. (2006). A Temporal Map of Transcription Factor Activity: Mef2 Directly Regulates Target Genes at All Stages of Muscle Development. Developmental Cell *10*, 797–807.

Saxena, S., Cabuy, E., and Caroni, P. (2009). A role for motoneuron subtype-selective ER stress in disease manifestations of FALS mice. Nat. Neurosci. *12*, 627–636.

Sellers, J.R. (2000). Myosins: a diverse superfamily. Biochimica et Biophysica Acta (BBA) - Molecular Cell Research *1496*, 3–22.

Sellier, C., Campanari, M., Julie Corbier, C., Gaucherot, A., Kolb-Cheynel, I., Oulad-Abdelghani, M., Ruffenach, F., Page, A., Ciura, S., Kabashi, E., et al. (2016). Loss of C9ORF72 impairs autophagy and synergizes with polyQ Ataxin-2 to induce motor neuron dysfunction and cell death. EMBO J *35*, 1276–1297.

Sephton, C.F., Cenik, C., Kucukural, A., Dammer, E.B., Cenik, B., Han, Y., Dewey, C.M., Roth, F.P., Herz, J., Peng, J., et al. (2011). Identification of neuronal RNA targets of TDP-43-containing ribonucleoprotein complexes. J. Biol. Chem. *286*, 1204–1215.

Shang, Y., and Huang, E.J. (2016). Mechanisms of FUS mutations in familial amyotrophic lateral sclerosis. Brain Research *1647*, 65–78.

Shaw, C.E., Al-Chalabi, A., and Leigh, N. (2001). Progress in the pathogenesis of amyotrophic lateral sclerosis. Curr Neurol Neurosci Rep *1*, 69–76.

Shiga, A., Ishihara, T., Miyashita, A., Kuwabara, M., Kato, T., Watanabe, N., Yamahira, A., Kondo, C., Yokoseki, A., Takahashi, M., et al. (2012).

Alteration of POLDIP3 Splicing Associated with Loss of Function of TDP-43 in Tissues Affected with ALS. PLoS One *7*.

Sivadasan, R., Hornburg, D., Drepper, C., Frank, N., Jablonka, S., Hansel, A., Lojewski, X., Sterneckert, J., Hermann, A., Shaw, P.J., et al. (2016). C9ORF72 interaction with cofilin modulates actin dynamics in motor neurons. Nat. Neurosci. *19*, 1610–1618.

Slater, C.R. (2017). The Structure of Human Neuromuscular Junctions: Some Unanswered Molecular Questions. Int J Mol Sci *18*.

Sreedharan, J., Blair, I.P., Tripathi, V.B., Hu, X., Vance, C., Rogelj, B., Ackerley, S., Durnall, J.C., Williams, K.L., Buratti, E., et al. (2008). TDP-43 mutations in familial and sporadic amyotrophic lateral sclerosis. Science *319*, 1668–1672.

Stallings, N.R., Puttaparthi, K., Dowling, K.J., Luther, C.M., Burns, D.K., Davis, K., and Elliott, J.L. (2013). TDP-43, an ALS Linked Protein, Regulates Fat Deposition and Glucose Homeostasis. PLOS ONE *8*, e71793.

Stavroulakis, T., Baird, W.O., Baxter, S.K., Walsh, T., Shaw, P.J., and McDermott, C.J. (2016). The impact of gastrostomy in motor neurone disease: challenges and benefits from a patient and carer perspective. BMJ Support Palliat Care *6*, 52–59.

Strong, M.J., and Yang, W. (2011). The frontotemporal syndromes of ALS. Clinicopathological correlates. J. Mol. Neurosci. *45*, 648–655.

Swanger, S.A., and Bassell, G.J. (2011). Making and breaking synapses through local mRNA regulation. Curr. Opin. Genet. Dev. *21*, 414–421.

Toivonen, J.M., Manzano, R., Oliván, S., Zaragoza, P., García-Redondo, A., and Osta, R. (2014). MicroRNA-206: A Potential Circulating Biomarker Candidate for Amyotrophic Lateral Sclerosis. PLOS ONE *9*, e89065.

Traynor, K. (2017). FDA approves edaravone for amyotrophic lateral sclerosis. Am J Health Syst Pharm *74*, 868.

Tsitkanou, S., Della Gatta, P.A., and Russell, A.P. (2016). Skeletal Muscle Satellite Cells, Mitochondria, and MicroRNAs: Their Involvement in the Pathogenesis of ALS. Front. Physiol. *7*.

Valentine, J.S., Doucette, P.A., and Zittin Potter, S. (2005). Copper-Zinc Superoxide Dismutase and Amyotrophic Lateral Sclerosis. Annual Review of Biochemistry *74*, 563–593.

Van Damme, P., Bogaert, E., Dewil, M., Hersmus, N., Kiraly, D., Scheveneels, W., Bockx, I., Braeken, D., Verpoorten, N., Verhoeven, K., et al. (2007). Astrocytes regulate GluR2 expression in motor neurons and their vulnerability to excitotoxicity. Proc. Natl. Acad. Sci. U.S.A. *104*, 14825–14830.

Van Deerlin, V.M., Leverenz, J.B., Bekris, L.M., Bird, T.D., Yuan, W., Elman, L.B., Clay, D., Wood, E.M., Chen-Plotkin, A.S., Martinez-Lage, M., et al. (2008). TARDBP mutations in amyotrophic lateral sclerosis with TDP-43 neuropathology: a genetic and histopathological analysis. Lancet Neurol *7*, 409–416.

Vance, C., Rogelj, B., Hortobágyi, T., De Vos, K.J., Nishimura, A.L., Sreedharan, J., Hu, X., Smith, B., Ruddy, D., Wright, P., et al. (2009). Mutations in FUS, an RNA processing protein, cause familial amyotrophic lateral sclerosis type 6. Science *323*, 1208–1211.

Vijayakumar, U.G., Milla, V., Cynthia Stafford, M.Y., Bjourson, A.J., Duddy, W., and Duguez, S.M.-R. (2019). A Systematic Review of Suggested Molecular Strata, Biomarkers and Their Tissue Sources in ALS. Front. Neurol. *10*.

Vogler, T.O., Wheeler, J.R., Nguyen, E.D., Hughes, M.P., Britson, K.A., Lester, E., Rao, B., Betta, N.D., Whitney, O.N., Ewachiw, T.E., et al. (2018). TDP-43 and RNA form amyloid-like myo-granules in regenerating muscle. Nature *563*, 508–513.

Volk, L., Chiu, S.-L., Sharma, K., and Huganir, R.L. (2015). Glutamate Synapses in Human Cognitive Disorders. Annual Review of Neuroscience *38*, 127–149.

Webster, C.P., Smith, E.F., Bauer, C.S., Moller, A., Hautbergue, G.M., Ferraiuolo, L., Myszczynska, M.A., Higginbottom, A., Walsh, M.J., Whitworth, A.J., et al. (2016). The C9orf72 protein interacts with Rab1a and the ULK1 complex to regulate initiation of autophagy. EMBO J. *35*, 1656–1676.

Wijesekera, L.C., and Leigh, P.N. (2009). Amyotrophic lateral sclerosis. Orphanet J Rare Dis *4*, 3.

Willard, S.S., and Koochekpour, S. (2013). Glutamate, Glutamate Receptors, and Downstream Signaling Pathways. Int J Biol Sci *9*, 948–959.

Williams, A.H., Valdez, G., Moresi, V., Qi, X., McAnally, J., Elliott, J.L., Bassel-Duby, R., Sanes, J.R., and Olson, E.N. (2009). MicroRNA-206 delays ALS progression and promotes regeneration of neuromuscular synapses in mice. Science *326*, 1549–1554.

Woods, D.F., and Bryant, P.J. (1991). The discs-large tumor suppressor gene of Drosophila encodes a guanylate kinase homolog localized at septate junctions. Cell *66*, 451–464.

Worms, P.M. (2001). The epidemiology of motor neuron diseases: a review of recent studies. J. Neurol. Sci. *191*, 3–9.

Wu, M.N., Fergestad, T., Lloyd, T.E., He, Y., Broadie, K., and Bellen, H.J. (1999). Syntaxin 1A interacts with multiple exocytic proteins to regulate neurotransmitter release in vivo. Neuron *23*, 593–605.

Zhang, Y.-J., Xu, Y.-F., Cook, C., Gendron, T.F., Roettges, P., Link, C.D., Lin, W.-L., Tong, J., Castanedes-Casey, M., Ash, P., et al. (2009). Aberrant cleavage of TDP-43 enhances aggregation and cellular toxicity. Proc. Natl. Acad. Sci. U.S.A. *106*, 7607–7612.

Zhou, J., Li, A., Li, X., and Yi, J. (2019). Dysregulated mitochondrial Ca2+ and ROS signaling in skeletal muscle of ALS mouse model. Archives of Biochemistry and Biophysics *663*, 249–258.

Zhou, W., Zhang, L., Guoxiang, X., Mojsilovic-Petrovic, J., Takamaya, K., Sattler, R., Huganir, R., and Kalb, R. (2008). GluR1 Controls Dendrite Growth through Its Binding Partner, SAP97. J. Neurosci. *28*, 10220–10233.

Zoccolella, S., Beghi, E., Palagano, G., Fraddosio, A., Guerra, V., Samarelli, V., Lepore, V., Simone, I.L., Lamberti, P., Serlenga, L., et al. (2008). Analysis of survival and prognostic factors in amyotrophic lateral sclerosis: a population based study. J. Neurol. Neurosurg. Psychiatry *79*, 33–37.

Zou, Z.-Y., Zhou, Z.-R., Che, C.-H., Liu, C.-Y., He, R.-L., and Huang, H.-P. (2017). Genetic epidemiology of amyotrophic lateral sclerosis: a systematic review and meta-analysis. J Neurol Neurosurg Psychiatry *88*, 540–549.

Zu, T., Liu, Y., Bañez-Coronel, M., Reid, T., Pletnikova, O., Lewis, J., Miller, T.M., Harms, M.B., Falchook, A.E., Subramony, S.H., et al. (2013). RAN proteins and RNA foci from antisense transcripts in C9ORF72 ALS

and frontotemporal dementia. Proc. Natl. Acad. Sci. U.S.A. *110*, E4968-4977.